Cranfield UNIVERSITY

Cranfield University

Ninghong Jia

Numerical Simulation of Two-Phase Gas and Non-Newtonian Shear-Thinning Fluid Flows in Pipelines

School of Engineering
Applied Mathematics and Computing Group

Ph.D. Thesis

Cranfield UNIVERSITY

Cranfield University

School of Engineering
Applied Mathematics and Computing Group

Ph.D. Thesis

Academic Year 2010-2011

Ninghong Jia

Numerical Simulation of Two-Phase Gas and Non-Newtonian Shear-Thinning Fluid Flows in Pipelines

Supervisor: Prof. C. P. Thompson
Dr. Mustapha Gourma

August 2011

This thesis is submitted in partial fulfilment of the requirements for the degree of Doctor of Philosophy

Acknowledgements

The author gratefully acknowledges the research grant from the Joint Project on Transient Multiphase Flows and Flow Assurance TMF. The author wish to acknowledge the contributions made to this project by the UK Engineering and Physical Sciences Research Council (EPSRC) and the following: ASCOMP; GL Noble Denton; BP Exploration; CD-adapco; Chevron; ConocoPhillips; ENI; ExxonMobil; FEESA; IFP Energies nouvelles; Institutt for Energiteknikk; PDVSA (INTEVEP); Petrobras; PETRONAS; SPT Group; Shell; SINTEF; Statoil and TOTAL. The authors wish to express their sincere gratitude for this support.

First and foremost I want to thank my supervisor Prof Chris Thompson, for having given me the opportunity and the financial support to continue my project on two-phase flow. I would like to thank him for the guidance and continuous support during my studies at Cranfield University.

In particular, I would like to express my deepest thanks and gratitude to the support of this work by Dr Mustapha Gourma who gave me very fruitful discussions throughout the current work. I also would like to specially thank him for the help in writing this work. This work would have taken much longer time without his sincere and patient advice. Thanks again, Mustapha.

Also, I would like to express my gratitude to Stamatis Kalogerakos, for having shared plenty of nice scripts and computer help, proof-reading of my article and friendship throughout the years.

I would to extend my gratitude to the other colleagues in the Applied Mathematics and Computing (AMAC) group: Dr Patrick Verdin, Robert Sawko, Dr Stuart Barnes, Dr Karl Jenkins, Dr Jiwan Han. They have all contributed to make the group a very enjoyable place to work. A very special thanks is due to Serena Slattery for her extremely good work and patience with all of us. I would also like to thank Dr Wei Yan, Lanchang Xing, from the Process Systems Engineering group (PSE), who discussed about experiment of multiphase flow.

I also wish to thank Dr R. P. Chhabra for providing us with experimental data.

Last, but not least, I would like to especially thank my parents for their unconditional love. I so appreciate their encouragement and patience. I wish to give specially thanks to my wife, Xiaowen, for all the years of love, support, patience, being a constant source of inspiration and especially for her understanding while depriving her of precious time and care during the duration of this work. I have also been refreshed by the smiling faces of my newborn son, Jingtai(uu). This work is a tribute to their sacrifices and continuous encouragement.

Ninghong Jia @ Cranfield University
21st Aug, 2011

献给我至爱的亲人们！

感谢你们给我的鼓励、支持，还有对我无限的包容！

To my family with love

Abstract

The one goal of this research is to present the adaptive mesh refinement (AMR) technique for one dimensional two-phase slug flows. Uniform fine meshes for these long devices are costly and, in general situations, the optimum space discretisation could not be determined a priori.

The adaptive mesh refinement (AMR) procedure permits this problem to be remedied by refining the mesh locally, within regions where sharp discontinuities and steep gradients are present. With the appropriate algorithm and data organisation, it helps to reduce CPU time and speed up simulations of flows in long pipes, while preserving accuracy and acceptable execution times.

The main objective of this research is to investigate the behaviour of the gas and non-Newtonian shear-thinning fluids in horizontal pipes. Predictions of drag reduction ratio and holdup are presented for the stratified flow of gas and non-Newtonian Ostwald-de Waele liquid. For slug flow regimes, the mechanistic slug unit model is adopted in order to estimate the pressure gradients along the slug unit. The slug unit model is rearranged and reinterpreted as inviscid Burgers's equation for incompressible phases.

For both stratified and slug flow regimes, three dimensional CFD (computational fluid dynamics) simulations were performed in order to compare the drag reduction ratio and pressure gradients. In stratified flows, CFD is also used in an attempt to evaluate the liquid wall friction factor and to compare the obtained values with those given by empirical standard correlations.

The estimated pressure gradient and drag reductions are compared with experimental data. Calculations showed an excellent agreement between the simulation and experimental data. Shear thinning effects are also correctly modelled in this work.

Contents

List of Figures

LIST OF FIGURES

LIST OF FIGURES

LIST OF FIGURES

List of Tables

LIST OF TABLES

Chapter 1

Introduction

1.1 Background

Two-phase flows are encountered in a wide range of industrial applications. Gas-liquid flows are commonly found in power plants, chemical processes, nuclear reactors, and petroleum and related industries. Problems arise in pipeline transport of such gas-liquid mixtures and in the design of equipment such as boilers, distillation towers, and condensers. Suspension of solids in gases in pneumatic conveying and fluidized bed are typical air-solid two-phase systems. The transport of some solid materials in finely divided form is accomplished by making a slurry of the solid particles in a liquid, and pumping the mixture through a pipe. Two immiscible liquids may also be considered to be another type of two-phase system which finds its application in emulsion, liquid-liquid solvent extraction.

The widespread presence of these multi-fluid systems suggests the utility of a general technique of description to understand their behaviour. However, each of these systems has distinguishing characteristics that keep any particular multiphase model from being generally applicable. The result is that many disjoint modelling communities use their own specific formulation and approximations, slowing the progress in better understanding these complex flows.

Despite the various forms of two-phase flow, the term "two-phase" will be used hereafter, to refer only to the case of one gas and one liquid phase in this thesis. They are commonly encountered in many types of process equipment, from boilers and condensers to refrigerators, heat exchangers and even air conditioners. They are also prevalent in hydrocarbon recovery onshore and offshore, because the oil that flows to the surface is often accompanied by gas through pipelines.

Although research on two-phase flows began as early as 18th century, it recently entered a state of rapid development and evolution. Previous research efforts have been heavily directed toward the flows of gases and Newtonian liquids, despite the increasing industrial importance of non-Newtonian liquids; for example, aeration of non-Newtonian broths in biochemical reactors, continuous polymerization, transport of such non-Newtonian liquid materials as drilling muds, greases, slurries, polymer solutions, etc. Significant differences can be expected between the two-phase flow behaviour of Newtonian liquids and that of non-Newtonian liquids, because of the latter's shear-dependent viscosity (usually shear-thinning). Thus, more attention should be concentrated on the simulation of a gas and a Non-Newtonian liquid.

1.2 Two-phase flow patterns

In this section, the most important hydrodynamic features in two-phase gas-liquid flow will be introduced, which are the flow patterns. The interface between the two phase can display in a wide variety of forms, depending on the flow rates, fluid properties of the phase and the geometry of the system. Classification of the flow interface into recognised patterns is very subjective, but most of them are still similar. In this thesis, only the flow patterns in horizontal or near horizontal pipes are focused on, and they are illustrated schematically in figure 1.1, which can be reviewed in the literature [Taitel and Dukler (1976), Barnea (1987), Shaha (1999)]:

- If both liquid and gas flow rates are low, gravitation effects the gas and liquid flow separately, with the gas phase in the higher portion of the pipe.

The stratified flow pattern is subdivided into stratified smooth flow, where the interface is smooth, and stratified wavy flow, where the interface is wavy. As the gas rate increases, instability of the interface of the stratified smooth flow results in the occurrence of stratified wavy flow.

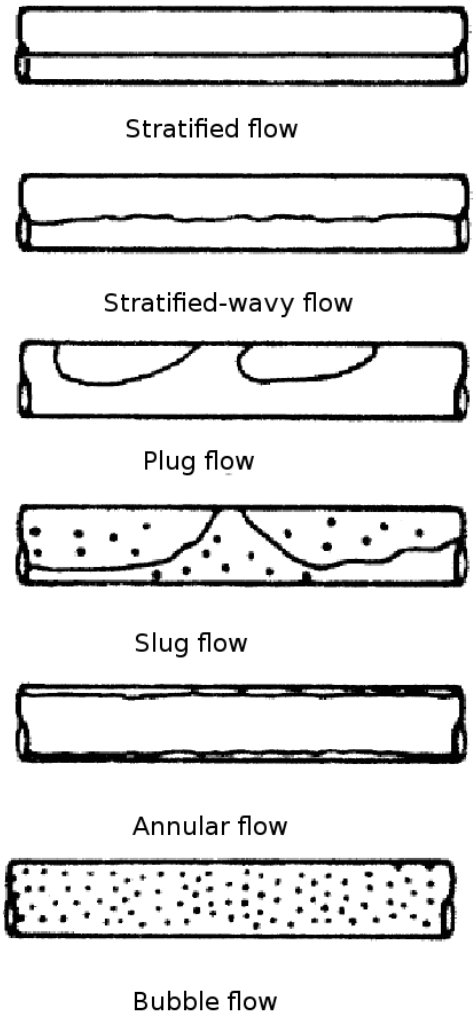

Figure 1.1: Schematic of gas-liquid flow patterns in horizontal pipes (Shaha, 1999)

- With increasing the gas and liquid velocity, the stratified wavy grows and blocks the whole cross section of the pipe. Intermittent flow is characterized by the alternate appearance of slugs and gas bubbles in the pipes. The

major difference between plug flow and slug flow is that in plug flow, there are no entrained gas bubbles in the slug body.

- When gas rate increases, annular flow occurs. The liquid flows as a film around the pipe wall and the gas flows in the centre of the pipe. The gas core may contain some entrained liquid droplets. In this flow pattern, the gas rate should be big enough to support the gas corn in the middle and prevent the liquid film from falling down.

- In dispersed bubble flow, liquid phase flows at very high flowrates. The liquid phase is continuous while the gas bubbles are dispersed in liquid phase, and bubbles tend to stay on the top of the pipe because of the effect of buoyancy.

1.3 Research objectives

This work is part of a project on **T**ransient **M**ultiphase **F**low (TMF) [Hewitt (2006)], funded by the UK Engineering and Physical Sciences Research Council (EPSRC) and the following: ASCOMP; GL Noble Denton; BP Exploration; CD-adapco; Chevron; ConocPhillips; ENI; ExxonMobil; FEESA; IFP Energies nouvelles; Institutt for Energiteknikk; PDVSA (INTEVEP); Petrobras; PETRONAS; SPT Group; Shell; SINTEF; Statoil and TOTAL.

The research described in this thesis comprises two parts:

- The first part will be dealing with the mathematical simulation of two-phase gas-liquid flow with Finite Volume methods.The first purpose is to validate the model by comparing calculated slug frequencies and slug lengths with their corresponding measured frequencies and measured lengths, the second aim is to implement an adaptive mesh refinement technique in the model that is developed in **E**ulerian **M**ultiphase **A**daptive **P**ipeline **S**olver (**EMAPS**), which is in-house FORTRAN code belonging to the AMAC group of Cranfield University;

- So far, the emphasis has been on multiphase flows of relatively simple Newtonian fluids; this has in itself been challenging enough. However, the reality has to be faced that real hydrocarbon production fluids are often very complex and difficult. They can have complex structures and extremely high viscosities (heavy oils), and they can be non-Newtonian in nature. However, predictive capability for variables like pressure drop and holdup for such two-phase flow of non-Newtonian liquids is, at present, practically limited. Very little information is available for the case when the liquid phase is non-Newtonian, especially in inclined pipes. Only for the two-phase flow of gas and Newtonian liquids does significant theoretical and experimental work exist, and a great deal of experimental investigations have been proposed in the literature for a gas-Newtonian fluid two-phase mixture in pipes.

  The second part concerns the behaviour of non-Newtonian liquid under gas injection in horizontal pipes. Both gas non-Newtonian stratified flow and slug flow regimes are studied. Gas injection in non Newtonian liquid results in drag reduction under certain flow conditions. These conditions were established experimentally. The objective here is to use numerical models in order to predict pressure drop and liquid holdup in gas non Newtonian shear thinning systems.

1.4 Chapter outline

This thesis is structured into five main chapters, (Chapter 2 to 7), followed by a short conclusion (Chapter 8), where the main results and achievements of this thesis are summarised, and suggestions for further work are provided.

Chapter 2: **Two phase flow modelling**, in this chapter, the one dimensional two-phase flow two-fluids model that is implemented in EMAPS code is introduced firstly. Following this, the three dimensional two-phase flow model Volume Of Fluids which is used to predict the gas-non-Newtonian stratified flow in chapter 6 and gas-non-Newtonian slug flow in chapter 7 will also be presented.

Chapter 3: **Gas/water slug flow modelling**, slug frequency, slug length and friction factor correlation will be thoroughly reviewed. Then a slug case is validated using the two-fluid model, followed by comparison of the slug frequency and slug length with results calculated from different correlations.

Chapter 4: **Adaptive mesh refinement(AMR) for gas/water slug flow**, the AMR strategy is introduced in the EMAPS framework, and two different error estimations will introduced in this work, which are gradient error criterion and Taitel-Dukler Kelvin-Helmholtz criterion coupled with gradient error criterion. Then, three slug test cases from Manolis (1995) will be used to validate these two criteria.

Chapter 5: **Non-Newtonian fluid behaviour**, a theoretical study of Steady non-Newtonian flow in circular tubes was conducted firstly, and the analytical velocity distribution about the laminar, steady, incompressible fully-developed non-Newtonian single phase flow was successfully obtained through the formula derivation from the steady invariant N-S momentum equation. The three most important factors in two-phase gas-non-Newtonian fluid flow are also reviewed here.

Chapter 6: **Two phase gas/shear-thinning liquid stratified flow**, in this chapter, a model extended from the gas-Newtonian fluid model, which is derived by Taitel and Dukler (1976), was used to predict the average liquid holdup and drag reduction for the gas/non-Newtonian shear-thinning stratified flow. Drag reduction was compared with experimental data and numerical results with 3D Fluent.

Chapter 7: **Two phase gas/shear-thinning liquid slug flow**, A mechanistic model of slug unit is reformulated and its capability to agree with experimental data in evaluating the pressure gradients is shown.

Fluent 3D CFD package Volume of fluid method was used, and simulations with an appropriate turbulence model, low Reynolds number $k - \epsilon$, initiated by Lam and Bremhorst (1981), were performed and supported the prediction of the previous slug unit model and its validity for wavy non-Newtonian flows.

References - 1

Barnea, D. (1987), 'A unified model for predicting flow-pattern transitions for the whole range of pipe inclinations', *International Journal of Multiphase Flow* **13**(1), 1 – 12. (cited at page 2)

Hewitt, G. F. (2006), 'Joint project on transient multiphase flow and flow assurance: Tmf4 prospectus'. [Online; accessed 1-August-2011].
URL: *http://multiphase.tech.cranfield.ac.uk/docs/TMF4_Prospectus.pdf*
(cited at page 4)

Lam, C. and Bremhorst, K. (1981), 'A modified form of the k-ϵ model for predicting wall turbulence', *Journal of Fluids Engineering, Transactions of the ASME* **103**(3), 456–460. (cited at page 6)

Manolis, I. G. (1995), High Pressure Gas-Liquid Slug Flow, PhD thesis, Department of Chemical Engineering and Chemical Technology, Imperial College of Science, Technology and Medicine, London, UK. (cited at page 6)

Shaha, J. (1999), Phase interactions in transient stratified flow, PhD thesis, Department of Chemical Engineering, Imperial College, London, UK. (cited at page xiii, 2, 3)

Taitel, Y. and Dukler, A. (1976), 'A theoretical approach to the lockhart-martinelli correlation for stratified flow', *International Journal of Multiphase Flow* **2**(5-6), 591 – 595. (cited at page 2, 6)

Chapter 2

Two phase flow modelling

2.1 Introduction

The governing equations describing two-phase flow systems, coupled with accurate numerical resolution techniques, should provide a tool for investigating and predicting the flow condition, with an understanding of limitations and uncertainties in their specifications. However, the most important part of the modelling process was that a proper physical model was built, because inappropriate conceptual numerical models can have large uncertainties that are difficult to quantify, and may lead to results that are significantly different with the physical systems that the researcher seeks to describe.

Of particular interest are the time-dependent phenomena in industry pipelines, operating under a two-phase stratified and slug flow regime. Therefore, the objective is to introduce mathematical two-phase flow models that have the capability of predicting the high viscous flow - especially non-Newtonian fluids.

In this chapter, one dimensional two-phase flow two-fluids model that is implemented in EMAPS code is introduced firstly. Following this, three dimensional two-phase flow model Volume Of Fluids (VOF), which is used to predict the gas-non-Newtonian stratified flow in chapter 6 and gas-non-Newtonian slug flow in chapter 7, will be presented as well.

2.2 One-dimensional two-phase flow model

The main subject of study is concentrated around flows in pipelines, where the fluid motion is mostly on one single dimension. By integrating the equations of motion over a cross section, it is possible to obtain a one-dimensional fluid model. The model investigated in this work is the two-fluid model. The derived version developed by Drew and Segel (1971) and detailed in Drew and Passman (1999) is considered.

2.2.1 Governing equations

Expressions of the ensemble-averaged continuity and momentum equations for isothermal two-phase flow in a pipe with constant diameter, using time-average (Chan and Banerjee, 1981), are given below:

Mass Conservation

$$\frac{\partial}{\partial t}\left(\rho_k \alpha_k\right) + \frac{\partial}{\partial x}\left(\rho_k \alpha_k u_k\right) = \Gamma_k \tag{2.1}$$

Momentum Conservation:

$$\begin{aligned}\frac{\partial}{\partial t}\left(\rho_k \alpha_k u_k\right) + \frac{\partial}{\partial x}\left(\rho_k \alpha_k {u_k}^2\right) = \; & -\alpha_k \frac{\partial P_k}{\partial x} - \Delta P_{ki} \frac{\partial \alpha_k}{\partial x} + \frac{\partial}{\partial x}\left[\alpha_k \left(\tau_k + {\tau_k}^{Re}\right)\right] \\ & + M_{kw} + M_{ki} + \Gamma_k u_{ki} - \rho_k \alpha_k g \sin\beta\end{aligned} \tag{2.2}$$

where the term β is the pipe inclination relative to a horizontal level, as shown in figure 2.1. The variables, ρ_k, P_k, α_k and u_k are the fluid density, pressure, volume fraction and velocity of phase-k, respectively. The parameter, ΔP_{ki} is the pressure correction term, and τ_k and ${\tau_k}^{Re}$ are the viscous stress and the Reynolds stress. The terms, M_{ki} and M_{kw} are the interfacial and wall shear stresses, while Γ_k is the mass transfer term, and u_{ki} is the interfacial velocity for each phase.

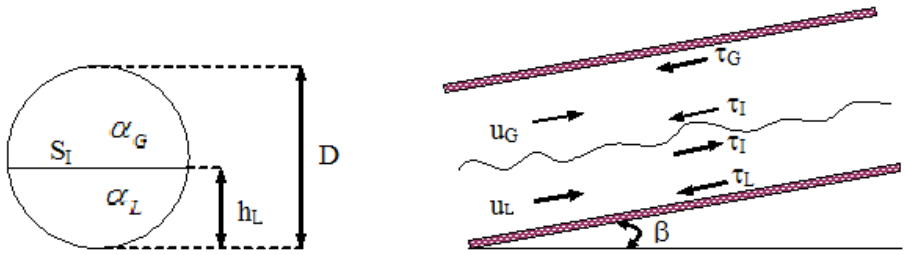

Figure 2.1: Two-phase flow in a circular pipe

2.2.2 Model formulation

The total volume fraction of the two phases is equal to one, and it is assumed that it is an ideal interface, which means there are no mass transfers, no chemical reactions and no phase change. Then, three closure equations are given:

$$\sum_k \alpha_k = 1 \tag{2.3}$$

$$\sum_k \Gamma_k = 0 \tag{2.4}$$

$$\sum_k M_{ki} + \Gamma_k u_{ki} = 0 \tag{2.5}$$

where subscript k takes the value G or L depending on the phase, and **i** indicates to the interfacial term.

Concerning engineering modelling, various assumptions and simplifications have to be made. It is out of reach to solve the momentum equation 2.2 as it is. First, we consider that no mass transfer nor phase change occur in the system, thus $\Gamma_k = 0$, second, non turbulent and inviscid flows are considered, this leads to $\tau_k = 0$ and to $\tau_k^{Re} = 0$. However, viscous and turbulent effects are modelled and represented via source terms M_{ki} and M_{kw}, more precisely via interfacial and wall friction factors as these will be shown in the section 2.2.3.

Dropping the weighted-average from the bulk-phase pressure P_k, the pressure jump between phases and the interface is represented in the non-conservative

term; $\Delta P_{ki} = P_k - P_{ki}$. Modelling and interpreting pressure forces arising from averaged two-phase flow equations are difficult ones. For dispersed flows, using averaging theorem, Prosperetti and Jones (1984) showed that ΔP_{ki} is a consequence of boundary integral along the interfaces. In Drew (1983), it was referred to as the buoyant force. In Sha and Soo (1979) and in Stuhmiller (1977), investigations on the influence of the inter-facial pressure forces on the character of the equations of two-phase flow models and their influence were outlined. For engineering problems, several expressions of this term exist in the literature [Stuhmiller (1977), Soo (1990), Bestion (1990) and Saurel and Abgrall (1999)]. In this work, the derivation given in Taitel and Dukler (1977) and Gu and Guo (2007) is considered. For a system inclined to the horizontal line with an angle β, that component is expressed by

$$\Delta P_{ki} \cdot \frac{\partial \alpha_k}{\partial x} = -\alpha_k \rho_k g cos\beta \cdot \frac{\partial \alpha_k}{\partial x} \tag{2.6}$$

resulting in the momentum exchange interaction due to interface liquid level or gas void gradients $\frac{\partial \alpha_k}{\partial x}$.

The two fluid model shown in the equation 2.1 and 2.2 can be rearranged as follows:

$$\begin{cases} \frac{\partial}{\partial t}(\alpha_G \rho_G) + \frac{\partial}{\partial x}(\alpha_G \rho_G u_G) & = 0 \\ \frac{\partial}{\partial t}(\alpha_L \rho_L) + \frac{\partial}{\partial x}(\alpha_L \rho_L u_L) & = 0 \end{cases} \tag{2.7}$$

$$\begin{cases} \dfrac{\partial}{\partial t}(\alpha_G \rho_G u_G) + \dfrac{\partial}{\partial x}(\alpha_G \rho_G u_G^2 + \alpha_G P_G) & = P_G \cdot \dfrac{\partial \alpha_G}{\partial x} - \alpha_G \rho_G g cos\beta \cdot \dfrac{\partial \alpha_G}{\partial x} + M_i \\ & \quad - M_{GW} - \rho_G \alpha_G g \sin\beta \\ \dfrac{\partial}{\partial t}(\alpha_L \rho_L u_L) + \dfrac{\partial}{\partial x}(\alpha_L \rho_L u_L^2 + \alpha_L P_L) & = P_L \cdot \dfrac{\partial \alpha_L}{\partial x} - \alpha_L \rho_L g cos\beta \cdot \dfrac{\partial \alpha_L}{\partial x} - M_i \\ & \quad - M_{LW} - \rho_L \alpha_L g \sin\beta \end{cases} \tag{2.8}$$

Above, ρ_k, α_k and u_k represent the density, the volume fraction and the velocity of the phase $k = G, L$, while P_k stands for its pressure.

2.2.3 Shear force

There are three shear stresses (M_{GW}, M_{LW}, M_i) involved in the momentum balances for the two-phase flow model; wall shear force represents the stresses acting on each phase at the wall. Different methodologies have been proposed to calculate it, and have been reviewed by Simonic (1992). The wall shear stress is generally based on closure laws derived from fully developed steady state two-phase flows and only express drag and friction forces, and it is usually given as:

$$M_{kw} = T_{kw} = -\frac{\tau_k \cdot S_k}{A} \tag{2.9}$$

where S_k is defined as wetted wall by the phase k, which is given for liquid and gas, respectively:

$$S_L = D(\pi - \cos^{-1}(2\frac{h_L}{D} - 1)) \tag{2.10}$$

$$S_G = \pi D - S_L \tag{2.11}$$

where h_L is the liquid height in the pipe.

In the equation 2.9, τ_k is the wall shear stress of the same phase. The constitutive relation for the wall shear stress is given in terms of the standard wall friction

factor, f_k that was shown as:

$$\tau_k = \frac{1}{2} f_k \rho_k u_k \left| u_k \right| \tag{2.12}$$

In a stratified or annular flow, the interfacial shear stress is defined by Ishii and Mishima (1984), and it is given as:

$$M_i = T_i = -\frac{\tau_{Gi} \cdot S_i}{A} \tag{2.13}$$

where A is the pipe cross-section and S_i is the wetted perimeter of the interface or the gas core, and is defined here:

$$S_i = D\sqrt{1 - (2\frac{h_L}{D} - 1)^2} \tag{2.14}$$

The gas interfacial shear stress, τ_{Gi} , which will be renamed τ_i in the following parts of the thesis, is given in terms of the standard interfacial friction factor as:

$$\tau_i = \frac{1}{2} f_i \rho_G (u_G - u_L) \left| u_G - u_L \right| \tag{2.15}$$

2.2.3.1 Wall friction factor

It is common that single phase fluids wall friction factors are used in the two-phase flow computations. In this section, some useful validated wall friction factors are reviewed.

For fully developed laminar flow in a circular pipe, a simple but famous Hagen-Poiseuille is given by:

$$f = \frac{16}{\mathrm{Re}} \tag{2.16}$$

New correlations have been derived from two-phase studies and have been used in the work of Taitel and Dukler (1976). The expression for the gas wall friction factor is:

$$f_G = c_G \mathrm{Re}_{\mathrm{G}}^{-\mathrm{d_G}} \tag{2.17}$$

where the Reynolds number is defined as

$$\mathrm{Re}_G = \frac{D_G u_G \rho_G}{\mu_G} \tag{2.18}$$

The hydraulic diameter D_G is defined as:

$$D_G = \frac{4A_G}{S_G + S_i} \tag{2.19}$$

The coefficients, c_G and d_G respectively have values of 0.046 and 0.25 if the flow is turbulent ($\mathrm{Re_G} > 2100$), or 16 and 1 if the flow is laminar ($\mathrm{Re_G} \leq 2100$)

The correlation used for calculating the liquid wall friction factor, f_L is derived by Kowalski (1987):

$$f_L = c_L(\alpha_L \mathrm{Re_L})^{-\mathrm{d_L}} \tag{2.20}$$

where c_L and d_L are correlated coefficients, α_L is the liquid holdup and $\mathrm{Re_L}$ is a Reynolds number based on the liquid superficial velocity and the pipe diameter. Kowalski (1987) proposed to use $c_L = 0.263$ and $d_L = 0.5$. Hand (1991) found that these values are not in agreement with his experimental results, and suggested the values 0.062 and 0.139 respectively for c_L and d_L. Srichai (1994) proposed using $c_L = 0.762$, $d_L = 0.562$.

2.2.3.2 Interfacial friction factor

The simplest relation for interfacial friction factor is that proposed by Taitel and Dukler (1976). They suggested taking the interfacial shear stress equal to the gas shear stress for smooth and wavy stratified flow.

$$f_i = f_G \tag{2.21}$$

Andreussi and Persen (1987) proposed an empirical correlation for the interfacial friction factor that is considered to be related to the gas friction factor via the dimensionless Froude number, Fr,

$$\frac{f_\mathrm{i}}{f_G} = \begin{cases} 1.0 & \text{if } Fr \leq 0.36 \\ 1.0 + 29.7 \cdot (Fr - 0.36)^{0.67} \cdot \left(\dfrac{h_L}{D}\right)^{0.2} & \text{if } Fr > 0.36 \end{cases}$$

The dimensionless Froude number Fr for horizontal pipes is given by

$$Fr = u_G \cdot \left(\frac{\rho_G}{\rho_L - \rho_G} \cdot \frac{S_\mathrm{i}}{g \cdot A_G}\right)^{0.5} \tag{2.22}$$

2.2.4 Single pressure model

In the following, incompressible liquid and ideal gas are assumed, and single pressure model (SPM-4) is considered. According to the thermodynamic equation of state (EOS), this model can be described by the following conservation equations:

- Mass Conservation

$$\begin{cases} \dfrac{\partial \rho_G \alpha_G}{\partial t} + \dfrac{\partial \rho_G \alpha_G u_G}{\partial x} = 0 \\ \dfrac{\partial \rho_L \alpha_L}{\partial t} + \dfrac{\partial \rho_L \alpha_L u_L}{\partial x} = 0 \end{cases} \tag{2.23}$$

- Momentum Conservation

$$\begin{cases} \dfrac{\partial \rho_G \alpha_G u_G}{\partial t} + \dfrac{\partial \rho_G \alpha_G u_G^2}{\partial x} = -\alpha_G \dfrac{\partial P}{\partial x} + B_{fG} + T_I + T_{Gw} \\ \dfrac{\partial \rho_L \alpha_L u_L}{\partial t} + \dfrac{\partial \rho_L \alpha_L u_L^2}{\partial x} = -\alpha_L \dfrac{\partial P}{\partial x} - P_c \dfrac{\partial \alpha_L}{\partial x} + B_{fL} - T_I + T_{Lw} \end{cases} \tag{2.24}$$

T_{kw} represents the wall shear stress for a phase k, T_i is the interfacial shear stress, and B_{fk} is the corresponding gravity force and is given as: $\rho_k \alpha_k g \sin\beta$. The gas pressure correction term has been dropped, and P_c is the liquid pressure correction term and is given by $P_c = \alpha_L \rho_L g cos\beta$.

2.2.5 Numerical solver for one-dimensional two-phase flow model

The aim of this section is intimately related to the numerical method in use. Today, there is a wide range of numerical methods that are trusted and reliable for a variety of applications allowed in engineering sciences.

Concerning multiphase flow fields, modelling flow regimes (Stratified, Slug, Bubbly, etc . . .) in horizontal or vertical pipes lead to various conservation laws that are differentiated with diverse source terms. The stiffness, derivability, characteristic time and space of these source terms are major factors in the loss of hyperbolicity, and hence, dictate the choice of adequate numerical schemes to describe appropriately the physics in the model [LeVeque and Yee (1988), LeVeque (1998) and Dumbser et al. (2008)]. In the last three decades, a new class of upwind schemes that are remarkably robust and stable for a variety of problems have been developed - these are named Advection Upstream Splitting Method $AUSM$, initiated by Liou and Steffen (1993) and Wada and Liou (1994). Later, for performing cures to shocks instabilities "carbuncle phenomenon"related to $AUSM$ schemes and in order to solve viscous flows at all speeds, improved versions, $AUSM$-family schemes such as $AUSM^{+}$, $AUSM^{+}-up$, $AUSMDV$, were introduced in Liou (1996) and Liou (2006) and tested in different situations in Tiselj and Petelin (1997), Mary et al. (2000), Evje and Fjelde (2003), Evje and Flatten (2003) and Garcia-Cascales and Paillere (2006), amongst others.

In Evje and Flatten (2003), a hybrid version named $AUSMDV^{*}$ was tested. The authors showed that although this numerical scheme does not offer a high level of robustness for high speed flows. For subsonic flows, as it is the case in slug flows, this scheme is efficient and accurate with reduced computational cost, and is suitable to simulate slow transitions occurring in multiphase flows in pipes. For these reasons, in this work, the $AUSMDV^{*}$ scheme was opted for.

It is common to rewrite the set of equations in 2.7 and 2.8 of the model in compact form.

Let U be the vector of unknown fields, $F(U)$ signifies the flux vector, $H(U)$ the non conservative coupling matrix $H(U)$ and source vector $S(U)$ be the inter-phase and wall frictions term

$$\frac{\partial U}{\partial t}+\frac{\partial F(U)}{\partial x}=H(P)\cdot\frac{\partial U}{\partial x}+S(U,Q) \tag{2.25}$$

The common step to $AUSM$-family schemes is to decompose the flux vector into

convective and to pressure components; $F(U) = F^c(U) + F^P(U)$ or

$$F^c(U) = \begin{pmatrix} \alpha_G\rho_G\cdot u_G \\ \alpha_G\rho_G\cdot u_G^2 \\ \alpha_L\rho_L\cdot u_L \\ \alpha_L\rho_L\cdot u_L^2 \end{pmatrix} \quad \text{and} \quad F^P(U) = \begin{pmatrix} 0 \\ \alpha_G\cdot P \\ 0 \\ \alpha_L\cdot P \end{pmatrix}$$

One starts to construct $AUSMDV^*$ scheme by using the generic form of the convective and pressure flux for each phase k, as follows

$$F_k^c(U) = \begin{pmatrix} \alpha_k\rho_k\cdot u_k \\ \alpha_k\rho_k\cdot u_k^2 \end{pmatrix} \quad \text{and} \quad F^P(U) = \begin{pmatrix} 0 \\ \alpha_k\cdot P \end{pmatrix}$$

In the following, the index k is dropped for simplicity, and the discretisation of the system (2.25) is considered at the cell interfaces $j + 1/2$, one has

$$\begin{aligned} F_{j+1/2}^c &= \begin{pmatrix} (\alpha\rho)_j\cdot\widetilde{u}_j^+ + (\alpha\rho)_{j+1}\cdot\widetilde{u}_{j+1}^- \\ s_f\cdot(\alpha\rho\cdot u^2)_V + (1-s_f)\cdot(\alpha\rho\cdot u^2)_D \end{pmatrix} \\ F_{j+1/2}^P &= \begin{pmatrix} 0 \\ (\alpha P)_j\cdot P_j^+ + (\alpha P)_{j+1}\cdot P_{j+1}^- \end{pmatrix} \end{aligned} \tag{2.26}$$

Indexes $(\alpha\rho\cdot u^2)_V$ and $(\alpha\rho\cdot u^2)_D$ stand for the discretisation of the term $\alpha\rho\cdot u^2$ with $AUSMV$ and $AUSMD$ schemes respectively, see, for example Trepanier et al. (1991), these are given below.

2.2.5.1 Convective flux discretisation

$$\begin{cases} (\alpha\rho\cdot u)_{1/2} &= (\alpha\rho)_j \cdot \widetilde{u}_j^+ + (\alpha\rho)_{j+1} \cdot \widetilde{u}_{j+1}^- \\ (\alpha\rho\cdot u^2)_V &= (\alpha\rho u)_j \cdot \widetilde{u}_j^+ + (\alpha\rho u)_{j+1} \cdot \widetilde{u}_{j+1}^- \\ (\alpha\rho\cdot u^2)_D &= \frac{1}{2}\Big[(\alpha\rho u)_{1/2} \cdot (u_{j+1}+u_j) - |\,(\alpha\rho u)_{1/2}\,| \cdot (u_{j+1}-u_j)\Big] \end{cases} \tag{2.27}$$

The velocities splitting needed in $AUSMDV^*$ are

$$\widetilde{u}_j^+ = \begin{cases} \xi_j \cdot \dfrac{\left(u_j + \widetilde{c}_{1/2}\right)^2}{4} + (1-\xi_j)\cdot \dfrac{(u_j + |u_j|)}{2} & \text{if } u_j \le \widetilde{c}_{1/2} \\ \dfrac{(u_j + |u_j|)}{2} & \text{if } u_j > \widetilde{c}_{1/2} \end{cases}$$

And

$$\widetilde{u}_{j+1}^- = \begin{cases} -\xi_{j+1} \cdot \dfrac{\left(u_{j+1} - \widetilde{c}_{1/2}\right)^2}{4} + (1-\xi_{j+1})\cdot \dfrac{(u_{j+1} - |u_{j+1}|)}{2} & \text{if } u_{j+1} \le \widetilde{c}_{1/2} \\ \dfrac{(u_j - |u_j|)}{2} & \text{if } u_{j+1} > \widetilde{c}_{1/2} \end{cases}$$

while the speed of sound is $\widetilde{c}_{1/2} = max(c_j, c_{j+1})$ and s_f is a switch function that is the function of local volume fraction.

The parameters ξ_j and ξ_{j+1} appearing above are density dependent, these are weighted coefficients that ensure the stability for continuous flow. In our case we used

$$\begin{aligned} \xi_j &= (1-\phi_j)\cdot \frac{(\rho/\alpha)_j}{(\rho/\alpha)_j + (\rho/\alpha)_{j+1}} + \phi_j \\ \xi_{j+1} &= (1-\phi_{j+1})\cdot \frac{(\rho/\alpha)_{j+1}}{(\rho/\alpha)_j + (\rho/\alpha)_{j+1}} + \phi_{j+1} \end{aligned} \tag{2.28}$$

$$\text{with} \quad \phi_j = \left[e^{-\kappa_1\cdot\alpha_g} + e^{-\kappa_2\cdot\alpha_l}\right]_j \quad and \quad s_f = max(\phi_j, \phi_{j+1})$$

Parameters $\kappa_1 = 50, \kappa_2 = 500$ are problem dependent, Wada and Liou (1997) hence adjustable coefficients. The values of κ_1 and κ_2 were validated in our

slug flow cases against experimental data from Manolis (1995), and these results were shown in Loilier (2006). The function ϕ_j is a smooth function that is close to unity in single phase regions. The quantity s_f appears only in the convective flux in the equation 2.26 to express $F^c_{j+1/2}$ ensures a combination between $AUSMV$ and $AUSMD$ fluxes. This is suitable because it keeps a balance between stability and accuracy.

2.2.5.2 Pressure flux discretisation

A similar approach to the one above is performed for the pressure splitting that is based on common speed of sound and is expressed by

$$P_j^+ = \begin{cases} \dfrac{1}{\widetilde{c}_{1/2}} \cdot \left(2 - \dfrac{u_j}{\widetilde{c}_{1/2}}\right) & \text{if } |u_j| \leq \widetilde{c}_{1/2} \\ \dfrac{1}{u_j} & \text{if } |u_j| > \widetilde{c}_{1/2} \end{cases}$$

And

$$P_{j+1}^- = \begin{cases} \dfrac{-1}{\widetilde{c}_{1/2}} \cdot \left(2 + \dfrac{u_{j+1}}{\widetilde{c}_{1/2}}\right) & \text{if } |u_{j+1}| \leq \widetilde{c}_{1/2} \\ \dfrac{1}{u_{j+1}} & \text{if } |u_{j+1}| > \widetilde{c}_{1/2} \end{cases}$$

2.2.5.3 Source terms discretisation

The index k representing the phase is restored; hence, source terms on the right hand side of the system 2.25 are discretised using the following second order spatial centred scheme.

$$\Sigma_k \left(U, Q, P\right)_j = H_k(\widetilde{P}_j, \widetilde{\rho}_j) \cdot \left(\frac{\widehat{Q}_j - \widehat{Q}_{j-1}}{\Delta x}\right)_k + S_k(U_j, Q_j) \tag{2.29}$$

where Δx is the cell size and averaged fields $\widetilde{U}_j$ and $\widehat{Q}_j$ are expressed as

$$\widetilde{U}_j = \frac{U_{j-1} + 2\cdot U_j - U_{j+1}}{4} \quad \text{and} \quad \widehat{Q_j} = \frac{Q_j + Q_{j+1}}{2} \tag{2.30}$$

$$Q_k = \begin{pmatrix} 1 \\ \\ \alpha_k \end{pmatrix}, \qquad S_k(U,Q) = \begin{pmatrix} 0 \\ \\ \pm\tau_i \cdot S_i - \tau_{kw} \cdot S_{kw} - \rho_k \cdot g sin\beta \end{pmatrix}$$

and the coupling sub-matrix $\quad H_k(P,\rho) = \begin{pmatrix} 0 & 0 \\ 0 & P_k - \rho_k \cdot g cos\beta \end{pmatrix}$

2.2.5.4 $AUSMDV^*$ numerical scheme

Collecting different discretised components in 2.25, the form of advancing the solution in time internals $t \in [t_n, t_{n+1}]$ with a time step Δt

$$\begin{aligned} U_{kj}^{n+1} &= U_{kj}^n - \frac{\Delta t}{\Delta x} \cdot \left[(F_{j+1/2}^c - F_{j-1/2}^c) + (F_{j+1/2}^P - F_{j-1/2}^P) \right]_k \\ &+ \Delta t \cdot \Sigma_k \left(U_j, Q_j, P_j \right) \end{aligned} \tag{2.31}$$

2.3 Three-dimensional two-phase flow model

Because of license problems, Ansys FLUENT was used to simulate the gas-non-Newtonian fluid two-phase flow in the present work. There are three main models to resolve a gas/liquid two-phase flow in Fluent: The Volume Of Fluid (VOF) model, the mixture model and the Eulerian model. It was mentioned in the Fluent user manual (ANSYS-Fluent Inc, 2008), for stratified and slug flows, the VOF model is advisable because it is the simplest and fastest one. In the present work, three-dimensional two-phase flow model Volume Of Fluid (VOF) in Ansys Fluent was used to simulate the gas-non-Newtonian fluid flow in stratified and slug regime, respectively in chapter 6 and chapter 7. In this

section, a description of Computational Fluid Dynamics (CFD) multiphase flow VOF model, turbulence model and discretisation will be presented.

2.3.1 VOF Model in Ansys FLUENT

The VOF formulation relies on the fact that two or more phases are not interpenetrating. For each additional phase that is added to the model, a variable is introduced: the volume fraction of the phase in the computational cell. The fields for all variables and properties are shared by the phases and represent volume-averaged values, as long as the volume fraction of each of the phases is known at each location.

2.3.1.1 Limitations of VOF method

Volume of fluid method is the simplest approach for multiphase flow that is implemented in CFD FLUENT software. It is a single fluid model in a sense that it considers momentum equation and turbulence transport only for mixture. Velocity, density, viscosity and turbulence of the mixture are averaged fields via volume fractions of individual phases. It is clear that at high densities or viscosities or velocities ratio; jumps in the material properties across the interface of the phases are smoothed. This lead to generation of diffusion and dispersion that cause the loss of the sharpness of the interface and therefore substantial error in the estimation of the surface tension and also erroneous calculation of shear stress transfer across the interface. The transport of the turbulence is also affected and diffused in the vicinity of the interface. In our case, the gas phase is turbulent while the shear thinning liquid is laminar. These in turn affect the shape of the interface. The use of a high resolution grid at the interface is a technique that helps to limit these effects, but it is computationally costly for compressible fluids especially in three dimensions.

Adaptive grid local refinement around the interface could be considered in the gas-liquid wavy and slug regime. In our case, the gas phase is turbulent while the shear thinning liquid is laminar. These in turn affect the shape of the interface.

The use of locally adaptive grid refinement around the interface can achieve a better prediction for the gas-liquid interface, with minimal transitional region and numerical diffusion(Theodorakakos and Bergeles (2004) and Malik et al. (2007)).

In the stratified flow, Fabre et al. (1987) showed a different behaviour in the liquid phase compared to normal shear flows in the interface. Interfacial correlations can be considered in order to enhance the VOF model. Issa (1988) used low and high Re $k-\epsilon$ models. The liquid pool height is obtained by fitting a special curvilinear mesh that fills the circular cross-section and has one chord denoting the interface position. Therefore only straight interfaces can be obtained and only steady solutions can be considered. Subsequently, Issa (1988) imposed mass fluxes and chose the position of the chord as to minimise the residuals in mass flux constraints. Egorov (2004) (Ansys CFX) and Ghorai and Nigam (2006) (Fluent) both used high Reynolds number models to simulate long channels. It is reported that the standard models in these commercial packages fail to predict the experimental data correctly. Then Ghorai and Nigam (2006) modified the profiles around the interface by imposing log-layers. This is only of limited applicability as a logarithmic profile does not necessarily emerge at the interface (see Biberg (2007)). Egorov (2004) included an additional dissipation term in the equation for specific dissipation.

2.3.1.2 Governing equations in VOF model

The governing equations behind the model are recalled. The volume of fluid (VOF) model was developed by Nichols et al. (1981) and it was implemented in several commercial fluid dynamics packages - and for detailed implementation and the description of turbulence modelling, please refer to the user manual for ANSYS-Fluent Inc (2008). The model considers a compressible gas and is augmented with the standard $k-\epsilon$ model to account for the presence of turbulence. Below, the continuity equation for liquid phase volume fraction α_L is shown

$$\partial_t \alpha_L + \nabla(\alpha_L \cdot \vec{u}) = 0 \tag{2.32}$$

The momentum equation below uses a single velocity field $\vec{u}$ for both phases and acts on the mixture density that is $\rho = \alpha_G \cdot \rho_G + \alpha_L \cdot \rho_L$, and where the mixture viscosity $\mu = \alpha_G \cdot \mu_G + \alpha_L \cdot \mu_L$ is similarly approximated by the barycentric relation of partial viscosities.

$$\partial_t \rho \cdot \vec{u} + \vec{\nabla}(\rho \cdot \vec{u} \cdot \vec{u} + p) = \vec{\nabla}(\mu \cdot (\nabla \cdot \vec{u} + \nabla \cdot \vec{u}^T)) + \rho \cdot \vec{g} + \vec{F} \tag{2.33}$$

The pressure, p is the pressure jump at the interface, and the last term, F in the right hand side represents the interfacial surface tension between phases and can be expressed as

$$F = \sum_{pairsij, i<j} \sigma_{ij} \frac{\alpha_i \rho_i \kappa_j \nabla \alpha_j + \alpha_j \rho_j \kappa_i \nabla \alpha_i}{\frac{1}{2}(\rho_i + \rho_j)} \tag{2.34}$$

where i and j are the indices representing two phases, σ_{ij} is the surface tension coefficient, and κ_i is the curvature at the interface where the surface tension is calculated.

If there are only two phases present, $\kappa_i = -\kappa_j$ and $\nabla \alpha_i = -\nabla \alpha_j$, this leads to

$$F = \sigma_{ij} \frac{\rho \kappa_i \nabla \alpha_i}{\frac{1}{2}(\rho_i + \rho_j)} \tag{2.35}$$

where $\rho = \sum_q \alpha_q \rho_q$ is the volume-averaged density.

2.3.2 Turbulence model

Several approaches are available for including turbulence in the Navier-Stokes equations. Most of these involve a process of time-averaging the conservation equations. When turbulence is included, the transported fields, for example velocity, are assumed to be the sum of an equilibrium and a fluctuating component $u = U + u'$.

Regarding the time averaging concept over a long period of time, many cycles of fluctuations stipulate that the only remaining terms are those that involve the product of two or more fluctuating components. Thus, the momentum equation

(Navier-Stokes) above becomes the so-called Reynolds-Averaged Navier-Stokes, or RANS equation for momentum.

$$\partial_t(\rho\cdot\vec{U}) + \vec{\nabla}(\rho\cdot\vec{U}\cdot\vec{U} + p) = \vec{\nabla}(\mu\cdot(\nabla\cdot\vec{U} + \nabla\cdot\vec{U}^T)) - \nabla(\rho\cdot<\vec{u'}\cdot\vec{u'}>) + \rho\cdot\vec{g} + \vec{F} \tag{2.36}$$

The new terms involving $<\vec{u'}\cdot\vec{u'}>$ are called the Reynolds stresses. The brackets indicate that these terms are time-averaged, these are new unknowns and need to be related to the other variables; thus, the turbulent kinetic energy k and ϵ the rate of dissipation of the turbulent energy are expressed by

$$\begin{aligned} k &= \frac{1}{2}\cdot<\vec{u'}\cdot\vec{u'}> \\ \epsilon &= \frac{\mu}{2}\cdot(<\nabla\cdot\vec{u'} + \nabla\cdot\vec{u'}^T>)^2 \end{aligned} \tag{2.37}$$

A variety of assumption on these terms leads to the availability of many turbulence models.

The $k-\epsilon$ model is part of a family of two-equation models, for which two additional transport equations must be solved in order to compute the Reynolds stresses. This model is commonly used in mixing applications. It is stable computationally and is applicable to various turbulent flows, and it has been largely adopted by the fluid modelling community for many years. It is semi-empirical, based in a large part on observations of mostly high Reynolds number flows. The two transport equations that need to be solved for this model are for the kinetic energy of turbulence, k, and the rate of dissipation of turbulence, ϵ.

$$\partial_t(\rho\cdot k) + \vec{\nabla}(\rho\cdot\vec{U}\cdot k) = \vec{\nabla}((\mu + \frac{\mu_t}{\sigma_k})\cdot\nabla\cdot k) + G_k - \rho\cdot\epsilon \tag{2.38}$$

$$\partial_t(\rho\cdot\epsilon) + \vec{\nabla}(\rho\cdot\vec{U}\cdot\epsilon) = \vec{\nabla}((\mu + \frac{\mu_t}{\sigma_\epsilon})\cdot\nabla\cdot\epsilon) + C_1\cdot f_1\cdot\frac{\epsilon}{k}\cdot G_k - C_2\cdot f_2\cdot\rho\cdot\frac{\epsilon^2}{k} \tag{2.39}$$

The quantities C_1, C_2, σ_ϵ and σ_k are empirical constants. The turbulent viscosity,

μ_t is derived from k and ϵ and it involves an experimental constant, C_μ that is approximately 0.09, and is given below with the apparent viscosity

$$\mu_t = \rho \cdot C_\mu \cdot f_\mu \cdot \frac{k^2}{\epsilon}$$

The quantity G_k, appearing in both equations, is a volumetric source or generation term of turbulence, and is a function of turbulent viscosity and velocity gradients.

$$G_k = \mu_t \cdot (\nabla \cdot \vec{U} + \nabla \cdot \vec{U}^T) \cdot \nabla \cdot \vec{U}^T \tag{2.40}$$

To summarise the solution process for the $k - \epsilon$ model, transport equations are solved for the turbulent kinetic energy and dissipation rate. The solutions for k and ϵ are used to compute the turbulent viscosity μ_t. Using the results for μ_t and k, the Reynolds stresses can be computed by substitution into the momentum equations. Once the momentum equations have been solved, the new velocity components are used to update the source terms on the right hand side, μ, f_1, f_2, f_μ, G_k, and the process is repeated.

2.3.3 Discretisation and method of solution

In order to numerically solve the system of partial and ordinary differential equations, discretisation of the equations has been carried out using Finite Volume Methods with an algebraic segregated solver and co-located grid arrangement, as implemented in Ansys FLUENT (ANSYS-Fluent Inc, 2008). Since FLUENT uses a segregated solver, the continuity and momentum equations need to be linked. The Pressure Implicit with Splitting of Operators (PISO) algorithm, which was introduced by Issa (1986), was used here to handle unsteady flow problems because of its good performance in finding a fast converged solution. PISO is a pressure-velocity calculation procedure that involves one predictor step and two corrector steps. It is strongly recommended in FLUENT to solve the unsteady flow problems. More detail about this numerical scheme was introduced in ANSYS-Fluent Inc (2008), and it will not be repeated in this thesis.

2.4 Summary

In order to solve two-phase flow problems, the one-dimensional two-fluids models which were used in this thesis are presented in this chapter. Single pressure two-fluids model (SPM-4), used in EMAPS codes to solve the slug flow condition in the next two chapters, was also introduced.

Closure claws for one-dimensional two-phase flow were thoroughly detailed. To formulate an accurate mathematical model for two-phase flows, accurate estimations of wall friction factors as well as the gas-liquid interfacial friction factor are required and reviewed. Numerical methods are required in order to solve the set of deferential equations, and $AUSMDV^*$ numerical scheme is chosen here because it is efficient and accurate, with reduced computational cost, and is suitable to simulate slow transitions occurring in multi-phase flows in pipes .

Additionally, VOF model was presented in this chapter in order to solve three dimensional two-phase flow later. Turbulence must be considered in the numerical simulation since, in slug flow, the velocity in the gas phase can easily be turbulent. Therefore, $k - \epsilon$ turbulence model is reviewed. It was also mentioned that PISO is the numerical method that we used in this work to solve the VOF model.

References - 2

Andreussi, P. and Persen, L. (1987), 'Stratified gas-liquid flow in downwardly inclined pipes', *International Journal of Multiphase Flow* **13**(4), 565 – 575. (cited at page 15)

ANSYS-Fluent Inc (2008), *Fluent 12.0 User Manual*, Lebanon, N. H. (cited at page 21, 23, 26)

Bestion, D. (1990), 'The physical closure laws in the cathare code', *Nuclear Engineering and Design* **124**(3), 229 – 245. (cited at page 12)

Biberg, D. (2007), 'A mathematical model for two-phase stratified turbulent duct flow', *Multiphase Science and Technology* **19**(1), 1–48. (cited at page 23)

Chan, A. M. C. and Banerjee, S. (1981), 'Refilling and rewetting of a hot horizontal tube: Part ii—structure of a two-fluid model', *Journal of Heat Transfer* **103**(2), 287–292. (cited at page 10)

Drew, D. A. (1983), 'Mathematical modeling of two-phase flow', *Annual Review of Fluid Mechanics* **15**(1), 261–291. (cited at page 12)

Drew, D. A. and Segel, L. A. (1971), 'Averaged equations for two-phase flows', *Studdies in Applied Mathematics* **L3**, 205 – 231. (cited at page 10)

Drew, D. and Passman, S. (1999), *Theory of multicomponent fluids*, Applied mathematical sciences, Springer. (cited at page 10)

Dumbser, M., Enaux, C. and Toro, E. F. (2008), 'Finite volume schemes of very high order of accuracy for stiff hyperbolic balance laws', *Journal of Computational Physics* **227**(8), 3971 – 4001. (cited at page 17)

Egorov, Y. (2004), Contact condensation in stratified stream-water flow, Technical report, ECORA. (cited at page 23)

Evje, S. and Fjelde, K. K. (2003), 'On a rough ausm scheme for a one-dimensional two-phase model', *Computers & Fluids* **32**(10), 1497 – 1530. (cited at page 17)

Evje, S. and Flatten, T. (2003), 'Hybrid flux-splitting schemes for a common two-fluid model', *Journal of Computational Physics* **192**(1), 175 – 210. (cited at page 17)

Fabre, J., Masbernat, L. and Suzanne, C. (1987), 'Experimental data set no. 7: Stratified flow, part i: Local structure', *Multiphase Science and Technology* **3**(1-4), 285–301. (cited at page 23)

Garcia-Cascales, J. and Paillere, H. (2006), 'Application of ausm schemes to multi-dimensional compressible two-phase flow problems', *Nuclear Engineering and Design* **236**(12), 1225 – 1239. (cited at page 17)

Ghorai, S. and Nigam, K. (2006), 'Cfd modeling of flow profiles and interfacial phenomena in two-phase flow in pipes', *Chemical Engineering and Processing* **45**(1), 55–65. (cited at page 23)

Gu, H. and Guo, L. (2007), 'Stability of stratified gas-liquid flow in horizontal and near horizontal pipes', *Chinese Journal of Chemical Engineering* **15**(5), 619 – 625. (cited at page 12)

Hand, N. P. (1991), Gas-Liquid Co-current Flow in a Horizontal Pipeline, PhD thesis, The Queen's University of Belfast, Belfast, UK. (cited at page 15)

Ishii, M. and Mishima, K. (1984), 'Two-fluid model and hydrodynamic constitutive relations', *Nuclear Engineering and Design* **82**(2-3), 107 – 126. (cited at page 14)

Issa, R. (1988), 'Prediction of turbulent, stratified, two-phase flow in inclined pipes and channels', *International Journal of Multiphase Flow* **14**(2), 141 – 154. (cited at page 23)

Issa, R. I. (1986), 'Solution of the implicitly discretised fluid flow equations by operator-splitting', *Journal of Computational Physics* **62**, 40–65. (cited at page 26)

Kowalski, J. E. (1987), 'Wall and interfacial shear stress in stratified flow in a horizontal pipe', *AIChE Journal* **33**(2), 274–281. (cited at page 15)

LeVeque, R. J. (1998), 'Balancing source terms and flux gradients in high-resolution godunov methods: The quasi-steady wave-propagation algorithm', *Journal of Computational Physics* **146**(1), 346 – 365. (cited at page 17)

LeVeque, R. J. and Yee, H. C. (1988), A study of numerical methods for hyperbolic conservation laws with stiff source terms, NASA Technical Memorandum 100075, Department of Mathematics, University of Washington, Seattle. (cited at page 17)

Liou, M.-S. (1996), 'A sequel to ausm: Ausm+', *Journal of Computational Physics* **129**(2), 364 – 382. (cited at page 17)

Liou, M.-S. (2006), 'A sequel to ausm, part ii: Ausm+-up for all speeds', *Journal of Computational Physics* **214**(1), 137 – 170. (cited at page 17)

Liou, M.-S. and Steffen, C. J. (1993), 'A new flux splitting scheme', *Journal of Computational Physics* **107**(1), 23 – 39. (cited at page 17)

Loilier, P. (2006), Numerical simulation of two-phase gas-liquid flows in inclined and vertical pipelines, PhD thesis, Cranfield University, UK. (cited at page 20)

Malik, M., Fan, E. S.-C. and Bussmann, M. (2007), 'Adaptive vof with curvature-based refinement', *International Journal for Numerical Methods in Fluids* **55**(7), 693–712.
URL: *http://dx.doi.org/10.1002/fld.1490* (cited at page 23)

Manolis, I. G. (1995), High Pressure Gas-Liquid Slug Flow, PhD thesis, Department of Chemical Engineering and Chemical Technology, Imperial College of Science, Technology and Medicine, London, UK. (cited at page 20)

Mary, I., Sagaut, P. and Deville, M. (2000), 'An algorithm for unsteady viscous flows at all speeds', *International Journal for Numerical Methods in Fluids* **34**(5), 371–401. (cited at page 17)

Nichols, B., Hirt, C. and Hotchkiss, R. (1981), 'A fractional volume of fluid method for free boundary dynamics', **141**, 304–309. (cited at page 23)

Prosperetti, A. and Jones, A. (1984), 'Pressure forces in disperse two-phase flow', *International Journal of Multiphase Flow* **10**(4), 425 – 440. (cited at page 12)

Saurel, R. and Abgrall, R. (1999), 'A multiphase godunov method for compressible multifluid and multiphase flows', *Journal of Computational Physics* **150**(2), 425 – 467. (cited at page 12)

Sha, W. T. and Soo, S. L. (1979), 'On the effect of $p\nabla\alpha$ term in multiphase mechanics', *International Journal of Multiphase Flow* **5**(2), 153 – 158. (cited at page 12)

Simonic, A. (1992), 'Matrix groups with positive spectra', *Linear Algebra and its Applications* **173**, 57 – 76. (cited at page 13)

Soo, S. L. (1990), *Multiphase fluid dynamics*, Butterworth-Heinemann. (cited at page 12)

Srichai, S. (1994), High pressure separated two phase flow, PhD thesis, Department of Chemical Engineering, Imperial College, London, UK. (cited at page 15)

Stuhmiller, J. (1977), 'The influence of interfacial pressure forces on the character of two-phase flow model equations', *International Journal of Multiphase Flow* **3**(6), 551 – 560. (cited at page 12)

Taitel, Y. and Dukler, A. (1977), 'A model for slug frequency during gas-liquid flow in horizontal and near horizontal pipes', *International Journal of Multiphase Flow* **3**(6), 585 – 596. (cited at page 12)

Taitel, Y. and Dukler, A. E. (1976), 'A model for predicting flow regime transitions in horizontal and near horizontal gas-liquid flow', *AIChE Journal* **22**(1), 47–55. (cited at page 14, 15)

Theodorakakos, A. and Bergeles, G. (2004), 'Simulation of sharp gasvliquid interface using vof method and adaptive grid local refinement around the interface', *International Journal for Numerical Methods in Fluids* **45**(4), 421–439.
URL: *http://dx.doi.org/10.1002/fld.706* (cited at page 23)

Tiselj, I. and Petelin, S. (1997), 'Modelling of two-phase flow with second-order accurate scheme', *Journal of Computational Physics* **136**(2), 503 – 521. (cited at page 17)

Trepanier, J., Reggio, M., Zhang, H. and Camarero, R. (1991), 'A finite-volume method for the euler equations on arbitrary lagrangian-eulerian grids', *Computers & Fluids* **20**(4), 399 – 409. (cited at page 18)

Wada, Y. and Liou, M.-S. (1994), A flux splitting scheme with high-resolution and robustness for discontinuities, *in* D. G. Fletcher, ed., 'Presented at the 32nd Aerospace Sciences Meeting and Exhibit, Reno, NV, 10-13 Jan. 1994; sponsored by AIAA', pp. 10–13. (cited at page 17)

Wada, Y. and Liou, M.-S. (1997), 'An accurate and robust flux splitting scheme for shock and contact discontinuities', *SIAM J. Sci. Comput.* **18**(3), 633 – 657. (cited at page 19)

Chapter 3

Gas/water slug flow modelling

3.1 Introduction

Two-phase flows in pipelines have been studied in the past few decades, due to their wide range of applications. The most common two-phase flow regime is called slug flow, in which the liquid flows intermittently along the pipes in a concentrated mass, called a slug. It takes place naturally inside pipes and occurs over a wide range of flow parameters.

The development of slug of liquid in two-phase pipelines is a major and expensive headache for the oil producer. The arrival of a slug at production or processing equipment is unwelcome to say the least. Severe slugging can even cause platform trips and plant shutdown. Slug flow plays an important role in a variety of industrial applications. Understanding slug flow becomes more important in pipe design and flow insurance.

3.2 Chapter outline

This chapter begins by reviewing the slug frequency, slug length and two phase friction factor correlations. Then, a slug case is validated using the two-fluid model, which has already been introduced in the chapter 2, followed by a

comparison of the slug frequency and slug length, with results calculated from different correlations.

3.3 Slug characteristics

Slug flow is composed of a sequence of liquid slugs and large stratified gas/liquid zones, as shown in the figure 3.1. A slug unit is defined as the combination of liquid film region and slug body region:

$$l_U = l_f + l_s \tag{3.1}$$

where l_U is the slug unit length, l_f is the length of the liquid film region, and l_s is the length of the slug body region.

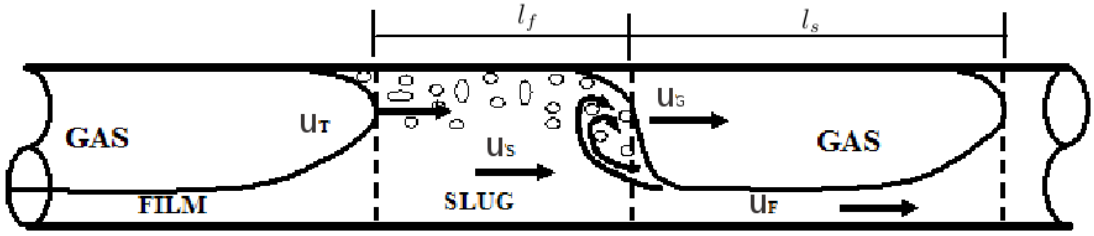

Figure 3.1: Slug unit model

3.4 Slug frequency

The liquid slug length and the slug frequency are closely related properties that are often used interchangeably. Slug frequency, ω_s, is defined as the average number of the slug units passing a fixed observer in the system over a unit of time, and increases with liquid flow rate and decreasing pipe diameter in Taitel and Dukler (1977).

$$\omega_s = \frac{N_t}{t} \tag{3.2}$$

where N_t is the number of slugs passing in time t.
Despite many slug frequency data reported in the literature [Omgba-Essama (2004), Manolis (1995)], it is still one of the least reliably modelled parameters. This is due to the statistical nature of the slug flow pattern, and the frequency parameter reflects the intermittency of the flow. However, due to its inclusion as a closure relation in many slug flow models, it is important to accurately predict this parameter.

3.4.1 Gregory and Scott (1969) correlation

Slug frequency had been measured for the system carbon dioxide-water flow in a horizontal pipe with a diameter of $19mm$. The measuring point was located approximately at 300 pipe diameters after the inlet. Based on measured values and combining the results with those obtained by Hubbard (1965), Gregory and Scott (1969) proposed one of the first slug frequency correlations expressions, and it was given as:

$$\omega_S = 0.0226[\frac{u_{SL}}{gD}(\frac{19.75}{u_m} + u_m)] \tag{3.3}$$

where mixture velocity $u_m = u_{SL} + u_{SG}$.

3.4.2 Greskovish and Shrier (1971) correlation

Greskovish and Shrier (1971) subsequently re-write this expression using the Froude number based on the mixture velocity u_m to obtain the following relationship:

$$\omega_S = 0.0226[\lambda_L(\frac{2.02}{D} + Fr_M^2)]^{1.2} \tag{3.4}$$

where λ_L is the the no-slip input liquid quality, defined as:

$$\lambda_L = \frac{u_{SL}}{u_{SL} + u_{SG}} \tag{3.5}$$

and Fr_m is the mixture Froude number, defined as:

$$Fr_m = \frac{u_m}{\sqrt{gD}} \tag{3.6}$$

However, based on data obtained from a $45mm$ internal diameter line, they suggested that the diameter effect is not properly taken into account by this expression. Therefore, they recommended using their graphical correlation instead for cases involving large diameters.

3.4.3 Heywood and Richardson (1979) correlation

Heywood and Richardson (1979) determined the probability density function and the power spectral densities of the holdup, through using the gamma densitometer for air-water flow in a $42mm$ diameter pipe. From these functions, they estimated the average slug frequency. By subsequently using a similar expression to Greskovish and Shrier (1971), they proposed that the slug frequency may be obtained by:

$$\omega_S = 0.0434[\lambda_L(\frac{2.02}{D} + Fr_m^2)]^{1.02} \tag{3.7}$$

3.4.4 Manolis (1995) correlation

Through studying the effect of pressure on the slug frequency, Manolis (1995) performed a large number of experiments on a $78mm$ diameter pipe for both air-water and air oil data at various system pressures, and he proposed the following expression to calculate the slug frequency:

$$\omega_S = \frac{u_{SG}}{D}(0.0363\frac{Fr_L}{\hat{F}r_G}\frac{Z_L}{Eo^{0.2}})^n \tag{3.8}$$

where n is a function of the viscosity number and is given by:

$$n = \frac{N_f}{260 + 0.85N_f} \tag{3.9}$$

the Eotvös number is define as:

$$Eo = gD^2 \frac{|\rho_g - \rho_l|}{\sigma} \tag{3.10}$$

while the viscosity number is expressed as:

$$N_f = \frac{D^{1.5}\sqrt{\rho_l \, |\rho_g - \rho_l| \, g}}{\sigma} \tag{3.11}$$

The liquid Froude number Fr_L and the modified gas Froude number $\hat{F}r_G$ are given by:

$$Fr_L = \frac{u_{SL}}{\sqrt{gD}}, \quad \hat{F}r_G = \frac{u_{SG}}{\sqrt{gD(\rho_l/|\rho_g - \rho_l|)}} \tag{3.12}$$

The parameter, Z_L is defined as the ratio of the liquid inertia to the liquid pressure drop. Its expression is:

$$Z_L = \left[\frac{\frac{\rho_L u_{SL}^2}{2D}}{\left(\frac{\mathrm{d}P}{\mathrm{d}x}\right)_L} \right]^{0.5} = \left[\frac{1}{4C_f \mathrm{Re}_{SL}^{-d}} \right]^{0.5} \tag{3.13}$$

The liquid Reynolds number is based on the liquid superficial velocity. C_f and d are respectively the friction factor constant coefficient and the exponent; they depend on the nature of the flow, laminar or turbulent. Hence, they are defined as:

$$\begin{cases} C_f = 0.046, \ d = 0.2, & if \ \mathrm{Re_L} < 2000 \\ C_f = 16, \ d = 1, & otherwise \end{cases} \tag{3.14}$$

3.4.5 Taitel and Dukler (1977) phenomenological models

A mechanistic model was built to predict the slug frequency by Taitel and Dukler (1977) for horizontal and near horizontal pipes. It is assumed that slug frequency is given by the inverse of the time taken for the film to rebuild its level and form a slug. The time interval was calculated using one-dimensional mass and momentum balances for each phase.

Hale (1994) modified this model by proposing a non-correlational approach to predict the slug frequency, in which the processes of slug initiation, growth and decay were take into account and had good agreement with his experiments.

3.5 Slug length

The liquid slug length, (l_s), which is introduced in figure 2, is an important design parameter for hydrocarbon pipelines. It is closely related to the slug frequency, but appears to be preferred in most slug flow models. In what follows, a brief review of the most common correlations for slug length in the literature is presented.

Table 3.1: Average slug lengths in horizontal pipes

Reference	$D(mm)$	Fluids	Average slug length
Dukler and Hubbard (1975)	38	air/water	$12 \sim 30D$
Nicholson et al. (1978)	25,51	air/light oil	$\sim 30D$
Gregory et al. (1978)	25,51	air/light oil	$\sim 30D$
Barnea and Brauner (1985)	Theory	Theory	32D
Andreussi et al. (1988)	50	air/water	22D
Nydal et al. (1992)	53,90	air/water	$15 \sim 20D$ (53 mm pipe) $12 \sim 30D$ (90 mm pipe)
Manolis (1995)	78	air/water air/oil	$10 \sim 25D$

Dukler and Hubbard (1975) and later Dukler et al. (1985) found that the minimum stable slug length increases with the slug Reynolds number, and from experiments on a $38mm$ horizontal pipe, they observed that the slug lengths are approximately $12 \sim 30D$ and appear to be relatively insensitive to the gas

and liquid flowrates. Other researchers have confirmed the same observations as indicated in table 3.1. Hence, constant values are generally used for the average slug length in slug flow models.

It can be summarised from the above reviews that in horizontal and nearly horizontal slug flow, the slug body length is dependent only on the pipe diameter, D (and not on physical properties or inlet velocities) and is:

$$l_S \approx 10D \sim 30D \tag{3.15}$$

3.6 Simulations

The two-phase flow of air and water in a horizontal pipe is simulated in EMAPS, using the two-fluids single pressure model (SPM-4), which were presented in chapter 2. The specifications are summarised as:

- Pipe length:$38m$
- Diameter: $78mm$
- Operating fluids: air and water ($\rho_G = 1.16kg/m^3$, $\rho_L = 1000kg/m^3$)
- Flow temperature: $T = 298$K
- Outlet flow pressure: $1bar$

The atmospheric properties of air and water are used (the outlet pressure is fixed to atmospheric). The initial conditions correspond to a flat stratified flow, and the boundary conditions at the pipe inlet are the same as with the initial input data. The only outflow boundary condition for the outlet is constant atmospheric pressure (1 bar). The rest of the conservative variables are considered as an open

boundary. Two tests were shown in the following. The inlet superficial velocities for the first test case are given as:

$$\begin{cases} u_{SG} = 4.64m \cdot s^{-1} \\ u_{SL} = 0.61m \cdot s^{-1} \\ \alpha_L^0 = 0.5 \end{cases} \tag{3.16}$$

The result obtained with the single pressure model is shown in the following.

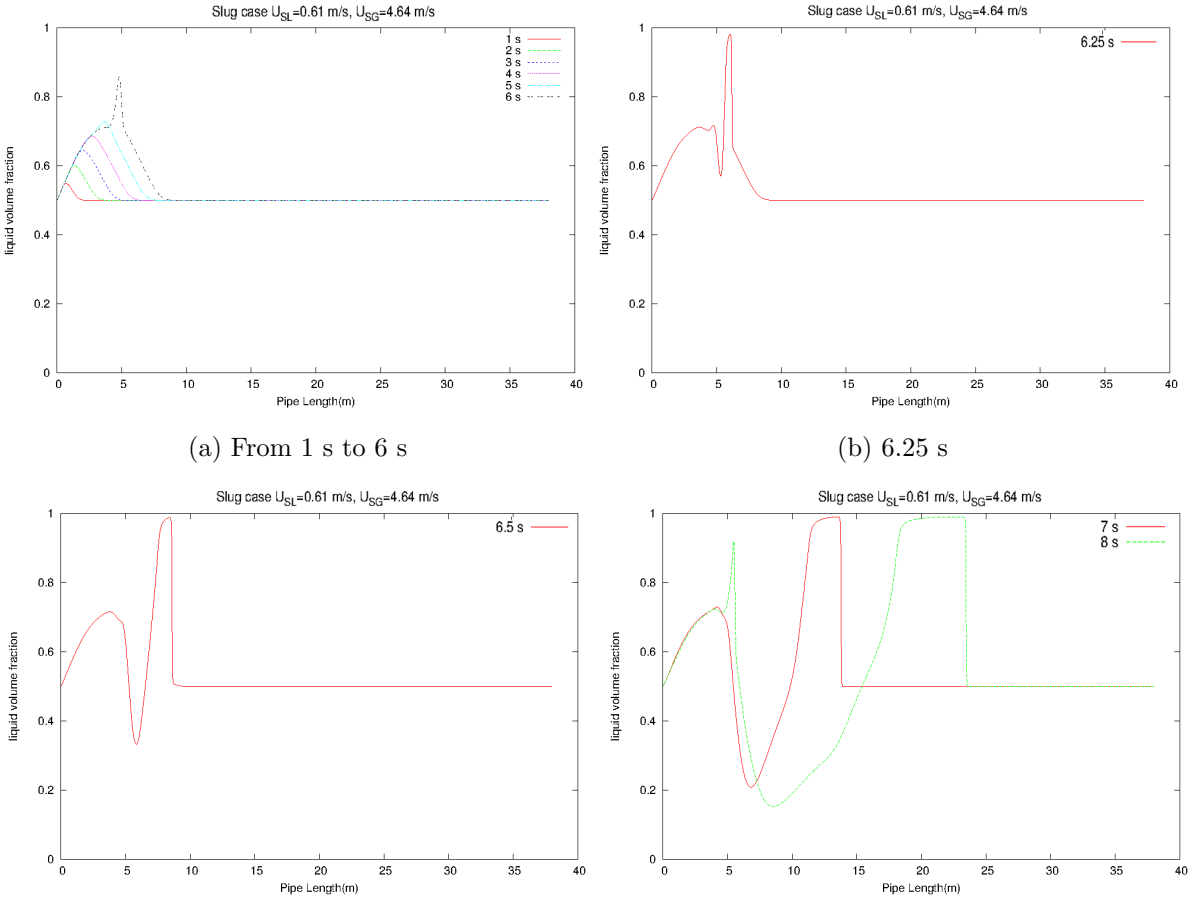

(a) From 1 s to 6 s

(b) 6.25 s

(c) 6.5 s

(d) 7 s and 8 s

Figure 3.2: Slug wave initiation - Liquid holdup profiles

As figure 3.2 indicates, the slug occurs in the pipe inlet. The wavy grows firstly, and then it transform from wavy to slug. The slug length for the first grows along the pipe, but the following slug length will be smaller.

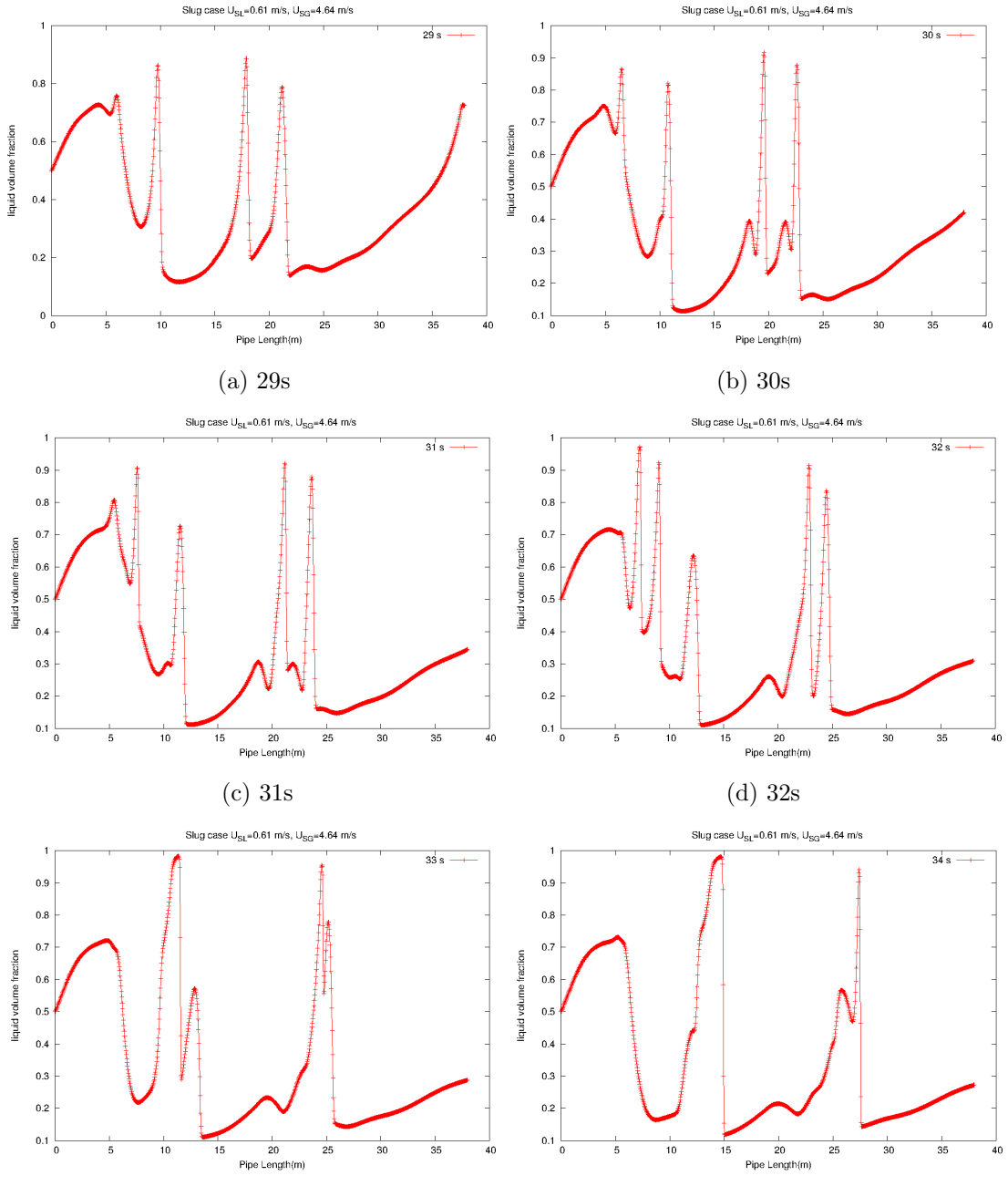

(a) 29s

(b) 30s

(c) 31s

(d) 32s

(e) 33s

(f) 34s

Figure 3.3: Slug growth and propagation - Liquid holdup profiles

The liquid holdup traces over the pipe length are shown in figure 3.3 for different times in the simulations. It can be seen from the figures 3.3 that slug wave initialises and grows in the inlet of the pipe, and it also clearly indicated that the big slug merged the wavy and small slug, which is in front of the big slug, to form a longer slug. This merging process continues until the liquid slugs are long enough to be stable, and slug length tends to increase as it moves from the entrance section to the end of the pipe.

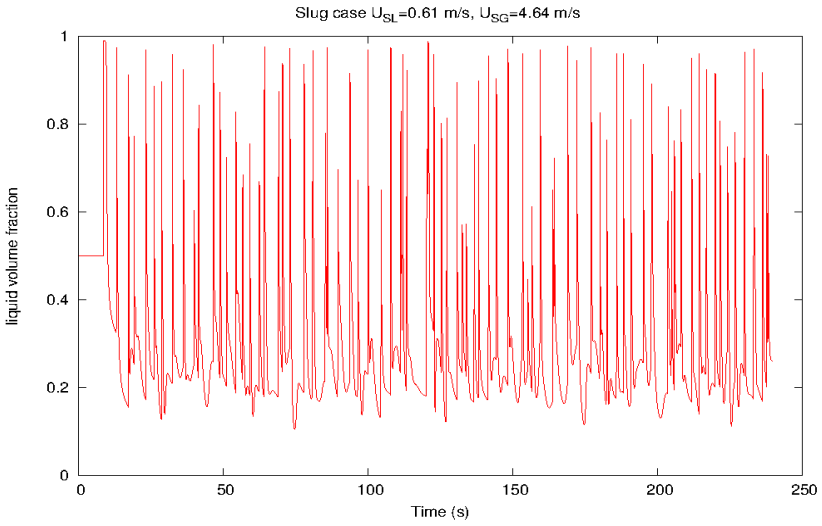

Figure 3.4: Time trace of the liquid holdup at $29m$.

The time trace of the liquid holdup at $29m$ from the pipe inlet is shown in figure 3.4, and it is regarded as a slug when the liquid holdup is greater than 0.8. Slug frequency strongly depends on the mesh size, and this part will be discussed in the next chapter. Slug frequency obtained from figure 3.4 compared with the correlations that have been reviewed already. The result is displayed in table 3.2.

The slug lengths range for EMAPS result is 0.376 to 1.285 m, except for the very first slug which was measured at 3.83m. The average slug length is approximately $10.5D$, and numerical result calculated by EMAPS gives a underestimation for slug length compared with the correlations listed in table 3.1. The calculated slug frequency using the two fluids single pressure model is in fair agreement with the correlations obtained by Gregory and Scott (1969) and Manolis (1995).

Table 3.2: Comparison of predicted slug characteristics with experimental correlation

Characteristic	EMAPS	Gregory and Scott (1969)	Manolis (1995)	Heywood and Richardson (1979)
Slug frequency (1/s)	0.2179	0.24	0.22	0.32
Average slug length	10.2D	-	$10 \sim 25D$	-

3.7 Conclusion

In this chapter, the two-phase slug flow was introduced, and many slug frequency and slug length correlations were reviewed. The present chapter also illustrated the slug flow in the EMAPS framework, using a two fluids single pressure model (SPM-4), and average slug length and slug frequency, calculated from simulations, were compared with the correlations. A good agreement of slug frequency was obtained compared with Manolis (1995) correlation. Slug lengths simulated by SPM-4 are smaller than the correlation.

References - 3

Andreussi, P., Paglianti, A., Vatistas, N., Minervini, A. and Bendiksen, K. (1988), Analysis of slug flow in near horizontal and horizontal pipes, *in* 'European Two-Phase Flow Group Meeting', Brussels, Belgium, p. B2. (cited at page 40)

Barnea, D. and Brauner, N. (1985), 'Holdup of the liquid slug in two phase intermittent flow', *International Journal of Multiphase Flow* **11**(1), 43 – 49. (cited at page 40)

Dukler, A. E. and Hubbard, M. G. (1975), 'A model for gas-liquid slug flow in horizontal and near horizontal tubes', *Industrial & Engineering Chemistry Fundamentals* **14**(4), 337 – 347. (cited at page 40)

Dukler, A. E., Maron, D. M. and Brauner, N. (1985), 'A physical model for predicting the minimum stable slug length', *Chemical Engineering Science* **40**(8), 1379 – 1385. (cited at page 40)

Gregory, G. A. and Scott, D. S. (1969), 'Correlation of liquid slug velocity and frequency in horizontal co-current gas-liquid slug flow', *AIChE Journal* **15**(6), 933 – 935. (cited at page viii, 37, 44, 45)

Gregory, G., Nicholson, M. and Aziz, K. (1978), 'Correlation of the liquid volume fraction in the slug for horizontal gas-liquid slug flow', *International Journal of Multiphase Flow* **4**(1), 33 – 39. (cited at page 40)

Greskovish, E. J. and Shrier, A. L. (1971), 'Pressure drop and holdup in horizontal slug flow', *AIChE Journal* **17**(5), 1214 – 1219. (cited at page viii, 37, 38)

Hale, C. P. (1994), Slug formation, growth and decay in gas-liquid glows, PhD thesis, Department of Chemical Engineering and Chemical Technology, Imperial College of Science, Technology and Medicine, London, UK. (cited at page 39)

Heywood, N. I. and Richardson, J. F. (1979), 'Slug flow of air - water mixtures in a horizontal pipe: Determination of liquid holdup by γ-ray absorption', *Chemical Engineering Science* **34**(1), 17 – 30. (cited at page viii, 38, 45)

Hubbard, M. (1965), An analysis of horizontal gas-liquid slug flow, PhD thesis, University of Houston. (cited at page 37)

Manolis, I. G. (1995), High Pressure Gas-Liquid Slug Flow, PhD thesis, Department of Chemical Engineering and Chemical Technology, Imperial College of Science, Technology and Medicine, London, UK. (cited at page viii, 37, 38, 40, 44, 45)

Nicholson, M. K., Aziz, K. and Gregory, G. A. (1978), 'Intermittent two phase flow in horizontal pipes: Predictive models', *The Canadian Journal of Chemical Engineering* **56**(6), 653 – 663. (cited at page 40)

Nydal, O., Pintus, S. and Andreussi, P. (1992), 'Statistical characterization of slug flow in horizontal pipes', *International Journal of Multiphase Flow* **18**(3), 439 – 453. (cited at page 40)

Omgba-Essama, C. (2004), Numerical Modelling of Transient Gas-Liquid Flows (Application to Stratified and Slug Flow Regimes, PhD thesis, Cranfield University, UK. (cited at page 37)

Taitel, Y. and Dukler, A. (1977), 'A model for slug frequency during gas-liquid flow in horizontal and near horizontal pipes', *International Journal of Multiphase Flow* **3**(6), 585 – 596. (cited at page viii, 36, 39)

Chapter 4

Adaptive mesh refinement(AMR) for gas/water slug flow

4.1 Introduction

The difficulties of modelling of multiphase flows in long pipes reside in capturing profiles of interfaces and discontinuities associated with them, along distances that can exceed several kilometres. These irregularities result from flow conditions combined with the nature of the topology of the terrain. Slugs and waves that characterise such systems undergo sudden mixing of phases and abrupt accelerations and decelerations. It follows that flow characteristics vary sharply from one region to another. Simulations of these problems and their complexities can be approached by reformulating the models in one space dimension. This approach attracted the attention of many researchers for obvious reasons [Lezeau and Thompson (1998), Omgba-Essama (2004), Sussman et al. (1999)], in addition to its applicability and capability to predict flow regimes and global phase's behaviour in extended configurations. For modelling industrial multiphase flows, various formulations use multi-fluid equations. These formulations are based on multi-field transport equations of interpenetrating media, and their physical closure relationships (constitutive laws) rely on numerous algebraic relations to account for inter-facial momenta and energies phases transfer.

The volume-averaged conservation laws resulting from these procedures require constitutive relations for closure. For engineering problems, the majority of these relations are algebraic, express inter-phases friction factors and phase pipes interaction, and are estimated from experimental measurements - these are Reynolds numbers, pipe diameter, smoothness and roughness dependent. Beside these empirical correlations, geometrical relations have to be performed in order to calculate phase heights, wetted perimeters and hydraulic diameters. For these reasons, simulations of two phase flows at an industrial scale keep causing problems regarding the CPU time consumption and precision.

In this work, an isothermal two fluid model is used to simulate the slug flow regime in long pipes with accidental topology. I implemented an adaptive mesh refinement method with Kelvin-Helmholtz criterion in order to keep execution time within an acceptable interval, plus a reasonable accuracy concerning the prediction of the flow distribution and behaviour along the system.

4.2 Adaptive mesh refinement (AMR)

The adaptive mesh refinement technique is now a mature approach, since it was pioneered by Pereyra and Sewell (1974), Oliger (1979), Berger and Oliger (1984), Berger and Colella (1989), Quirk (1991), Sussman et al. (1999) and many others. It is widely associated to transient problems involving ideal or real interfaces, see Fuster et al. (2009), Zuzio and Estivalezes (2011), to shock waves in multi-material media Nourgaliev et al. (2005) and Sambasivan and UdayKumar (2010), for example, to systems transitioning from a metastable state to another, see Provatas et al. (1999), Beckett et al. (2001) - for instance, phase transitions take place and materials are submitted to large gradients in confined regions.

The AMR technique refines the numerical solution of the systems (2.31) in space and time. The technique used here, Berger and Colella (1989), Quirk (1991), is based on a hierarchy of grids ranging from coarsest, labelled level zero $l_0 = 0$, to finest, labelled $l = l_{max}$. These grids are genuinely nested by mean so that the union of grids at level l is contained in the union of grids at level $(l-1)$ for

$0 \leq l \leq l_{max}$, except at physical boundaries where the cells level $(l-1)$ are large to contain the cells level l.

Each level has a given resolution. The refinement ratio between successive level, r is constant and even; $r = \dfrac{\Delta x_{l+1}}{\Delta_{x_l}} = ... = \dfrac{\Delta x_1}{\Delta x_0}$. In order to fulfil the stability condition ($CFL < 1$), the time step must be cycled, thus $r = \dfrac{\Delta t_l}{\Delta t_{l-1}}$.

The idea of the process of this automatic grid refinement is to adapt a computational grid to an evolving flow solution. The adaptation process will be divided into two operations. In the first, the regions that have to be refined will be identified and flagged through the following error estimation. Then, a refined mesh will be created in a higher level to cover this patch. This adaptive mesh refinement algorithm refines not only the space of the mesh, but also the time step of the simulation. Smaller time steps are taken on the finer grids than on the coarse grids. This process of adaptive mesh refinement is repeatedly working as the simulation evolves. More detail about data structure and automatic grid refinement process about using this criterion can be found in Omgba-Essama (2004). Here, two error estimation criteria were used to test the slug flow cases.

4.2.1 Gradient error criterion

In this work, Lezeau and Thompson (1998) the type of gradient detector was chosen to start with. This gradient error estimation was depicted in the following: the average gradient is figured out for each half of each patch k which belongs to level l.

$$Grad_{l,k,left} = \sqrt{\frac{\sum_{j=1}^{M} (U_{2,j} - U_{1,j})^2 + \sum_{i=3}^{N_k/2} \sum_{j=1}^{M} (U_{i,j} - U_{i-2,j})^2}{M \times N_k/2}}$$

$$Grad_{l,k,right} = \sqrt{\frac{\sum_{i=N_k/2+1}^{N_k} \sum_{j=1}^{M} (U_{i,j} - U_{i-2,j})^2 + \sum_{j=1}^{M} (U_{N_k,j} - U_{N_k-1,j})^2}{M \times N_k/2}} \tag{4.1}$$

where N_k is the number of cells in patch k, and M is the number of equation of system solved. In present work, M is 4 when single pressure model (SPM4) is used.

A half patch on level l will be flagged for refinement if its average gradient $Grad$ is greater than or equal to the following threshold:

$$t_l = \left(\frac{\sum_{k=1}^{L_p} Grad^{\gamma}_{l,k,left} + Grad^{\gamma}_{l,k,right}}{2L_p} \right)^{(\frac{1}{2})} \tag{4.2}$$

where L_p is the total number of sub-patches in level l.

4.2.2 Gradient error criterion coupled with Taitel-Dukler Kelvin-Helmholtz criterion

Taitel and Dukler (1976) studied wave growth on a smooth stratified layer in a horizontal channel, and derived a stability criterion Taitel-Dukler Kelvin-Helmholtz (TD KH) criterion to locate the transition between stratified and slug flow. This criterion is shown here:

$$u_G > (1 - K_{TD}) \sqrt{\frac{(\rho_L - \rho_G) g \cos\beta}{\rho_G} \frac{A_G}{dA_L/dh_L}} \tag{4.3}$$

$$K_{TD} = \left(1 - \frac{h_L}{D}\right) \tag{4.4}$$

The following express can be obtained through to move all of term to left hand side in equation 4.3:

$$u_G - (1 - \frac{h_L}{D}) \sqrt{\frac{(\rho_L - \rho_G) g \cos\beta}{\rho_G} \frac{A_G}{dA_L/dh_L}} > 0 \tag{4.5}$$

Equation 4.3 can locate the transition between stratified and slug flow since it was satisfied.

4.3 Hydrodynamic slug cases

Numerical simulations are performed with initial and boundary conditions corresponding to data from Manolis (1995). In these experiments, various flow rates of air/water in $38m$ horizontal pipe and diameter $D = 0.078m$ at atmospheric pressure were analysed. Here, the test cases are dealt with.

Pipe geometry and fluids properties are shown in the table 4.1, while initial conditions for concerned cases are specified in the

Table 4.1: Cases references and air-water physical properties

Case reference	Air density kg/m^3	Water density kg/m^3	Temperature K	Pressure Bar
22	1.25	998.4	292.5	1.034
36	1.23	998.2	293.5	1.024
37	1.02	998.4	292.5	1.020

Gas and water inlet superficial velocities are depicted in table 4.2, and water volume fractions ,α_l, correspond to the numerical input.

4.3.1 Transition to slug flow regime

Barnea and Taitel (1994) performed a linear Kelvin-Helmholtz (KH) analysis to study the onset of instability for both inviscid Kelvin-Helmholtz (IKH) and viscous Kelvin-Helmholtz (VKH) flow, using the two-fluid model. The criteria they found are:

Table 4.2: Initial conditions at the inlet s and water superficial velocity and liquid holdup

Case reference	Mixture flow rate m/s	Air flow rate m/s	Water flow rate m/s	$\alpha_L^{equilibrium}$ in %
22	4.54	4.016	0.519	67.0
36	2.07	1.548	0.519	80.8
37	3.67	3.135	0.534	71.5

$$(u_G - u_L) \leq K\sqrt{\frac{(\rho_L - \rho_G)g\cos\beta}{\rho_G\rho_L}(\rho_G\alpha_L + \rho_L\alpha_G)\frac{A}{dA_L/dh_L}} \tag{4.6}$$

where for the inviscid case the factor $K = 1$, and for the viscous case:

$$K = K_V = \sqrt{1 - \frac{(C_v - C_{iv})^2}{\frac{\rho_L - \rho_G}{\rho_L/\alpha_L - \rho_G/\alpha_G}g\cos\beta\frac{A}{dA_L/dh_L}}} \tag{4.7}$$

and the critical wave velocities from the viscid and inviscous stability analyses are C_v and C_{iv}, respectively.

After comparing K_{TD}, which is shown in the equation 4.3, with K_V in the equation 4.7, it was shown in Barnea and Taitel (1994) that K_{TD} and K_V are almost identical which was shown in figure 4.1 when the liquid viscosity is $1cP$, which corresponds to very similar transitional lines on the $u_{SL} - u_{SG}$ map. In the present work, K_{TD} will be used here rather than K_V, since the present work will focus on the gas water ($\mu = 1cP$) two phase slug flow.

It can be seen in figure 4.2 that these three cases are within the slug flow region, in which they are above the Taitel & Dukler Kelvin-Helmholtz line for transition from stratified to slug flow, and more precisely, they are all below the inviscid

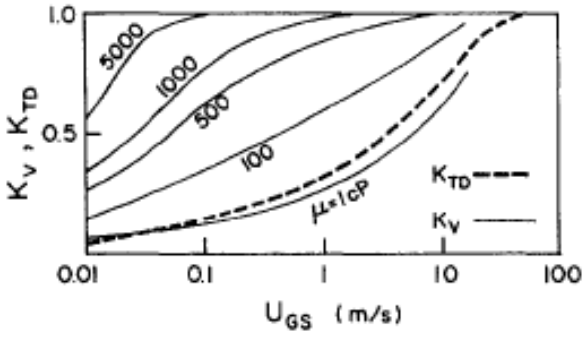

Figure 4.1: The influence of liquid viscosity on the coefficients K_{TD} and K_V. Air-liquid, atmospheric pressure, horizontal pipe, $D = 5\ cm$ (Barnea and Taitel, 1994)

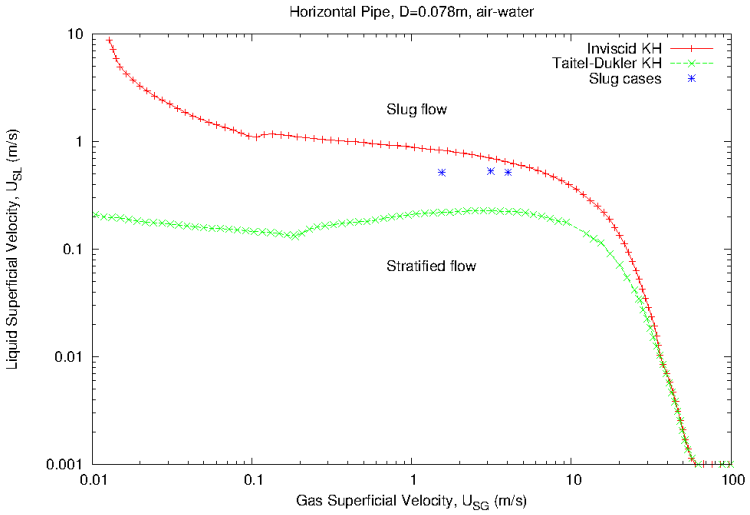

Figure 4.2: Taitel and Dukler (1976) & inviscid Kelvin-Helmholtz transitions from stratified to slug flow

Kelvin-Helmholtz line, which is also the limit of stability of the model (Louaked et al., 2003). The velocity above the inviscid Kelvin-Helmholtz line will result in an ill-posed problem [Taitel and Dukler (1976), Barnea (1991)]. A system with the velocity between the IKH and VKH limits leads to real characteristics, and this system will be well-posed [Barnea (1991), Issa and Kempf (2003)].

4.3.2 Slug frequency

In this section, we present a series of computations that were completed in order to evaluate slug frequencies dependency on mesh size in uniform meshes. In gures 4.3, horizontal dashed lines represent experimental measurement of slug frequencies obtained Manolis (1995). It can be clearly seen that the slug frequency is a function of mesh size, and the slug frequencies of all of these three slug cases are both mesh dependent and they are converged to the experimental slug frequency.

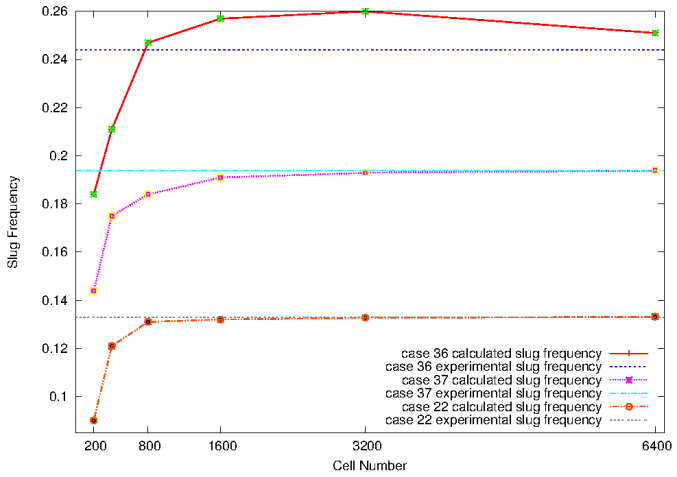

Figure 4.3: Comparison of experimental slug frequency with calculated slug frequency as function of mesh size

It can be seen from figure 4.3 that the finer the grid is, the better the quality of numerical simulation. However, it is too expensive to generate uniform fine grids every where in the pipe computationally, especially in long industrial pipelines. So, more computing resources should be focused on steep gradients, shocks and discontinuities, especially on where the slug is. The number of nodes per unit of length is not required to be the same everywhere. Adaptive mesh refinement will be used to handle such kinds of flows.

4.4 Evaluation result

4.4.1 Verification result using gradient error criterion

Figure 4.4 are the time evolution of the liquid holdup with adaptive grid, using gradient error criterion that is equation 4.1. It can be seen from figure 4.4, the highest level was put where the slug zone is, and the highest level is moved with the slug.

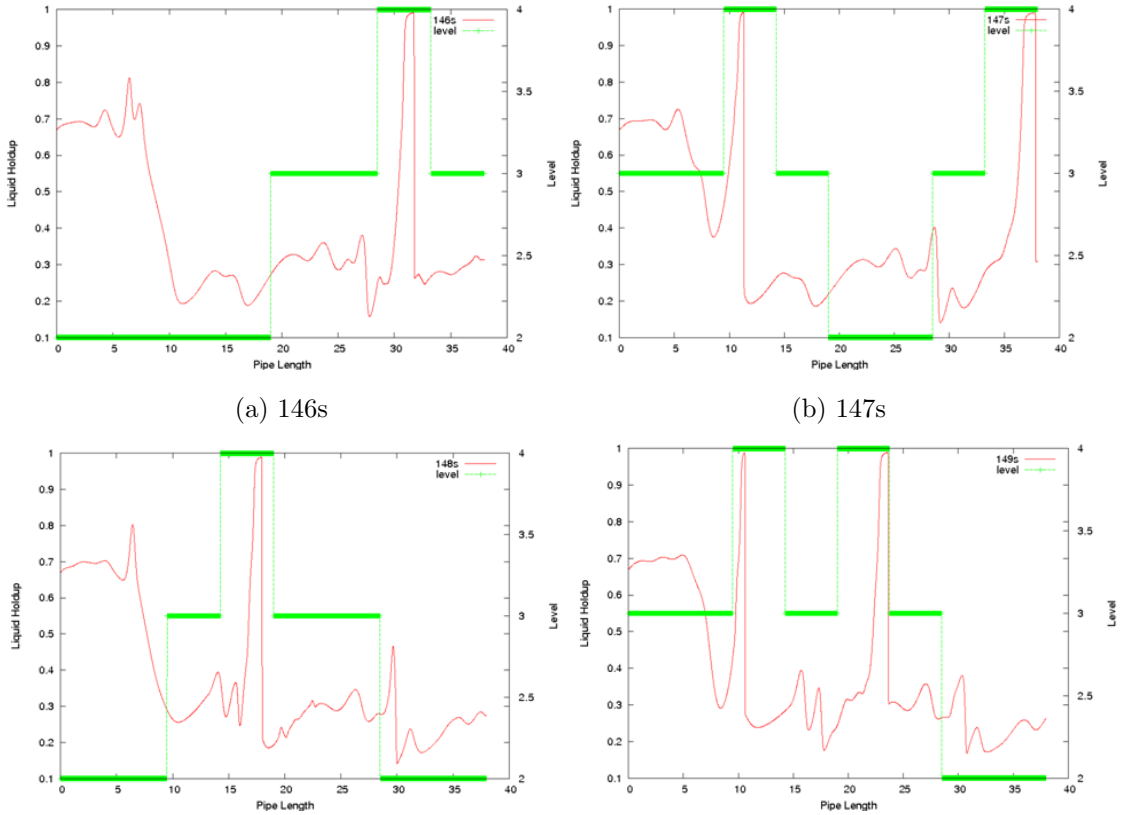

(a) 146s (b) 147s

(c) 148s (d) 149s

Figure 4.4: Time evolution of the liquid holdup with adaptive grid using gradient error criterion

Table 4.3 shows the execution time for the integration of slug case 22 after 240 seconds flow time. It is clearly seen that the adaptive mesh refinement method significantly accelerates the computation compared to fine uniform grid.

Comparing the slug frequency calculated by the uniform and AMR methods, the slug frequency is overestimated for the AMR method and less accurate than the uniform.

Table 4.3: Running time and slug frequency for different grid types and levels for slug case 22 using gradient error criterion

Level of Refinement (Based on 200 cells)	Cells of Uniform	Timings (s)		Speed-up	Slug Frequency	
		Uniform	AMR		Uniform	AMR
1	200	365.45s	-	-	0.09	-
2	400	27 m45s	14m53s	1.93	0.121	0.116
3	800	105m27s	47m8s	2.23	0.131	0.141
4	1600	6h56m18s	134m58s	3.1	0.1326	0.142
5	3200	15h23m06s	3h12m24s	4.9	0.1327	0.142
6	6400	37h52m14s	5h47m35s	6.2	0.1332	0.144

4.4.2 Validation result using gradient error criterion coupled with Taitel-Dukler Kelvin-Helmholtz criterion

Adaptive mesh refinement using gradient error criterion lacks of ability of dealing with the slug cases. In this section, these three Manolis (1995) slug cases and one slug case with long and complex geometry pipe will be validated using the gradient error criterion coupled with Taitel-Dukler Kelvin-Helmholtz criterion. The main purpose is to validate this error estimate criterion and compare the result with the one with a uniform grid.

Time evolution of the liquid holdup (left label) and Taitel-Dukler Kelvin-Helmholtz results (right label) were plotted here in figure 4.5. It is clearly

shown that they have a similar shape - and the line that equation 4.5 equals to zero was plotted as well in figure 4.5. This line means that the flow is in the slug regime or will transit from stratified to slug regime if the liquid holdup value is above it. It can be seen, except in the slug body, that the inlet zone is also quite important and is not stable, and so a new slug will generate from there. Therefore, this area should be refined as well. However, the gradient error criterion does not detect this part - that is why the result for slug case 22 was not good when only the gradient error criterion was used as an indication for the AMR error estimation.

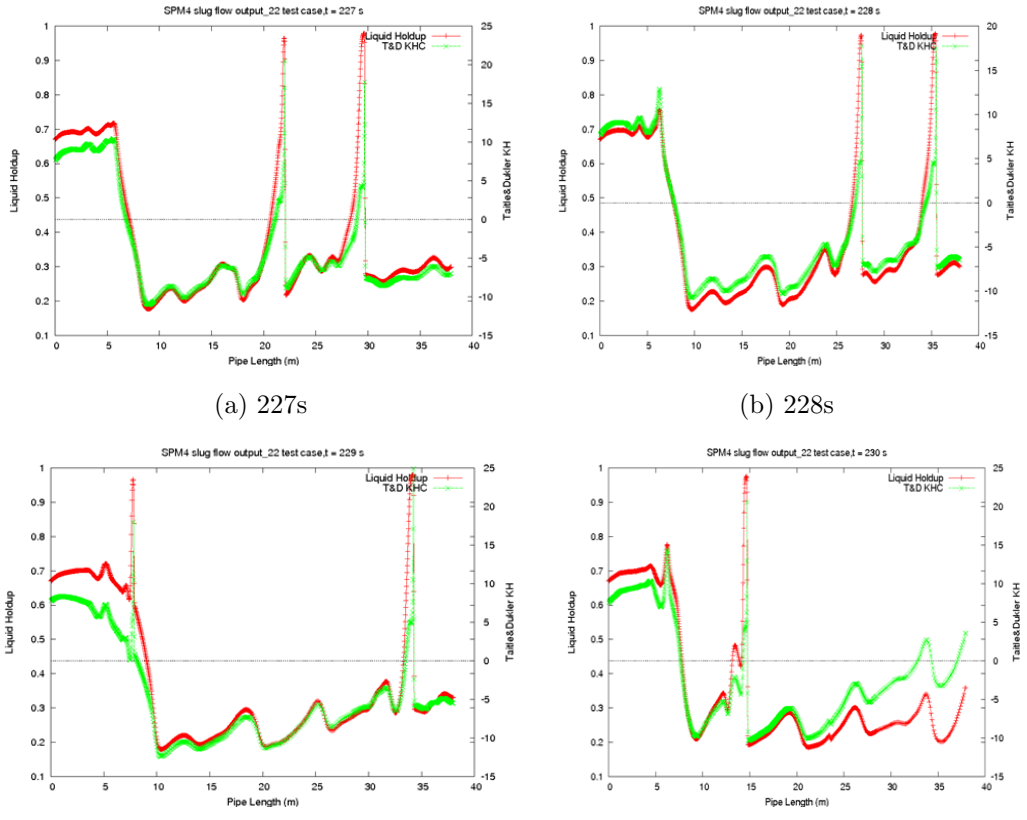

(a) 227s (b) 228s

(c) 229s (d) 230s

Figure 4.5: Time evolution of the liquid holdup with Taitel-Dukler Kelvin-Helmholtz criterion

Here, slug case 22 was validated with new error estimation criterion, and its time evolution of the liquid holdup with adaptive grid was displayed in the figure 4.6.

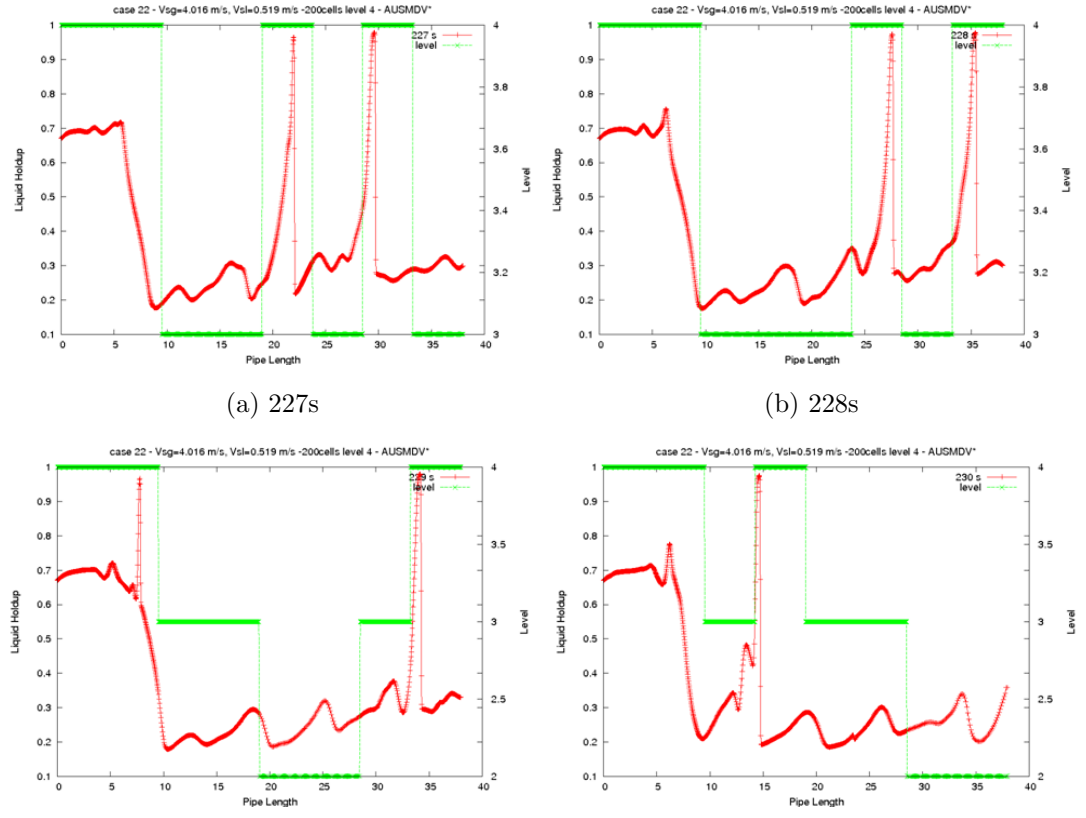

(a) 227s (b) 228s

(c) 229s (d) 230s

Figure 4.6: Time evolution of the liquid holdup with adaptive grid (Slug case 22, gradient error criterion coupled with Taitel & Dukler Kelvin-Helmholtz criterion)

It can be seen from figure 4.6 that the finest grids were located in the steep gradients where the slug is, and also was put in the inlet of the pipe where the flow is in the transition from stratified to slug flow. The slug frequency and running time of the simulation for case 22 were compared here with those obtained with a uniform grid, as shown in table 4.4. Compared with the slug frequency in table 4.3, the slug frequency computed with the new coupled error estimation criterion is more accurate. However, it can be seen that more running time was used because more regions were refined when this new criterion was adopted. Differences of the running time for different levels using different criterion was

compared in table 4.5, it can be seen that the difference of the running time is less when the high level was used.

Table 4.4: Running time and slug frequency for different grid types and levels for slug case 22 using coupled error estimation criterion

Level of Refinement (Based on 200 cells)	Cells of Uniform	Timings (s)		Speed-up	Slug Frequency	
		Uniform	AMR		Uniform	AMR
1	200	365.45s	-	-	0.09	-
2	400	27m45s	21m39s	1.28	0.121	0.121
3	800	105m27s	65m45s	1.6	0.131	0.1263
4	1600	6h56m18s	182m50s	2.28	0.132	0.132
5	3200	15h23m06s	4h15m29s	3.61	0.1327	0.133
6	6400	37h52m14s	7h28m48s	5.08	0.1332	0.1335

Table 4.5: Comparison of Running time for different levels for slug case 22 using gradient error criterion with coupled error estimation criterion

Level of Refinement (Based on 200 cells)	Timings (s)		Difference
	Gradient error	Coupled	
2	14m53s	21m39s	30.8%
3	47m8s	65m45s	27.9%
4	134m58s	182m50s	26.1%
5	3h12m24s	4h15m29s	24.6%
6	5h47m35s	7h28m48s	22.6%

The results for Manolis (1995) case 36 and 37 are shown in tables 4.6 and

4.7 separately. These tables show that the the computed frequencies are in good agreement with the experimental measurements, more significantly, the performances gained in the computational times were about 5 times faster compared to computational times needed when uniform meshes were used.

Table 4.6: Running time and slug frequency for different grid types and levels for slug case 36 using coupled error estimation criterion

Level of Refinement (Based on 200 cells)	Cells of Uniform	Timings (s)		Speed-up	Slug Frequency	
		Uniform	AMR		Uniform	AMR
1	200	305.114s	-	-	0.184	-
2	400	23m57s	18m55s	1.26	0.211	0.201
3	800	79m29s	52m48s	1.52	0.247	0.240
4	1600	5h17m38s	148m32s	2.14	0.257	0.248
5	3200	12h43m37s	3h40m26s	3.40	0. 260	0.252
6	6400	29h16m52s	5h56m06s	4.91	0.251	0.245

Table 4.7: Running time and slug frequency for different grid types and levels for slug case 37 using coupled error estimation criterion

Level of Refinement (Based on 200 cells)	Cells of Uniform	Timings (s)		Speed-up	Slug Frequency	
		Uniform	AMR		Uniform	AMR
1	200	409.1215s	-	-	0.144	-
2	400	28m40s	22m19s	1.31	0.175	0.170
3	800	94m7s	55m38s	1.69	0.184	0.175
4	1600	6h15m32s	160m5s	2.35	0.191	0.19
5	3200	19h09m48s	4h57m40s	3.81	0.193	0.192
6	6400	44h21m46s	8h16m18s	5.45	0.194	0.193

4.4.3 Effect of different criterion on refinement

Figure 4.7 showed the liquid holdup profile that was captured at 29m in case 22. The slug frequency that was put in the figure 4.3 can be calculated from figure 4.7.

Figure 4.8 shows the liquid holdup, along with flow time, at a location 29 meters from the inlet of the pipe, the whole pipe being 38 meters, using gradient error criterion that is equation 4.1. Comparing figure 4.8 with figure 4.7, it can be seen that the liquid holdup in figure 4.8 is quite uniform, and some small waves disappeared compared with figure 4.7. There must be some regions which are quite important, but they were not refined because of this gradient error criterion, which produced quite good results for the other two-phase cases, such as faucet, wave growth and stratified flow which is reported in Omgba-Essama (2004), Jia (2007) and Appendix A.

Now, more attention should be focused on figure 4.9 in which the slug was not uniform any more compared with figure 4.8. Figure 4.9 depicts the same spectrum when the error gradient in conjunction with Kelvin-Helmholtz is applied. The

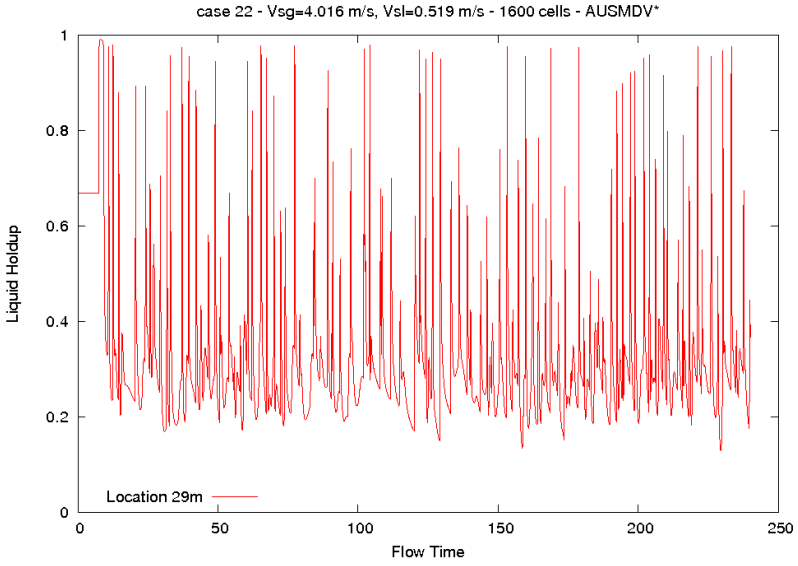

Figure 4.7: Time trace of liquid holdup at 29m from inlet (1600 uniform cells)

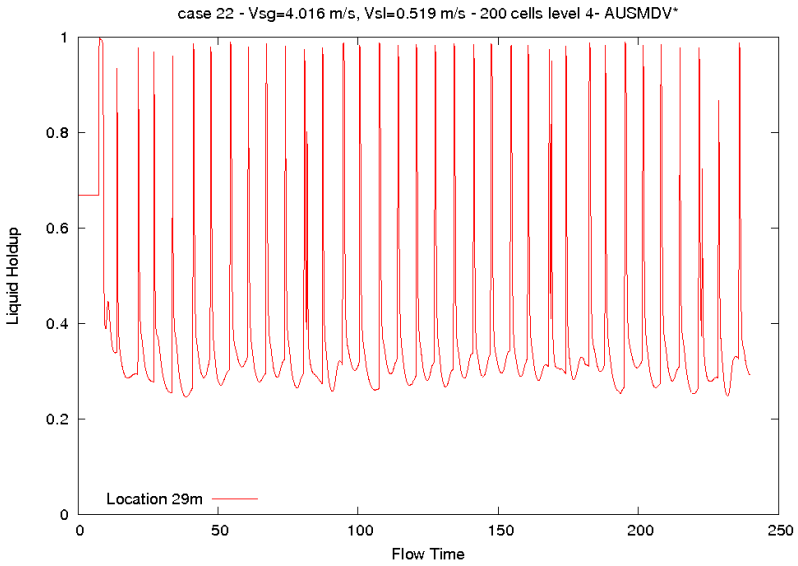

Figure 4.8: Time trace of liquid holdup at $29m$ (Level 4 based on 200 cells, gradient error criterion was used)

application of the complete criteria along with AMR shows no major effect on the spectrum distribution as global, only local changes can be observed. Small waves and slug were all captured.

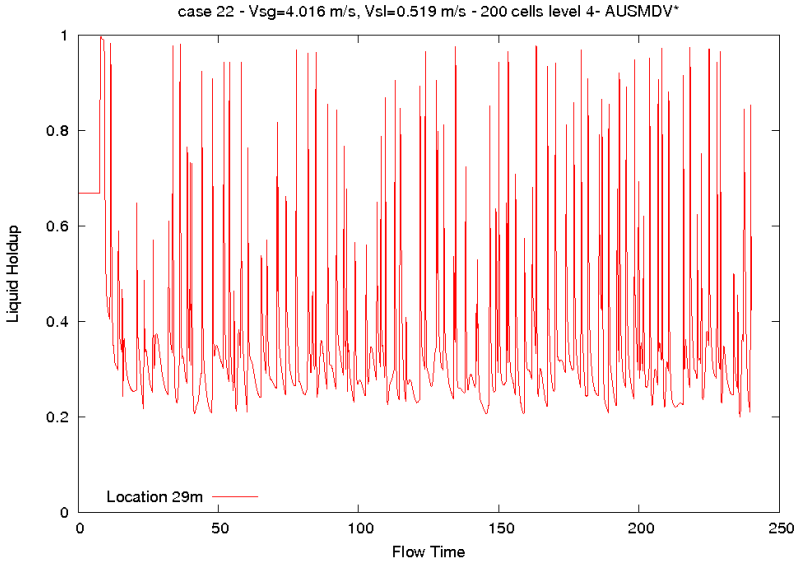

Figure 4.9: Time trace of liquid holdup at $29m$ (Level 4 based on 200 cells, coupled error estimation criterion was used)

The use of the coupled criterion is necessary and figure 4.9 shows that its application keeps the global mean features of the spectra. The use of the gradient error criterion in combination with K-H condition is necessary for the estimation of accurate slug frequencies. Comparing figure 4.9 with figure 4.7 shows the criteria affects the spectra locally. But globally it keeps the main features and essentially it produces the correct frequency of slugs.

4.4.4 Slug flow in non uniform pipe

In this section, we consider a slug ow with conditions of the case 22 ow in a non uniform pipe with length of $l = 520m$. The topology of the system is plotted in figure 4.10.

The aim here is to assess the capability and sensitivity of TD-KH with gradient error criteria along with the AMR technique to detect the inception of topological slugs, or slugs resulting from accidental terrains.

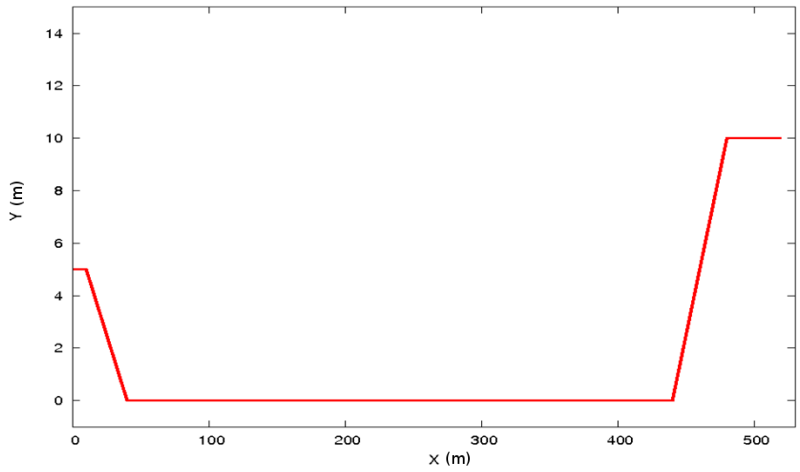

Figure 4.10: Topography of the pipelines ($L = 520m$)

Figure 4.11 shows the time evolution of the liquid holdup with adaptive grid in a long pipe and complex geometry. As figure 4.11 indicates, the onset of slugging occurs in the dip regions, at the beginning of the horizontal pipe and at the beginning of the upward section, these areas are primary candidates for renement. The flow in the downward section is always stratified in this flow condition.

Table 4.8 indicates the running time for both uniform grid and AMR grid. It can be seen that the better speed-up can be obtained in the long pipe rather than the short one.

4.5 Conclusion

The AMR presented in this chapter uses two different error estimations to simulate time dependent gas-water two-phase flow.

The adaptive mesh refinement gradient error criterion approach alone did not allow an acceptable agreement with slug cases 22. The adaptive mesh refinement gradient error criterion approach, combined with Taitel & Dukler Kelvin-Helmholtz criterion, permitted gaining a speed-up factor of around 5.45 when level is 6 and gave a good agreement of the slug frequency with Manolis

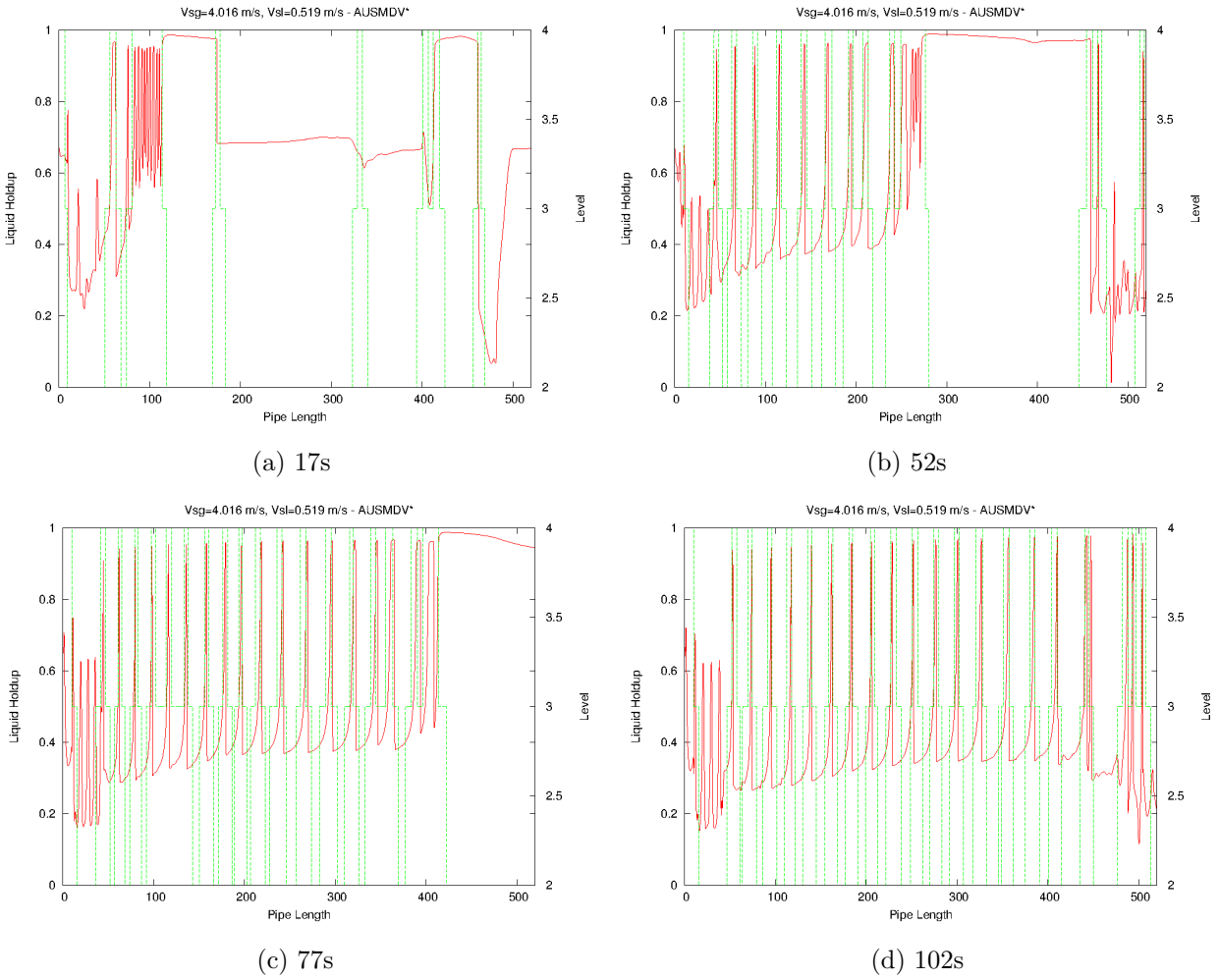

(a) 17s

(b) 52s

(c) 77s

(d) 102s

Figure 4.11: Time evolution of the liquid holdup(solid red line) with adaptive grid(dashed green line) - Long pipe case, gradient error criterion coupled with Taitel & Dukler Kelvin-Helmholtz criterion

cases. For a long pipe and non uniform geometry, the higher speed-up factor obtained is 7.39.

In the end, success in implementing an accurate scheme for slug flow in the EMAPS framework is achieved.

Table 4.8: Running time for different grid types and levels for slug case with long pipe using coupled error estimation criterion

Level of Refinement (Based on 200 cells)	Cells of Uniform	Timings (s)		Speed-up
		Uniform	AMR	
1	1000	5h12m38s	-	-
2	2000	20h47m52s	15h24m40s	1.35
3	4000	68h59m25s	29h58m49s	2.34
4	8000	153h43m12s	41h34m25s	3.68
5	16000	376h34m30s	73h12m06s	5.15
6	32000	917h45m23s	124h52m17s	7.39

References - 4

Barnea, D. (1991), 'On the effect of viscosity on stability of stratified gas - liquid flow - application to flow pattern transition at various pipe inclinations', *Chemical Engineering Science* **46**(8), 2123 – 2131. (cited at page 55)

Barnea, D. and Taitel, Y. (1994), 'Interfacial and structural stability of separated flow', *International Journal of Multiphase Flow* **20**(Supplement 1), 387 – 414. (cited at page xiii, 53, 54, 55)

Beckett, G., Mackenzie, J. A. and Robertson, M. L. (2001), 'A moving mesh finite element method for the solution of two-dimensional stefan problems', *Journal of Computational Physics* **168**(2), 500 – 518. (cited at page 50)

Berger, M. J. and Colella, P. (1989), 'Local adaptive mesh refinement for shock hydrodynamics', *Journal of Computational Physics* **82**, 64–84. (cited at page 50)

Berger, M. J. and Oliger, J. (1984), 'Adaptive mesh refinement for hyperbolic partial differential equations', *Journal of Computational Physics* **53**(3), 484 – 512. (cited at page 50)

Fuster, D., Bague, A., Boeck, T., Moyne, L. L., Leboissetier, A., Popinet, S., Ray, P., Scardovelli, R. and Zaleski, S. (2009), 'Simulation of primary atomization with an octree adaptive mesh refinement and VOF method', *International Journal of Multiphase Flow* **35**(6), 550 – 565. (cited at page 50)

Issa, R. I. and Kempf, M. H. W. (2003), 'Simulation of slug flow in horizontal and nearly horizontal pipes with the two-fluid model', *International Journal of Multiphase Flow* **29**(1), 69 – 95. (cited at page 55)

Jia, N. (2007), Adaptive mesh refinement in solution of two-phase flow problems, Master's thesis, Cranfield University, UK. (cited at page 63)

Lezeau, P. and Thompson, C. P. (1998), Numerical simulation of multi-phase flow: Speed, error control & robustness, Technical report, AMAC, Cranfield University. (cited at page 49, 51)

Louaked, M., Hanich, L. and Thompson, C. P. (2003), 'Well-posedness of incompressible models of two- and three-phase flow', *IMA Journal of Applied Mathematics* **68**(6), 595–620. (cited at page 55)

Manolis, I. G. (1995), High Pressure Gas-Liquid Slug Flow, PhD thesis, Department of Chemical Engineering and Chemical Technology, Imperial College of Science, Technology and Medicine, London, UK. (cited at page 53, 56, 58, 61)

Nourgaliev, R., Sushchikh, S., Dinh, T. and Theofanous, T. (2005), 'Shock wave refraction patterns at interfaces', *International Journal of Multiphase Flow* **31**(9), 969 – 995. (cited at page 50)

Oliger, J. (1979), Approximate methods for atmospheric and oceanographic circulation problems, *in* R. Glowinski and J. Lions, eds, 'Computing Methods in Applied Sciences and Engineering, 1977, II', Vol. 91 of *Lecture Notes in Physics*, Springer Berlin / Heidelberg, pp. 169–184. (cited at page 50)

Omgba-Essama, C. (2004), Numerical Modelling of Transient Gas-Liquid Flows (Application to Stratified and Slug Flow Regimes, PhD thesis, Cranfield University, UK. (cited at page 49, 51, 63)

Pereyra, V. and Sewell, E. G. (1974), 'Mesh selection for discrete solution of boundary problems in ordinary differential equations', *Numerische Mathematik* **23**, 261–268. (cited at page 50)

Provatas, N., Goldenfeld, N. and Dantzig, J. (1999), 'Adaptive mesh refinement computation of solidification microstructures using dynamic data structures', *Journal of Computational Physics* **148**(1), 265 – 290. (cited at page 50)

Quirk, J. J. (1991), An adaptive grid algorithm for computational shock hydrodynamics, PhD thesis, College of Aeronautics. Cranfield Institut of Technology UK. (cited at page 50)

Sambasivan, S. K. and UdayKumar, H. (2010), 'Sharp interface simulations with local mesh refinement for multi-material dynamics in strongly shocked flows', *Computers & Fluids* **39**(9), 1456 – 1479. (cited at page 50)

Sussman, M., Almgren, A. S., Bell, J. B., Colella, P., Howell, L. H. and Welcome, M. L. (1999), 'An adaptive level set approach for incompressible two-phase flows', *Journal of Computational Physics* **148**(1), 81 – 124. (cited at page 49, 50)

Taitel, Y. and Dukler, A. E. (1976), 'A model for predicting flow regime transitions in horizontal and near horizontal gas-liquid flow', *AIChE Journal* **22**(1), 47–55. (cited at page xiii, 52, 55)

Zuzio, D. and Estivalezes, J. (2011), 'An efficient block parallel amr method for two phase interfacial flow simulations', *Computers & Fluids* **44**(1), 339 – 357. (cited at page 50)

Chapter 5

Non-Newtonian fluid behaviour

5.1 Introduction

Studies on two-phase gas-liquid co-current flow with non-Newtonian liquid system has attracted the attention of researchers over the years[Chhabra and Richardson (1984), Dziubinski et al. (2004), Xu et al. (2007), Farooqi et al. (1980)], due to its wide-spread applications and importance in various different processes in the chemical and biochemical industries, such as the process of two-phase in oil and gas wells, transportation systems of crude and refined products, and food processing in biochemical engineering and bio-reactors.

The objective of this chapter is to introduce the non-Newtonian fluid and the constitutive equation of time independent viscosity shear-thinning fluid, investigate the behaviour of the shear thinning fluid, and compare with Newtonian and shear-thickening fluid. Furthermore, the velocity profile in a pipe influences the flow behaviours; Thus, different velocity profiles in different non-Newtonian fluids will be introduced in this chapter. Pressure drop for different fluid will also be studied in this chapter. Other non-Newtonian properties such as elastic effects are not included in this work.

5.2 Definition of a non-Newtonian flow

Fluids such as water and air are Newtonian, which means shear stress τ versus shear rate $\dot{\gamma}$ at a given temperature is linear and crosses the origin. The constant slope is known as the Newtonian viscosity μ that is independent with shear rate, which can be expressed as the velocity gradient, i.e.

$$\tau = \mu \left(-\frac{\mathrm{d}u}{\mathrm{d}y} \right) = \mu\dot{\gamma} \tag{5.1}$$

where u is the velocity of the fluid, y is a position coordinate, du/dy is the velocity gradient called the shear rate.

The fluid will be called non-Newtonian if this fluid does not obey the Newtonian relationship between the shear stress and shear rate. High molecular weight liquids, which include polymer melts and solutions of polymer, are usually non-Newtonian. In this case, the proportionality of the shear stress against shear rate will not be constant, as the shear rate was changed.

Such materials may be conveniently grouped into three general classes:

1. fluids for which the rate of shear at any point is determined only by the value of the shear stress at that point at that instant; these fluids are variously known as time independent.

2. more complex fluids for which the relation between shear stress and shear rate depends, in addition, upon the duration of shearing and their kinematic history; they are called time-dependent fluids.

3. substances exhibiting characteristics of both ideal fluids and elastic solids and showing partial elastic recovery, after deformation; these are categorised as visco-elastic fluids

5.2.1 Viscous time-independent non-Newtonian fluids

For these kinds of non-Newtonian fluids, their shear rate and shear stress relationship can be expressed as:

$$\frac{\mathrm{du}}{\mathrm{dy}} = f(\tau) \tag{5.2}$$

where f is a non-linear function. Figure 5.1 shows several types of such fluids.

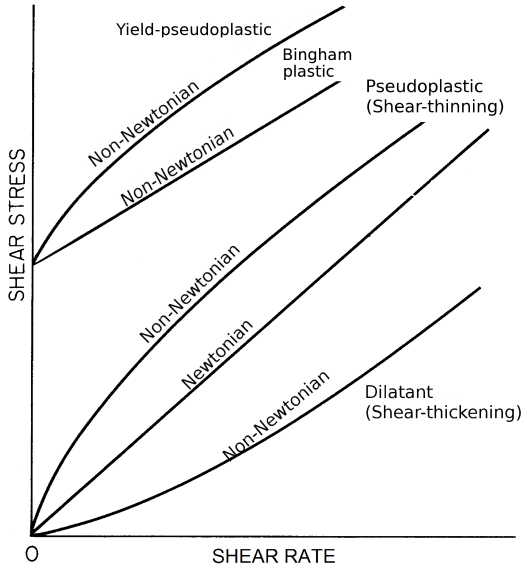

Figure 5.1: Type of fluid behaviour

5.2.1.1 Shear-thinning and shear-thickening fluids

Shear-thinning fluid is the most common type of the non-Newtonian fluid. For Shear-thinning and shear-thickening fluids, μ is called the "apparent viscosity" of the fluid, and is a function of the shear rate. It can be seen from Figure 5.2, the viscosity decreases with increasing shear rate, and the viscosity of this fluid has a shear-thinning behaviour. In the opposite case, the viscosity of liquid increases with an increase of shear rate - this kind of fluid is called shear-thickening.

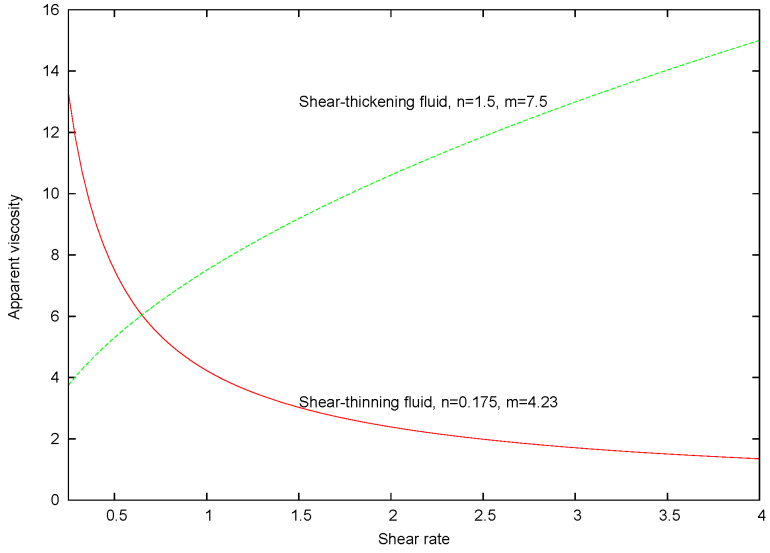

Figure 5.2: Apparent viscosity as function of shear rate

5.2.1.2 Viscoplastic fluids

This kind of fluid behaviour is characterised by the existence of a yield stress, (τ_0). The fluid will flow only when the externally applied stress exceeds the yield stress (τ_0). As shown in figure 5.1, the shear stress versus shear rate curve was linear or non-linear, but it will start from a certain stress threshold rather than the original point. If the externally applied stress is bigger than the yield stress, viscoplastic fluids will present the normal viscous behaviour.

There are two types of viscoplastic fluid. One is called Bingham plastic fluid, which is like solid for low shear stress exhibiting and like Newtonian fluid when the yield stress is surpassed. The other one is called yield-pseudoplastic fluid, and it will present shear-thinning behaviour when external stress is greater than yield stress.

5.2.2 Viscous time-dependent non-Newtonian fluids

The present behaviour was influenced by what happened to them in the recent past. These fluids seem to have a "memory" which fades with time. The relationship between shear rate and shear stress can be expressed as:

$$\frac{\mathrm{du}}{\mathrm{dy}} = f(\tau, t) \tag{5.3}$$

where t is the time. Time-dependent non-Newtonian fluids are further classified into two groups: thixotropic fluids and rheopectic fluids, depending on whether the shear stresses decrease or increase with time at a given shear rate and constant temperature.

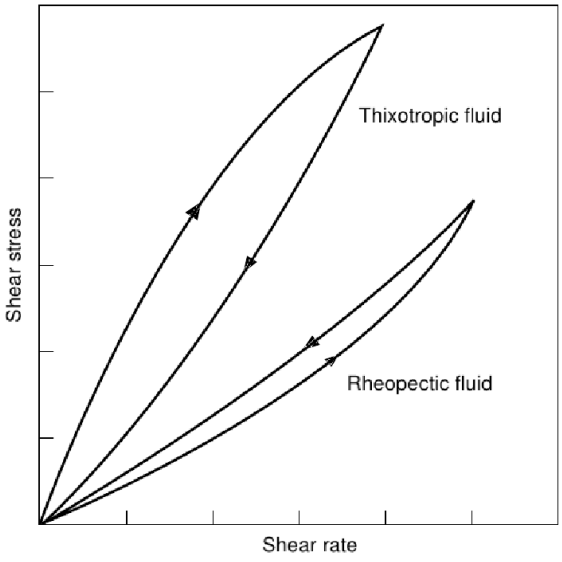

Figure 5.3: Time-dependent fluid behaviour (shear stress versus shear rate) (Chhabra and Richardson, 1999)

The thixotropic fluids exhibit a reversible decrease in shear stress with time at a given shear rate and constant temperature. If the flow curve is measured in a single experiment in which shear rate is steadily increased from zero to a maximum value, and then immediately decreased steadily toward zero, a form

of hysteresis loop would be obtained, as shown in figure 5.3. The arrows in this figure indicate the chronological progress of the experiment.

For rheopectic fluids, the materials exhibit a reversible increase in shear stress with time at a constant shear rate under isothermal conditions. The location of the hysteresis loop for a given fluid is again dependent on the time history of the material, including the rate at which du/dy is increased and decreased during the experiment.

5.2.3 Visco-elastic fluid behaviour

Visco-elastic fluids combine the elastic properties of solids with the flow behaviour of fluids. In a purely Hookean elastic solid, the stress corresponding to a given strain is independent of time, whereas for visco-elastic substances, the stress will gradually dissipate. In contrast to purely viscous liquids, on the other hand, visco-elastic fluids flow when subjected to stress, but part of their deformation is gradually recovered upon removal of the stress.

5.3 Typical mathematical models for shear-thinning fluid

The mathematical model is fundamental to non-Newtonian fluid flow. It is used to establish the momentum equation, which, together with the continuity and energy equations, lays down a model for flow behaviour. Here, some widely used shear-thinning fluid viscosity models were chosen to for this section - more detail about these models can be found in Chhabra and Richardson (1999), Carreau et al. (1997) and Macosko (1994). Many of these models were developed for applications in the fields of liquid food products, blood, polymer melts, etc.

In this work, the power-law model was chosen to express the shear-thinning fluid only because of the limited availability of experimental data. However, the expressions of Carreau-Yasuda model and Cross model were introduced in this section as well.

5.3.1 Power-law model

Here, the so-called power-law (or Ostwald de Waele) model is one of the most widely used expressions for shear-thinning fluid (Macosko, 1994). It is presented as follows:

$$\tau_{ij} = m|\pi_{2D}|^{(n-1)/2}\,(2D_{ij}) \tag{5.4}$$

where D is the rate of deformation tensor, π_{2D} is the second invariant of D, and τ is the shear stress. The first subscript in equation 5.4 refers to the plane on which the components of shear stress are acting, and the second indicates the direction of the component on that plane. This equation is often applied to steady simple shear flow in which the absolute value of the second invariant becomes

$$|\pi_{2D}| = \dot{\gamma}^2 \tag{5.5}$$

Noting that $2D_{ij} = \dfrac{du}{dy}$ for a steady simple shear flow, the power-law model becomes

$$\tau_{ij} = m(\dot{\gamma}_{ij})^{n-1}\frac{du}{dy} \tag{5.6}$$

and $\dot{\gamma} = \dfrac{du}{dy}$ is the shear rate. Then, this implies that apparent viscosity is given by:

$$\mu = \tau_{ij}/\dot{\gamma}_{ij} = m(\dot{\gamma}_{ij})^{n-1} \tag{5.7}$$

where m and n are called consistency index and power-law index, respectively. They are two empirical curve-fitting parameters. The relationship between logarithmic apparent viscosity and logarithmic shear rate can be plotted by a straight line, as shown in figure 5.4. It can be seen from figure 5.4 that the power-law model only applies over a limited range of shear rates, and this model does not predict the zero apparent viscosity μ_0 and infinite apparent viscosity μ_∞. This model is given by:

- For n < 1, the fluid is called shear-thinning fluid
- For n $= 1$, the fluid is Newtonian fluid
- For n > 1, the fluid is called shear-thickening fluid

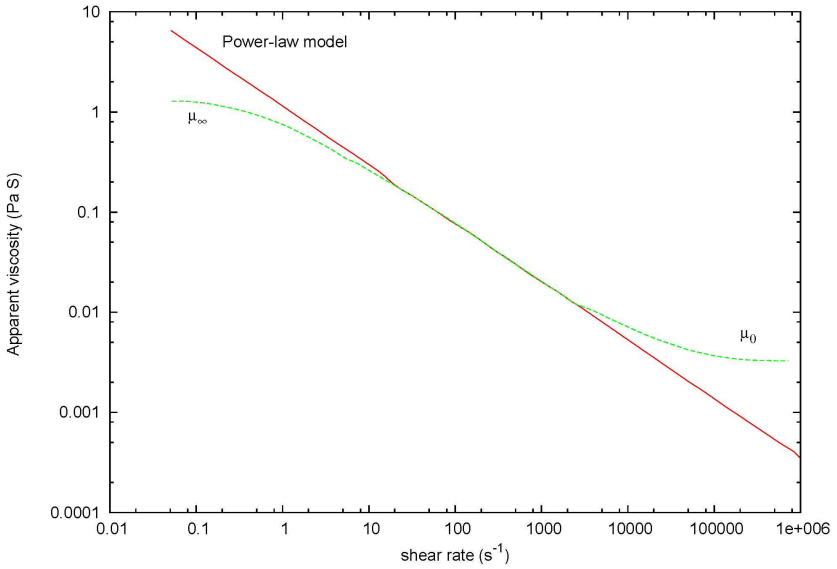

Figure 5.4: Comparison of power-law model with shear-thinning fluid in zero shear and infinite apparent viscosities

For a shear-thinning fluid, the power-law index, n may have any value between 0 and 1. Shear-thinning fluids are also called pseudoplastic fluids. Shear-thinning behaviour is more common than shear-thickening.

In this work, the power-law model was chosen to express the shear-thinning fluid, because this model offers the simplest representation of shear-thinning behaviour. However, there is shortcoming in predicting the zero apparent viscosity μ_0 and infinite apparent viscosity μ_∞ in this model. The commercial computational fluid dynamics (CFD) software Fluent that was used in this work allows placement of zero apparent viscosity μ_0 and infinite apparent viscosity μ_∞ on the power-law function(ANSYS-Fluent Inc (2008)), see figure 5.5. If the viscosity computed from the power-law model is smaller than μ_0, the number of μ_0 will be chosen instead. Likewise, if the computed apparent viscosity is bigger than μ_∞, the value of μ_∞ will be used instead.

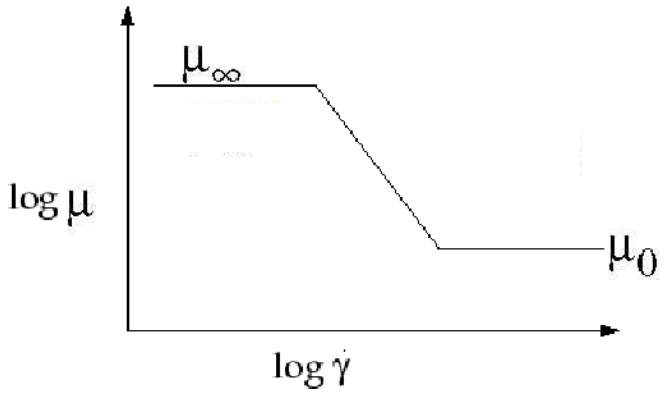

Figure 5.5: Variation of apparent viscosity with shear rate (ANSYS-Fluent Inc, 2008)

5.3.2 Carreau-Yasuda model

The model is used when the significant discrepancy is predicted at low and high shear-rates, and it is given by:

$$\frac{\mu - \mu_\infty}{\mu_0 - \mu_\infty} = (1 + (\lambda\dot{\gamma})^a)^{(n-1)/a} \tag{5.8}$$

For $a = 2$, the equation is known as Carreau equation.

5.3.3 Cross model

Here is the Cross model expression, giving viscosity as a function of shear rate:

$$\frac{\mu - \mu_\infty}{\mu_0 - \mu_\infty} = \frac{1}{1 + (\lambda\dot{\gamma})^{(n-1)/2}} \tag{5.9}$$

where λ is natural time that is inverse of the shear rate at which the fluid changes from Newtonian to power-law behaviour. Typically, $\mu_0 \gg \mu_\infty$, so

$$\mu = \frac{\mu_0}{1 + (\lambda\dot{\gamma})^{(n-1)/2}} \tag{5.10}$$

This Cross model is usually chosen while the zero shear rate behaviour of the viscosity has to be described.

5.4 Single-phase flow of power-law fluids

Frictional pressure gradient and velocity profile were the two most important considerations for fluid power designers, especially in long pipe systems for industry. Frictional pressure gradient could influence the pipe design, and velocity profile in a given flow could affect the mass and heat transfer. To understand more detail about non-Newtonian power-law fluids, friction pressure gradient and velocity were studied in a single-phase power-law fluids pipeline in both laminar and turbulent flow in this section.

5.4.1 Steady laminar flow in circular pipe

The time-independent laminar flow is assumed to be fully developed and in steady-state situation in a circular pipe, as shown in figure 5.6.

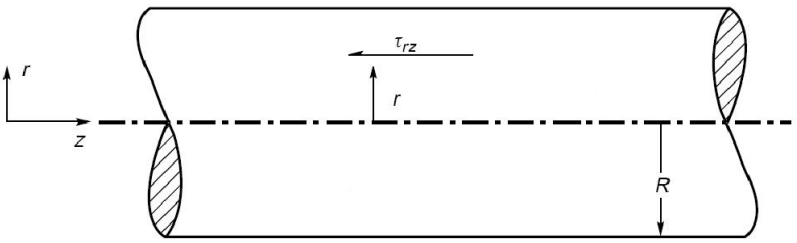

Figure 5.6: Steady flow in a horizontal pipe (Chhabra and Richardson, 1999)

The steady invariant Navier-Stokes momentum equation in cylindrical coordinate can be simplified in the following expression.

$$\begin{cases} 0 = -\dfrac{\partial p}{\partial r} + \dfrac{\partial \tau_{rr}}{\partial r} + \dfrac{\tau_{rr} - \tau_{\theta\theta}}{r} & (5.11) \\ 0 = -\dfrac{1}{r}\dfrac{\partial p}{\partial \theta} & (5.12) \\ 0 = \dfrac{1}{r}\dfrac{\partial (r\tau_{rz})}{\partial r} - \dfrac{\partial p}{\partial z} & (5.13) \end{cases}$$

Equation 5.12 shows that p is independent of θ. Therefore:

$$p = p(r, z) \tag{5.14}$$

In equation 5.11, $\frac{\partial \tau_{rr}}{\partial r}$ and $\frac{\tau_{rr} - \tau_{\theta\theta}}{r}$ are all the function of r, so the equation 5.14 can be rewritten:

$$p = f(r) + g(z)$$

therefore:

$$\frac{\partial p}{\partial z} = \frac{dg}{dz} = g'(z)$$

But $\frac{1}{r}\frac{\partial (r\tau_{rz})}{\partial r}$ is only the function of r, So

$$\frac{\partial p}{\partial z} = \text{constant} = -\frac{\Delta p}{L} \tag{5.15}$$

Substitution of equation 5.15 into equation 5.13, followed by integration gives:

$$\tau_{rz} = \frac{-\Delta p}{L}\frac{r}{2} + C_1 \tag{5.16}$$

Figure 5.7 shows the linear shear stress distribution across the pipe cross-section, the shear stress being zero at the axis of the pipe.

So $C_1 = 0$, therefore:

$$\tau_{rz} = \frac{-\Delta p}{L} \cdot \frac{r}{2} \tag{5.17}$$

For a non-Newtonian flow in a pipe, the power-law model was adopted. Now combing equations 5.7 and 5.17, the following expression can be obtained:

$$\tau_{rz} = \frac{-\Delta p}{L} \cdot \frac{r}{2} = m(-\frac{du_z}{dr})^n \tag{5.18}$$

Then, equation 5.18 can be rewritten as:

$$du_z = (\frac{-\Delta p}{L} \cdot \frac{r}{2m})^{1/n} dr \tag{5.19}$$

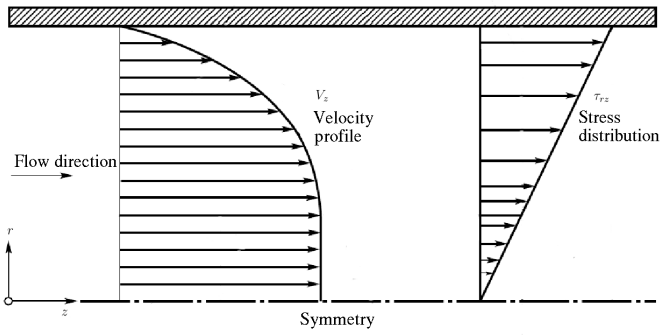

Figure 5.7: Shear stress and velocity distribution in fully developed laminar flow in a pipe (Chhabra and Richardson, 1999)

The velocity distribution is shown in the following expression by integration of the equation 5.19:

$$u_z = -\frac{n}{n+1}\left(\frac{-\Delta p}{L}\cdot\frac{1}{2m}\right)^{1/n}\cdot r^{(n+1)/n} + \text{constant} \tag{5.20}$$

Since no-slip boundary condition is applied at the wall along the pipe, $r = R$, the velocity u_z must be zero, as shown in the figure 5.7. Substituting the value $u_z = 0$, when $r = R$:

$$\text{constant} = \frac{n}{n+1}\left(\frac{-\Delta p}{L}\cdot\frac{1}{2m}\right)^{1/n}\cdot R^{(n+1)/n}$$

therefore:

$$u_z = \frac{n}{n+1}\left(\frac{-\Delta p}{L}\cdot\frac{R}{2m}\right)^{1/n}\cdot R\cdot\left\{1-\left(\frac{r}{R}\right)^{(n+1/n)}\right\} \tag{5.21}$$

The velocity profile may be expressed in terms of the average velocity, u, which is given by:

$$u = \frac{Q}{\pi R^2} = \frac{1}{\pi R^2}\int_0^R 2\pi r u_z dr \tag{5.22}$$

where Q is the volumetric flow rate of the non-Newtonian power-law fluid. On substitution for u_z from equation 5.22, and integration yields,

$$
\begin{aligned}
u &= \frac{2\pi}{\pi R^2}\left(\frac{n}{n+1}\right)\left(\frac{-\Delta p}{L}\cdot\frac{R}{2m}\right)^{1/n}\cdot R\cdot\int_0^R r\left(1-\left(\frac{r}{R}\right)^{(n+1)/n}\right)dr \\
&= 2\left(\frac{n}{n+1}\right)\left(\frac{-\Delta p}{L}\cdot\frac{R}{2m}\right)^{1/n}\cdot R\cdot\int_0^R \frac{r}{R}\left(1-\left(\frac{r}{R}\right)^{(n+1)/n}\right)d(\frac{r}{R}) \\
&= \left(\frac{n}{n+1}\right)\left(\frac{-\Delta p}{L}\cdot\frac{R}{2m}\right)^{1/n}\cdot R\cdot\left(\frac{1}{2}-\frac{n}{3n+1}\right)
\end{aligned}
$$

therefore:

$$u = \frac{n}{3n+1}\left(\frac{-\Delta p}{L}\cdot\frac{R}{2m}\right)^{1/n}\cdot R \tag{5.23}$$

Velocity distribution can be written as:

$$\frac{u_z}{u} = \frac{3n+1}{n+1}\left[1-\left(\frac{r}{R}\right)^{(n+1)/n}\right] \tag{5.24}$$

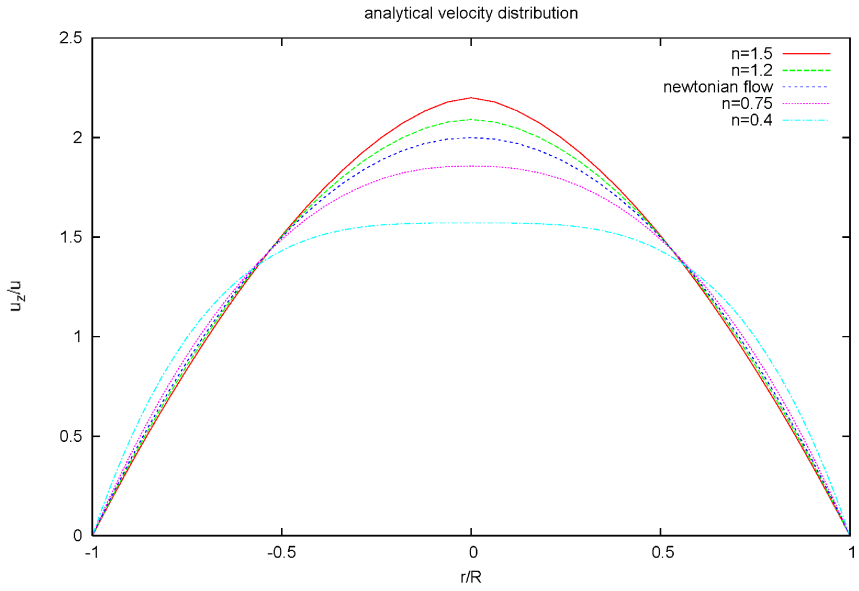

Figure 5.8: Analytical dimensionless velocity distribution for power-law fluids in laminar flow

The velocity profiles for different values of n, calculated from equation 5.24, are shown in figure 5.8. Compared with the parabolic distribution for a Newtonian fluid ($n = 1$), the profile is flatter for a shear-thinning fluid and sharper for a shear-thickening fluid. The maximum velocity is achieved at the pipe axis, $r = 0$.

Commercial computational fluid dynamics (CFD) software, Fluent software, was used here to study the non-Newtonian power-law fluids velocity profile and compared with figure 5.8.

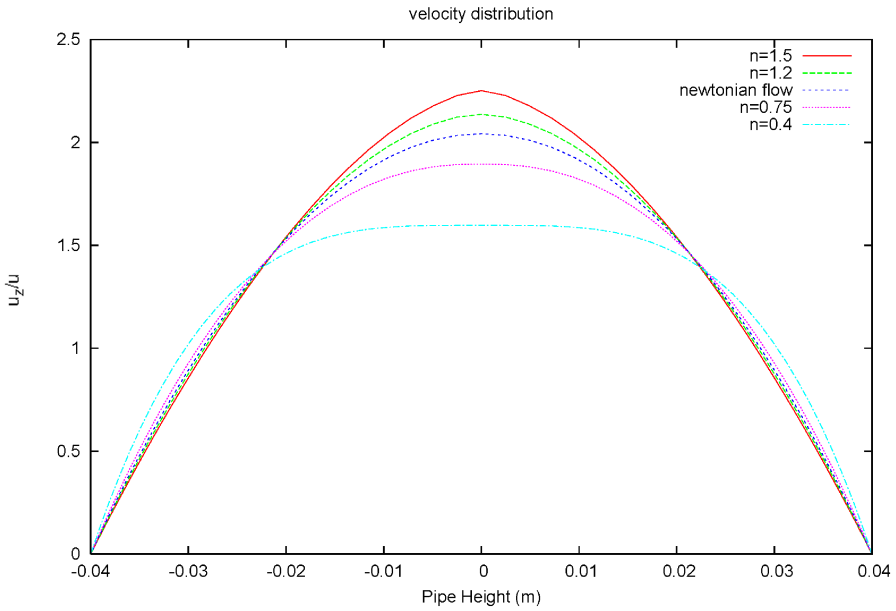

Figure 5.9: Dimensionless velocity distribution calculated by FLUENT for power-law fluids in laminar flow with inlet velocity $v = 0.1m/s$

Here, a 2-dimensional test case was built to run in Fluent. The specifications are summarised as:

- Diameter: $78mm$
- Pipe Length: $38m$
- Operating fluids: Different power-law fluids
- Inlet velocity: $0.1m/s$ in laminar flow, $1m/s$ in turbulent flow

- Flow temperature: $T = 298\text{K}$
- Outlet flow pressure: $1bar$

The pipe length was set to $38m$ in order to fully develop the flow. The figure 5.9 is the dimensionless velocity distribution for different power-law fluids with inlet velocity $v = 0.1m/s$ in laminar flow monitored in $37.5m$ from inlet. The velocity profiles for different values of n, simulated by CFD Fluent software, are shown in figure 5.9.

Velocity profiles calculated from analytical equation 5.24 and CFD Fluent are compared in figure 5.10, the solid lines are CFD resluts for different power-law index n, and the dotted lines are analytical velocity profiles for different power-law index n, it clearly shows that a excellent agreement can be yielded between the analysis velocity distribution and CFD result near the pipe wall. At the pipe axis, $r/R = 0$, the velocities calculated by CFD Fluent are always slightly higher than the analytical results and maximum difference is in error by 4.5% .

Re-writing equation 5.23 to obtain the expression for the volumetric flow rate:

$$Q = \pi R^2 u = \pi \frac{n}{3n+1} \left(\frac{-\Delta p}{L} \cdot \frac{1}{2m} \right)^{1/n} \cdot R^{\frac{3n+1}{n}} \tag{5.25}$$

It is easy to obtain from equation 5.25 that $-\Delta p \propto Q^n$ in a given power-law index n and pipe radius R. Therefore, the pressure gradient of shear thickening fluids is higher than that of Newtonian fluids and is much more sensitive to changes in power-law index compared to shear thinning fluids. This result was also verified in table 5.1 using CFD software. Here, pressure gradient for different power-law fluids was also studied in CFD Fluent. It can be shown from table 5.1 that the pressure gradient increases with an increase in power-law index, n, and pressure gradient for shear-thickening fluid is much higher than shear-thinning fluid.

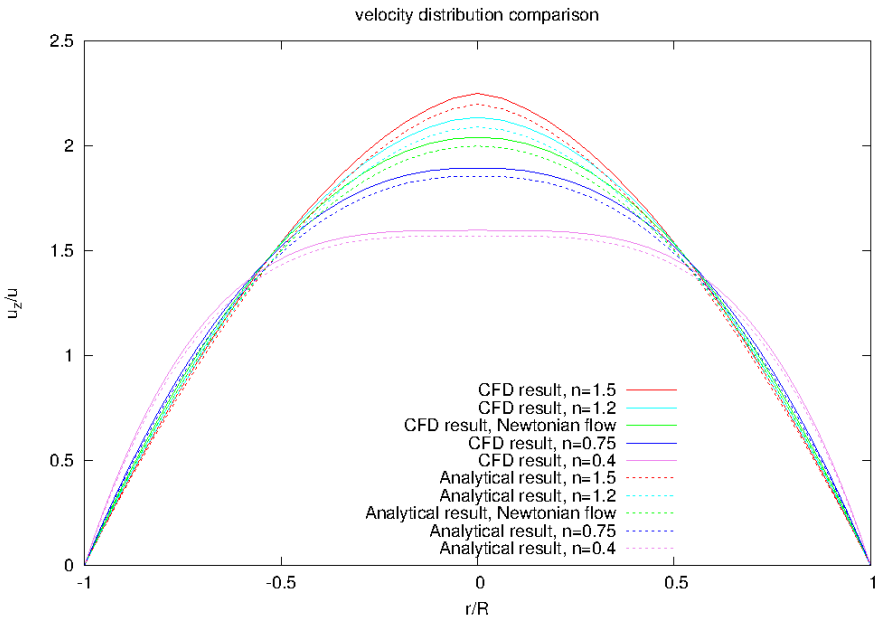

Figure 5.10: Comparison of dimensionless velocity distribution calculated by Fluent for power-law fluids in laminar flow with inlet velocity $v = 0.1m/s$ with analytical results

n	$-\frac{dp}{dz}$
0.4	2.84737
0.75	5.4437
1 (Newtonian flow)	8.31579
1.2	11.57895
1.5	18.97368

Table 5.1: Pressure gradient for different power law index n with inlet velocity $v = 0.1m/s$ in laminar flow

5.4.2 Steady turbulent flow in circular tubes

Since Newtonian and non-Newtonian fluids exhibit different flow behaviours, the definition of Reynolds number for Newtonian fluids is invalid for non-Newtonian fluids. In this study, the generalized Reynolds number for power-law fluids, proposed by Metzner and Reed (1955) to yield the same laminar friction factor $f = \frac{16}{\mathrm{Re}}$, was described as:

$$\mathrm{Re}_{MR} = \frac{\rho u^{2-n} D^n}{8^{n-1} m \left(\frac{3n+1}{4n}\right)^n} \tag{5.26}$$

The accepted critical value of the Reynolds number of transition from laminar to turbulent flow will no longer be 2100, which it is for Newtonian fluids. For power-law fluids, the critical value of the Reynolds number of transition from laminar to turbulent flow depends on the type and the degree of non-Newtonian behaviour. For power-law fluids, the criterion of Ryan and Johnson (1959) can be used,

$$\mathrm{Re}_{MR} = \frac{6464n}{(3n+1)^2} \cdot (2+n)^{\frac{2+n}{1+n}} \tag{5.27}$$

As shown in the figure 5.11, equation 5.27 still predicts the critical Reynolds number of 2100 for Newtonian fluids, and the critical Reynolds number increases with decreasing values of the power law index from Newtonian fluids $n = 1$, reaching a maximum of about 2400 at $n = 0.4$ and then dropping to 1600 at $n = 0.1$.

Figure 5.12 shows the dimensionless velocity distribution for different power-law fluids with inlet velocity $v = 1m/s$ in turbulent flow captured in $37.5m$ where the flow is fully developed already. The same conclusion can be obtained that the velocity profile is flatter for a shear-thinning fluid and sharper for a shear-thickening fluid. Comparing the velocity distribution in laminar flow, as shown in figure 5.9 and in turbulent flow, see figure 5.12, it clearly shows that, for shear thinning fluid with power-law index $n = 0.4$ in turbulent flow, a fairly

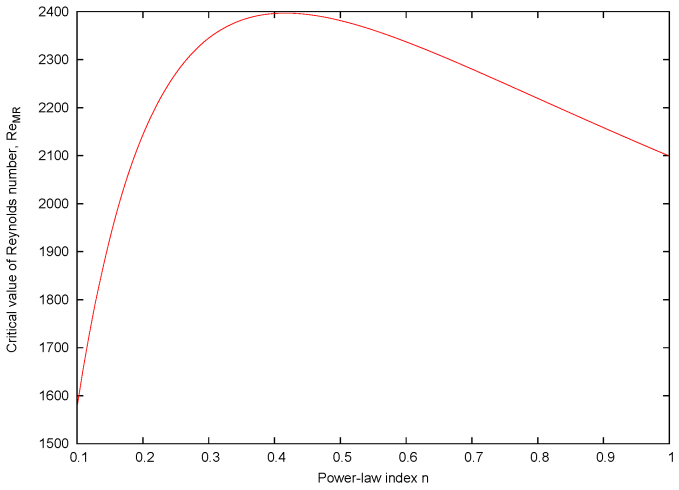

Figure 5.11: Critical value of the Reynolds number of power-law fluids transition from laminar to turbulence depends on the power-law index n

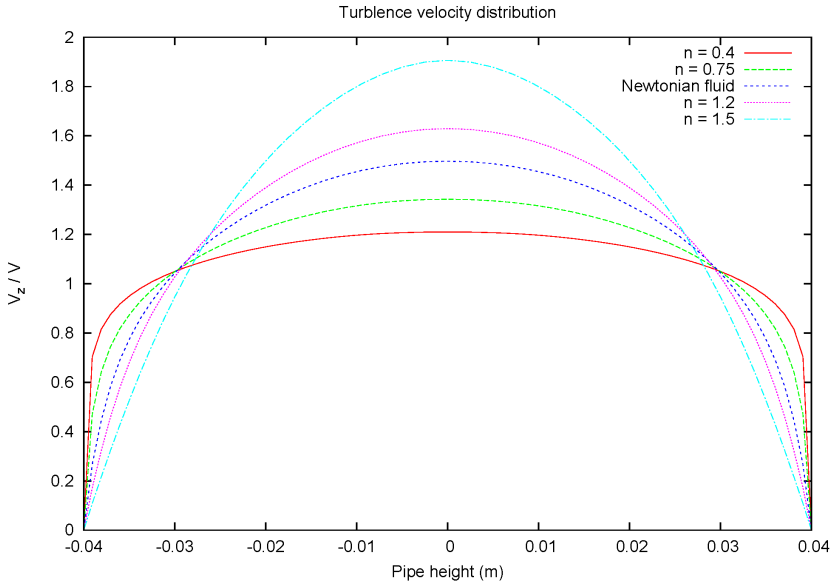

Figure 5.12: Dimensionless velocity distribution calculated by FLUENT for power-law fluids in turbulent flow with inlet velocity $v = 1m/s$

flat velocity distribution exists across the section of pipe, with the result that the entire fluid flows at a single value.

Five different inlet velocity cases using the same shear-thinning fluid, $n = 0.75$, were studied here. The critical Reynolds number is 2249.9 because the value of the power law index is 0.75.

Inlet velocities

- $v = 0.1, Re_{MR} = 258.81$
- $v = 0.3, Re_{MR} = 1021.85$
- $v = 1, Re_{MR} = 4602.4$
- $v = 1.2, Re_{MR} = 5780.44$
- $v = 1.5, Re_{MR} = 7640.09$

v	$-\frac{dp}{dz}$
0.1	5.44737
0.3	12.83684
1	159.6842
1.2	198.8421
1.5	258.3684

Table 5.2: Pressure gradient for different inlet velocity when $n = 0.75$

Table 5.2 shows the pressure gradient for different inlet velocities for shear-thinning fluids, $n = 0.75$. The pressure gradient in turbulent flow is much higher than in laminar flow. Table 5.3 shows that pressure gradient of shear-thickening fluids is much more sensitive than for shear thinning fluids - the

n	$-\frac{dp}{dz}$
0.4	54.47368
0.75	159.6842
1 (Newtonian flow)	330
1.2	501.8421
1.5	950

Table 5.3: Pressure gradient for different power law index n with inlet velocity $v = 1m/s$ in turbulent flow

same as in laminar flow, and the similar tendency can be found in Chhabra and Richardson (1999).

5.4.3 Friction factor

The normal way to obtain pressure drops for turbulent flow of power-law fluids in pipelines is to adopt the Darcy-Weisbach equation, and then the fanning friction factor, f, will be determined. Most of them have a study of logarithmic region behaviour attached(El-emam et al. (2003)). In this section, several equations for predicting the friction factor will be reviewed.

5.4.3.1 Laminar flow

As already mentioned in the previous section, Metzner and Reed (1955) suggested using the same friction factor expression with the Newtonian fluids for non-Newtonian power-law fluids, that is :

$$f = \frac{16}{\mathrm{Re_{MR}}} \tag{5.28}$$

In order to satisfy this laminar friction factor expression, Metzner and Reed (1955) Reynolds number $\mathrm{Re}_{MR} = \dfrac{\rho u^{2-n} D^n}{8^{n-1} m \left(\dfrac{3n+1}{4n}\right)^n}$ was used.

5.4.3.2 Turbulent flow

Dodge and Metzner (1959) developed a semi-empirical expression to calculate the pressure drop of the fully developed turbulent flow of power-law fluids in smooth pipes, using a solution of CarboxyMethylo Cellulose (CMC), carbopol and clay. In the special case of fluids that follow the model of Ostwald-de Waele, this friction factor correlation, f can be obtained by the following equation 5.29, where the Metzner and Reed (1955) Reynolds number was used in this correlation.

$$\frac{1}{\sqrt{f}} = \frac{4}{n^{0.75}} \log\left[Re_{MR} f^{1-n/2}\right] - \frac{0.4}{n^{1.2}} \tag{5.29}$$

For $n = 1$, equation 5.29 reduces to the well-known Karman-Nikuradse friction factor correlation ($\dfrac{1}{\sqrt{f}} = 4.0 \cdot \log\left(Re \cdot \sqrt{f}\right) - 0.4$), which is valid for the Newtonian flow in a smooth pipe.

Irvine (1988) presented a Blasius like expression for power-law fluids, which is not logarithmic behaviour, as shown in the following:

$$f = [(\frac{2^{n+4}}{7^7 n}(\frac{4n}{3n+1})^{3n^2})/Re_{MR}]^{1/(3n+1)} \tag{5.30}$$

and this correlation was shown graphically in figure 5.13.

More correlation of friction factor for turbulent power-law fluids was listed in the table 5.4. A more complete review can be found in El-emam et al. (2003) and Gao and Zhang (2007).

Table 5.4: Friction factor correlations for power-law fluids in turbulent flow.

Reference	Correlation
Dodge and Metzner (1959)	$\frac{1}{\sqrt{f}} = \frac{4}{n'^{0.75}} \log\left[Re_{MR} f^{1-n/2}\right] - \frac{0.2}{n^{1.2}}$
Kemblowski and Kolodziejski (1973)	$f = 0.00225 \cdot exp(3.57n^2) \cdot exp[572(1-n^{4.2})/n^{0.435} Re_{MR}]/Re_{MR}^{(0.314n^{2.3}-0.064)}$ $when\ \ Re_{MR} > 31600/n^{0.435},\ \ then\ \ f = 0.0791/Re_{MR}^{0.25}$
Szilas et al. (1981)	$\frac{1}{\sqrt{f}} = \frac{4}{n} \cdot \log Re_{MR}(4f)^{1-n/2} + 1.511^{1/n}(4.242 + 1.414/n) - 8.03/n - 2.114$
Hemeida (1993)	$\frac{1}{\sqrt{f}} = 3.536 - 392.081(f/n')^{0.9013} - 305.624(f/n')^{0.9013}$ $\cdot \left[\ln(1 - \sqrt{1 - 14.142/Re_{MR}\sqrt{f}}) + \sqrt{1 - 14.142/Re_{MR}\sqrt{f}}\right]$
El-emam et al. (2003)	$f = \left[n'/\left(3.072 - 0.1433n'\right) Re_{MR}^{n'/(0.282-4.211n')} - 0.00065\right]/4$
Clapp (1961)	$\frac{1}{\sqrt{f}} = \frac{2.69}{n} - 2.95 + \frac{4.53}{n} = \log Re_{MR}(\sqrt{f})^{2-n} + 0.69\left(\frac{5n-8}{n}\right)$

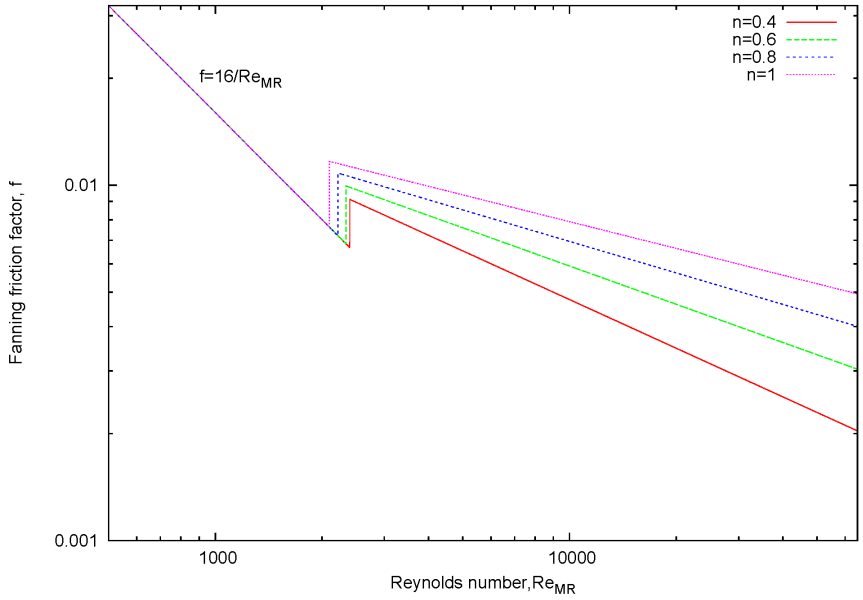

Figure 5.13: Friction factor - Reynolds number behaviour for shear-thinning fluids using friction factor correlation of Irvine (1988)

5.5 Two phase gas/non-Newtonian fluid flow

5.5.1 Introduction

After being concerned with the behaviour of single phase non-Newtonian fluid, more consideration should be concentrated on the far more complex two-phase problem. Despite large differences in rheology, gas-liquid two-phase flow exhibits many common features, whether the liquid is Newtonian or follows a shear-thinning behaviour. Applications in the chemical, food and processing industries range from the flow of mixtures of crude oil (which exhibit non-Newtonian characteristics) and gas from oil well heads, to that of vapour-liquid mixtures in boilers and evaporators. Just like two-phase gas-Newtonian flow, the three most important hydrodynamic features, which are the flow pattern, holdup, and the pressure drop of two-phase flows, will be studied in this work.

5.5.2 Flow patterns

The regions over which the different types of flow patterns can occur are conveniently shown as a 'flow pattern map', in which a function of the liquid flowrate is plotted against a function of the gas flowrate and boundary lines are drawn to delineate the various regions. For the flow of gas-Newtonian two-phase flow, a wide variety of flow patterns have been examined, depending upon their physical properties and input fluxes of two phases, and the size and inclination of the pipe. Most of the data used for constructing such maps have been obtained with the air-water system at atmospheric conditions. Although the physical properties of the two phases were expected intuitively to play significant roles in determining the transition from one flow pattern to another, it is now generally recognised that the liquid properties indeed have very little effect for the flow pattern map [Mandhane et al. (1974); Weisman et al. (1979); Chhabra and Richardson (1984)]. Even shear-thinning behaviour seems to play virtually no role in governing the transition from one flow pattern to another [Chhabra and Richardson (1984)]. Chhabra and Richardson slightly modified the horizontal flow pattern map of Mandhane et al. (1974) on the basis of these considerations and taking into account the extensive experimental study of Weisman et al. (1979), as shown in figure 5.14. More recently, Xu et al. (2007) did some work on CMC solution using transparent tubes of 20, 40 and 60 mm in diameter with different angle.

In vertical flow, gravity acts in the axial direction, giving symmetry across the pipe cross-section. The flow pattern appears more stable. Recent works reporting data of flow pattern maps of gas-non-Newtonian liquid mixture vertical flow are Khatib and Richardson (1984) and Dziubinski et al. (2004). Khatib and Richardson (1984) worked on suspensions of china clay in vertical upward flowing pipes, and their results compared well with the predictions of Taitel et al. (1980) for air-water mixtures - and this suggests that the transition boundaries between the various flow pattern are largely unaffected by the rheology of the liquid. The flow patterns map is shown in Figure 5.15. Dziubinski et al. (2004) obtained data for tubes with diameters $25.3 - 50.5mm$ and lengths of $5m$, and the map for the determination of flow patterns for two-phase gas-non-Newtonian liquid flow in a

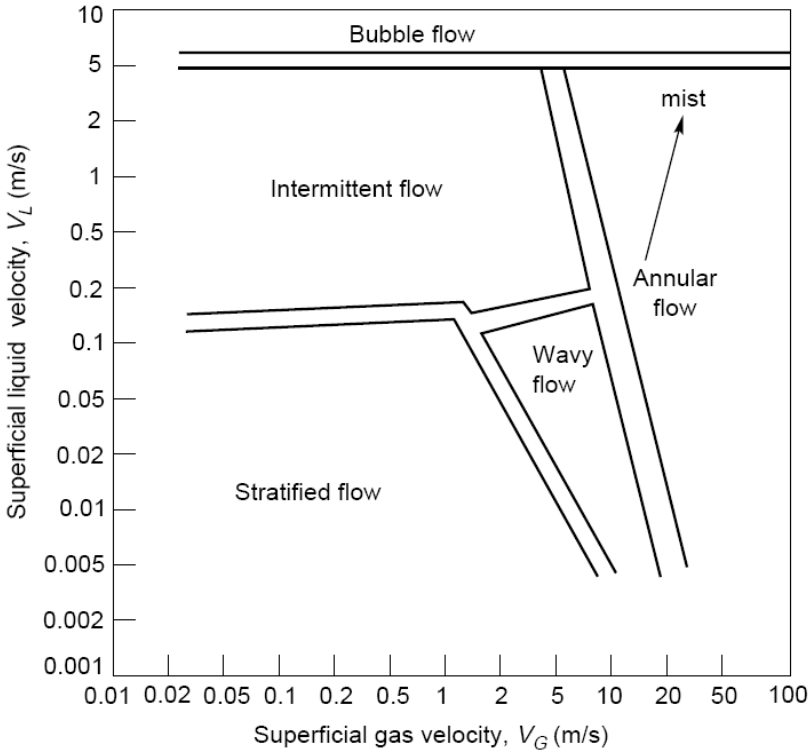

Figure 5.14: Modified flow pattern map (Chhabra and Richardson, 1984)

vertical pipe was presented.

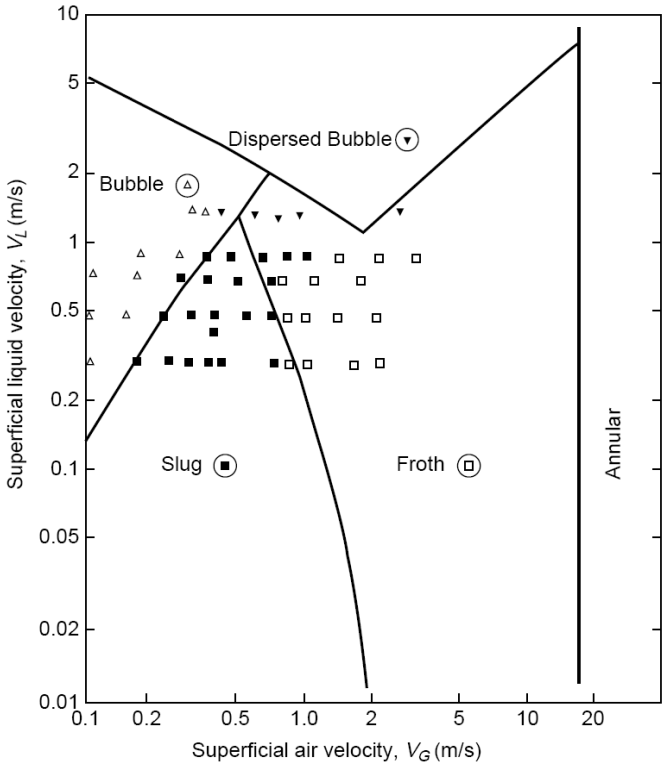

Figure 5.15: Experimental Khatib and Richardson (1984) flow patterns for upward flow of air and china clay suspensions ($D = 38mm$)

5.5.3 Pressure drop and liquid holdup

Two phase pressure drop with non-Newtonian shear-thinning liquid properties was studied by Oliver and Young-Hoon (1968), Farooqi and Richardson (1982b), Farooqi et al. (1980), Chhabra et al. (1983), Chhabra and Richardson (1984) and Dziubinski (1995). These studies indicate that gas/non-Newtonian liquid two-phase flow hydrodynamics in pipes behaviour is different with gas/Newtonian liquid two-phase flow, which is of great industrial importance in the transport of

fluids and related operations. For example, gas/non-Newtonian liquid two-phase flow in pipelines has a significant reduction in the average pressure gradient.

Lockhart and Martinelli (1949) (L-M) approach led to the definition of a factor, which is shown in equation 5.31, that correlates the liquid holdup, wetted angle and other fields to the ratio of two-phase pressure gradient over the single gas phase pressure gradient. Two phase liquid holdup or void fraction with non-Newtonian shear-thinning liquid properties was reviewed in Oliver and Young-Hoon (1968), Heywood and Charles (1979), Farooqi and Richardson (1982a) and Das et al. (1992).

$$\chi = (\frac{\Delta P_L/L}{\Delta P_G/L})^{1/2} \tag{5.31}$$

5.5.3.1 Drag reduction phenomenon

Increasing pipeline capabilities, production rates, faster transportation and ships are some of the objectives of various industries, including those of hydrocarbons. Reducing internal frictions and pressures is a natural route to accomplish that purpose. For hydrocarbon multiphase flows in pipes, seven decades ago, two perceptions cropped up simultaneously: drag reduction by chemical agents (DRA), first observed by Toms (1949), also known as Toms effect, and drag reduction by gas injection initiated by Clark and Shapiro (1949).

The investigation presented here is concerned with drag reduction by gas injection in non-Newtonian liquid for stratified and slug flow regimes. It was established by Clark and Shapiro (1949) that the pressure gradient of a high viscosity liquid flowing in pipelines may be reduced by the injection of a much lower viscosity liquid than is immiscible with the viscous fluid. Agarwal et al. (1973) performed their gas oil experiments and observed that a reduction of pressure gradient by 30 to 50 percent can be achieved, depending on the oil velocity. Earlier mathematical approaches by Charles and Redberger (1962) and Russell and Charles (1959) were able to predict substantial pressure gradient reduction in two phase flows.

Drag reduction by gas injection has been known for six decades, and 25 years ago, Chhabra et al. (1983) and Farooqi et al. (1980), and more recently, Xu et al.

(2007) confirmed some of the existing experimental results. Drag reduction by chemical agent DRA and solvents is another technique for reducing resistance of liquid to flow.

Moreover, another type of drag reduction, mainly dealing with liquid-liquid systems that is based on lubrication of oil by water in pipes, was first mentioned by Isaacs and Speed (1904). These authors noted that concentric flow regime may be established, and the denser fluid separates from the lighter and envelops it, resulting in core annular flow (CAF). Consequently, the reduction of the frictional resistance of the lighter fluid to the flow is obtained. Core annular flow regimes and lubrications in pipes were extensively analysed, both experimentally and theoretically, in Joseph et al. (1984), Bai et al. (1992), Joseph et al. (1992), Bannwart (2001) and Rodriguez and Bannwart (2008).

The comparison between the pressure drop, with and without air injection, has been traditionally carried out in the form of the drag ratio coefficient in equation 5.32, which is applicable to any flow pattern:

$$\phi_L^2 = \frac{(\Delta P_{TP}/L)}{(\Delta P_L/L)} \tag{5.32}$$

where $(\Delta P_{TP}/L)$ is the two-phase pressure gradient and $(\Delta P_L/L)$ is the pressure gradient for a liquid flowing alone at the same superficial velocity as in the two phase flow. There is extensive literature on two phase gas/non-Newtonian fluid friction factors. This interest is easily explained by the fact that non-Newtonian fluids are typically fluids of high viscosity and their transport can pose serious engineering difficulties.

It has to be mentioned that the drag reduction phenomenon was observed not only in high viscosity liquid with non-Newtonian properties, but also in Newtonian liquid, such as water. However, this drag reduction phenomenon was more obvious in gas/non-Newtonian liquid two-phase flow.

5.5.3.2 Oliver and Young-Hoon (1968)

Oliver and Young-Hoon (1968) is the forerunner of researching the gas/non-Newtonian liquid two-phase flow. They theoretically analyse the

slug flow and annular flow and propose single models for these two flow regimes. They also conducted some experiments using non-Newtonian power-law liquids, which are sodium salt of carboxymethyl cellulose (SCMC) solution and polymer-Polyethylene oxide solution (Polyox WSR 301). Pressure drop and liquid holdup was obtained from this experiment and compared with Lockhart-Martinelli correlation (Lockhart and Martinelli, 1949). However, this correlation is over estimated. Although Oliver and Young-Hoon (1968) did not propose a new correlation, the work that they did was fundamental for subsequent research of the gas-non-Newtonian shear-thinning liquid two-phase flow.

5.5.3.3 Heywood and Charles (1979)

The Taitel and Dukler (1976) technique that was initially developed for fully stratified Newtonian flows, was extended to gas non-Newtonian stratified flows by Heywood and Charles (1979).

Drag reduction has eventually led to:

$$\phi_L^2 = \frac{\widetilde{u}_L^n}{\widetilde{D}_L^{1+n}} \cdot \frac{(\widetilde{S}_G + \widetilde{S}_i)}{\widetilde{S}_G + \frac{\pi}{4}\frac{\widetilde{S}_i}{\widetilde{A}_L}} \tag{5.33}$$

where $\widetilde{u_k} = \dfrac{u_k}{u_{Sk}}$, $\widetilde{D_k} = \dfrac{D_k}{D}$, $\widetilde{S_k} = \dfrac{S_k}{D}$ and $\widetilde{A_k} = \dfrac{A_k}{D^2}$, They all are dimensionless factors. Heywood and Charles (1979) proposed this drag reduction correlation although the validation was not possible due to the absence of experimental data.

5.5.3.4 Farrooqi and Richardson

Farooqi and Richardson (1982a) modified the Lockhart and Martinelli (1949) model to predict the average liquid holdup for co-current flow of air and Newtonian and non-Newtonian (shear-thinning) liquids in either laminar or turbulent flow before air injection. Experiments also have been performed in a $42mm$ diameter horizontal pipe, and holdup was measured using $\gamma-$ray absorption method. The non-Newtonian liquid used in this experiment is

kaolin, water and glycerol mixture. Farooqi and Richardson (1982a) proposed a correction factor, J to be applied to the Lockhart-Martinelli parameter, and then they suggested using a modified parameter, χ_{mod} to replace χ, which is defined as:

$$\chi_{mod} = J\chi \tag{5.34}$$

where correction factor J is defined as:

$$J = \frac{u_{SL}}{u_{SL_c}} \tag{5.35}$$

u_{SL_c} is the critical velocity for the transition from laminar to turbulent flow. For a known power-law liquid, u_{SL_c} can satisfy the Reynolds number to 2000.

$$Re_{MR} = \frac{\rho u_{SL_c}^{2-n} D^n}{8^{n-1} m \left(\frac{3n+1}{4n}\right)^n} \tag{5.36}$$

Now, the average liquid holdup is suggested by Farooqi and Richardson (1982a):

$$\begin{aligned}
&\alpha_L = 0.24(\chi_{mod})^{0.8} && 0.01 \leq \chi_{mod} \leq 0.5 \\
&\alpha_L = 0.175(\chi_{mod})^{0.32} && 0.5 \leq \chi_{mod} \leq 5 \\
&\alpha_L = 0.143(\chi_{mod})^{0.42} && 5 \leq \chi_{mod} \leq 50 \\
&\alpha_L = \frac{1}{0.97 + \frac{19}{\chi_{mod}}} && 50 \leq \chi_{mod} \leq 500
\end{aligned} \tag{5.37}$$

Farooqi and Richardson (1982b) studies included drag reduction phenomenon in shear thinning suspensions, which has been reported to occur when air is injected into a laminar flow of liquid suspension and gives drag ratio, ϕ_L^2, obtained as:

$$\phi_L^2 = (\lambda_L)^{1-n} \tag{5.38}$$

The maximum drag reduction has been correlated with a ratio of apparent viscosity to apparent viscosity under $Re_{MR} = 2000$. An empirical correlation of this maximum drag reduction has been obtained and is the following:

$$\begin{aligned}
&\min(\phi_L^2) = J^{0.205}, && 0.6 \leq J \leq 1 \\
&\min(\phi_L^2) = 1 - 0.0315J^{-2.25}, && 0.35 \leq J <\leq 0.6 \\
&\min(\phi_L^2) = 1.9J, && 0.05 \leq J \leq 0.35
\end{aligned} \tag{5.39}$$

5.5.3.5 Dziubinski (1995)

Dziubinski (1995) has put forward an alternative formulation for the prediction of the two-phase pressure drop for a gas and shear-thinning liquid two-phase flow in the intermittent. His analysis was based on a loss coefficient which is of the form:

$$\Lambda = \frac{\tau_w \rho D^2}{\mu^2} \tag{5.40}$$

for non-Newtonian power-law fluids and:

$$\Lambda = m(\frac{4n}{3n+1})Re_{MR}^2 \tag{5.41}$$

For non-Newtonian power-law liquid in laminar flow, he suggests the drag reduction is:

$$\phi_L^2 = (\frac{1 + 1.036 \times 10^{-4} Re_{TP}^{1.235}}{1 + 1.036 \times 10^{-4} Re_L^{1.235}}) \cdot \lambda_L^{1-n} \tag{5.42}$$

where λ_L is the input liquid fraction, which is expressed in the following:

$$\lambda_L = \frac{u_{SL}}{u_{SL} + u_{SG}} \tag{5.43}$$

Reynolds numbers in equation 5.42, Re_L is based on the superficial velocity of the power-law liquid, and Reynolds number Re_{TP} is defined as:

$$Re_{TP} = \frac{\rho u_m^{2-n} D^n}{8^{n-1} m \left(\frac{3n+1}{4n}\right)^n} \tag{5.44}$$

and he report that the resulting formulae for coefficient loss for non-Newtonian power-law liquid in laminar flow, which have a form:

$$\Lambda_{TP} = 8\lambda_L^n \phi_L^2 Re_{TP} \tag{5.45}$$

and for non-Newtonian power-law liquid in turbulent flow ($Re_{TP} > 2000$), Dziubinski (1995) suggested that the expression in terms of the loss coefficient Λ_{TP} is,

$$\Lambda_{TP} = 0.0131\lambda_L \left(\frac{3n+1}{4n}\right)^{-5} \cdot \exp\left(1.745 \cdot \frac{3n+1}{4n} - 0.634\lambda_L\right) \cdot [(\frac{3n+1}{4n})^2 Re_{TP}]^{7/4} \tag{5.46}$$

Dziubinski (1995) compared equation 5.42 and extensive experimental data, giving an error ±15%.

5.5.3.6 Other literature reviews

Ruiz-Viera et al. (2006) experimentally observed the mixture flows of air/lubricating grease, using different geometries with both smooth and rough surfaces, and finally, a combination of a power-law and a sigmoidal-type equation was proposed to describe the experimental evolution of the drag ratio. These methods need extra information about two-phase flow structures, so it is easy to solve the void fraction and pressure drop of two-phase flows. However, these methods are entirely empirical, and the extrapolation beyond the range of experimental conditions must be treated with reserve.

Xu et al. (2007) and Xu et al. (2009) extended the analysis of Heywood and Charles (1979) for inclined pipes. Two flow patterns were considered: stratified flow, which is more common in downward inclined pipe, and plug flow, which appears more often in upward inclined pipes.

An experimental and theoretical study of gas-shear-thinning liquid flows through an inclined pipe was conducted. They did propose an average void fraction and pressure drop with a reasonable estimate. The proposed models were tested extensively against air/different CMC solutions flows over wide ranges of inclination angles and pipe diameters. Comparison with experimental data has shown that proposed equations deviated 30% and 20% in case of stratified and slug flow, respectively.

5.6 Conclusion

In this chapter, different non-Newtonian fluids and their mathematical models were reviewed first. Then, the analytical velocity distribution concerning the laminar, steady, incompressible fully-developed non-Newtonian single phase flow was successfully obtained through the formula derivation from the steady invariant N-S momentum equation in cylindrical coordinate. Compared with the parabolic distribution for a Newtonian fluid ($n = 1$), the profile is flatter for a shear-thinning fluid and sharper for a shear-thickening fluid. The maximum velocity is achieved at the pipe axis, $r = 0$. This is the same as the result

which was calculated using Fluent software and shown in the Appendix B. The pressure gradient calculated from Fluent software shows that it sharply increases with increasing power-law index, no matter whether flow is laminar or turbulence. However, the pressure gradient increases linearly when the inlet velocity is enhanced with a given power-law index.

Two phase gas-shear-thinning fluid flow was introduced in the last section, and three of the most important factors of two phase flow, namely flow pattern map, pressure drop and liquid holdup, were reviewed in the last section. Gas-non-Newtonian fluid two-phase flow have usually received less attention compared with gas-water and gas-oil two-phase flow, it was observed that the properties of non-Newtonian fluid had a minimal effect on the flow pattern in horizontal and near horizontal flows. Drag reduction phenomenon is noticed by Farooqi and Richardson (1982b), Heywood and Charles (1979) and Dziubinski (1995), and different correlations are reviewed in the last section. Xu et al. (2009) extended the analysis of Heywood and Charles (1979) for inclined pipes, a theoretical drag reduction correlation was proposed although the interfacial friction factor f_i is considered to be equal to the gas friction factor f_G.

In this work, for non Newtonian two phase flow, the reformulation of previous work by Xu et al. (2009) is performed and is also extended to the case where the ratio of interfacial friction factor and gas friction factor is Froude number dependent according to Andreussi and Persen (1987) correlation. This extension showed the existence of non-uniqueness distribution of the shear thinning hold up. Moreover, it also indicates that extra drag reduction zones can appear.

References - 5

Agarwal, S. S., Gregory, G. A. and Govier, G. W. (1973), 'An analysis of horizontal stratified two-phase flow in pipes', *The Canadian Journal of Chemical Engineering* **51**(3), 280 – 286. (cited at page 99)

Andreussi, P. and Persen, L. (1987), 'Stratified gas-liquid flow in downwardly inclined pipes', *International Journal of Multiphase Flow* **13**(4), 565 – 575. (cited at page 105)

ANSYS-Fluent Inc (2008), *Fluent 12.0 User Manual*, Lebanon, N. H. (cited at page xiv, 80, 81)

Bai, R., Chen, K. and Joseph, D. D. (1992), 'Lubricated pipelining: stability of core annular flow. part 5. experiments and comparison with theory', *Journal of Fluid Mechanics* **240**, 97 – 132. (cited at page 100)

Bannwart, A. C. (2001), 'Modeling aspects of oil-water core-annular flows', *Journal of Petroleum Science and Engineering* **32**(2-4), 127 – 143. (cited at page 100)

Carreau, P. J., DeKee, D. and Chhabra, R. P. (1997), *Rheology of polymeric systems: principles and applications*, Hanser Gardner Publications. (cited at page 78)

Charles, M. E. and Redberger, P. J. (1962), 'The reduction of pressure gradients in oil pipelines by the addition of water: Numerical analysis of stratified flow', *The Canadian Journal of Chemical Engineering* **40**(2), 70 – 75. (cited at page 99)

Chhabra, R. P., Farooqi, S. I., Richardson, J. F. and Wardle (1983), 'Co-current flow of air and shear-thinning suspensions in pipes of large diameter', *Chemical Engineering Research and Design* **61**, 56 – 61. (cited at page 98, 99)

Chhabra, R. P. and Richardson, J. F. (1984), 'Prediction of flow pattern for the co-current flow of gas and non-newtonian liquid in horizontal pipes', *The Canadian Journal of Chemical Engineering* **62**(4), 449 – 454. (cited at page xv, 73, 96, 97, 98)

Chhabra, R. P. and Richardson, J. F. (1999), *Non-Newtonian flow in the process industries*, Butterworth-Heinemann. (cited at page xiv, 77, 78, 82, 84, 92)

Clapp, R. (1961), Turbulent heat transfer in pseudoplastic non-newtonian fluids, *in* 'International Development in Heat Transfer', Vol. Part III, New York. (cited at page 94)

Clark, A. F. and Shapiro, A. (1949), 'U.S. Patent'. (cited at page 99)

Das, S. K., Biswas, M. N. and Mitra, A. K. (1992), 'Holdup for two-phase flow of gas-non-newtonian liquid mixtures in horizontal and vertical pipes', *The Canadian Journal of Chemical Engineering* **70**(3), 431–437. (cited at page 99)

Dodge, D. and Metzner, A. (1959), 'Turbulent flow of non-newtonian systems', *AIChE Journal* **5**(2), 189 – 204. (cited at page 93, 94)

Dziubinski, M. (1995), 'A general correlation for two-phase pressure drop in intermittent flow of gas and non-newtonian liquid mixtures in a pipe', *Chemical Engineering Research and Design* **73**(5), 528 – 534. (cited at page x, 98, 103, 105)

Dziubinski, M., Fidos, H. and Sosno, M. (2004), 'The flow pattern map of a two-phase non-newtonian liquid-gas flow in the vertical pipe', *International Journal of Multiphase Flow* **30**(6), 551 – 563. (cited at page 73, 96)

El-emam, N., Kamel, A. H., El-shafei, M. and El-batrawy, A. (2003), 'New equation calculates friction factor for turbulent flow on non-newtonian fluids', *Oil and Gas Journal* **101**(36), 74. (cited at page 92, 93, 94)

Farooqi, S. I., Heywood, N. I. and Richardson, J. F. (1980), 'Drag reduction by air injection for suspension flow in a horizontal pipeline', *Transactions of the Institution of Chemical Engineers* **58**(1), 16–27. (cited at page 73, 98, 99)

Farooqi, S. and Richardson, J. (1982a), 'Horizontal flow of air and liquid (newtonian and non-newtonian) in a smooth pipe. part i: A correlation for average liquid holdup', *Trans. IChemE* **60**, 292 – 305. (cited at page 99, 101, 102)

Farooqi, S. and Richardson, J. (1982b), 'Horizontal flow of air and liquid (newtonian and non-newtonian) in a smooth pipe. part ii: Average pressure drop', *Trans. IChemE* **60**(6), 323 – 333. (cited at page 98, 102, 105)

Gao, P. and Zhang, J.-j. (2007), 'New assessment of friction factor correlations for power law fluids in turbulent pipe flow: A statistical approach', *Journal of Central South University of Technology* **14**, 77–81. (cited at page 93)

Hemeida, A. M. (1993), 'Friction factors for yieldless fluids in turbulent pipe flow in turbulent pipe flow', *The Journal of Canadian Petroleum Technology* **32**(1), 32 – 35. (cited at page 94)

Heywood, N. I. and Charles, M. E. (1979), 'The stratified flow of gas and non-newtonian liquid in horizontal pipes', *International Journal of Multiphase Flow* **5**(5), 341 – 352. (cited at page x, 99, 101, 104, 105)

Irvine, T. F. (1988), 'A generalized blasius equation for power law fluids', *Chemical Engineering Communications* **65**(1), 39–47. (cited at page xv, 93, 95)

Isaacs, J. D. and Speed, J. B. (1904), 'Method of piping fluids'. (cited at page 100)

Joseph, D. D., Bai, R., Chen, K. P. and Renardy, Y. Y. (1992), 'Core-annular flows', *ANNUAL REVIEW OF FLUID MECHANICS* **29**, 65 – 90. (cited at page 100)

Joseph, D. D., Nguyen, K. and Beavers, G. S. (1984), 'Non-uniqueness and stability of the configuration of flow of immiscible fluids with different viscosities', *Journal of Fluid Mechanics* **141**, 319 – 345. (cited at page 100)

Kemblowski, Z. and Kolodziejski, J. (1973), 'Flow resistances of non-newtonian fluids in transitional and turbulent flow', *International Chemical Engineering* **13**, 265. (cited at page 94)

Khatib, Z. and Richardson, J. F. (1984), 'Vertical co-current flow of air and shear thinning suspensions of kaolin', *Chemical Engineering Research Design* **62**(3), 139 – 154. (cited at page xv, 96, 98)

Lockhart, R. W. and Martinelli, R. C. (1949), 'Proposed correlation of data for isothermal two-phase, two-component flow in pipes', *Chemical Engineering Progress* **45**(1), 39 – 48. (cited at page 99, 101)

Macosko, C. (1994), *Rheology: Principles, measurements, and applications*, VCH Publishers. (cited at page 78, 79)

Mandhane, J. M., Gregory, G. A. and Aziz, K. (1974), 'A flow pattern map for gas - liquid flow in horizontal pipes', *International Journal of Multiphase Flow* **1**(4), 537 – 553. (cited at page 96)

Metzner, A. B. and Reed, J. C. (1955), 'Flow of non-newtonian fluids - correlation of the laminar, transition, and turbulent-flow regions', *AIChE Journal* **1**(4), 434 – 440. (cited at page 89, 92, 93)

Oliver, D. and Young-Hoon, A. (1968), 'Two-phase non-newtonian flow. part i: Pressure drop and holdup', *Trans. IChemE* **46**, 106 – 115. (cited at page x, 98, 99, 100, 101)

Rodriguez, O. M. H. and Bannwart, A. C. (2008), 'Stability analysis of core-annular flow and neutral stability wave number', *AIChE Journal* **54**(1), 20–31. (cited at page 100)

Ruiz-Viera, M., Delgado, M., Franco, J., S?nchez, M. and Gallegos, C. (2006), 'On the drag reduction for the two-phase horizontal pipe flow of highly viscous non-newtonian liquid/air mixtures: Case of lubricating grease', *International Journal of Multiphase Flow* **32**(2), 232 – 247. (cited at page 104)

Russell, T. W. F. and Charles, M. E. (1959), 'The effect of the less viscous liquid in the laminar flow of two immiscible liquids', *The Canadian Journal of Chemical Engineering* **37**(1), 18 – 24. (cited at page 99)

Ryan, N. W. and Johnson, M. M. (1959), 'Transistion from laminar to turbulent flow in pipes', *AIChE Journal* **5**(4), 433 – 435. (cited at page 89)

Szilas, A., Bobok, E. and Navratil, L. (1981), 'Determination of turbulent pressure loss of non-newtonian oil flow in rough pipes', *Rheologica Acta* **20**(5), 487 – 496. (cited at page 94)

Taitel, Y., Bornea, D. and Dukler, A. E. (1980), 'Modelling flow pattern transitions for steady upward gas-liquid flow in vertical tubes', *AIChE Journal* **26**(3), 345 – 354. (cited at page 96)

Taitel, Y. and Dukler, A. (1976), 'A theoretical approach to the lockhart-martinelli correlation for stratified flow', *International Journal of Multiphase Flow* **2**(5-6), 591 – 595. (cited at page 101)

Toms, B. (1949), 'Some observations on the flow of linear polymer solutions through straight tubes at large reynolds numbers', *Proceedings at 1st International Congress On Rheology, Holland, Amsterdam, section II* **13**, 135 – 141. (cited at page 99)

Weisman, J., Duncan, D., Gibson, J. and Crawford, T. (1979), 'Effects of fluid properties and pipe diameter on two-phase flow patterns in horizontal lines', *International Journal of Multiphase Flow* **5**(6), 437 – 462. (cited at page 96)

Xu, J., Wu, Y., Shi, Z., Lao, L. and Li, D. (2007), 'Studies on two-phase co-current air/non-newtonian shear-thinning fluid flows in inclined smooth pipes', *International Journal of Multiphase Flow* **33**(9), 948 – 969. (cited at page 73, 96, 99, 104)

Xu, J., xiang Wu, Y., Li, H., Guo, J. and Chang, Y. (2009), 'Study of drag reduction by gas injection for power-law fluid flow in horizontal stratified and slug flow regimes', *Chemical Engineering Journal* **147**(2-3), 235 – 244. (cited at page 104, 105)

Chapter 6

Two phase gas/shear-thinning liquid stratified flow

6.1 Introduction

This chapter deals with issues associated with the drag reduction of stratified gas-non-Newtonian shear-thinning liquid flow in horizontal pipes. There are three reasons for starting from this specific flow regime.

4. Stratified flow presents the simplest interface configuration considered in two-phase flows, and experimental data for validating stratified flow is available. Either increasing the gas velocity to get annular flow, or increasing the liquid velocity to achieve the slug flow, an accurate prediction and a further understanding of stratified flow will be necessary.

5. Although topology of the interface in annular flow has a core configuration, the interfacial behaviour in stratified and annular flows is similar. Better understanding of stratified flow will help us to understand more complex features occurring in annular flow.

6. More importantly, stratified flow plays an important role in the slug flow regime, which is the primary objective of this study. As previously described, a slug unit is composed of two parts - a dispersed bubble region

and stratified film region, which are also called slug body and film zone separately in Chapter 7.

6.2 Chapter outline

For the prediction of the average liquid holdup and drag reduction for the gas/non-Newtonian shear-thinning stratified flow, the present work attempts to investigate approximated limit Lockhart-Martinelli (L-M) correlation validation in established stratified flow, also extending this approach when interfacial friction is gas friction dependent; for example, by means of Andreussi and Persen (1987) correlation. Firstly, a steady state model of stratified gas-non-Newtonian flow in horizontal pipes was introduced, which is derived by Taitel and Dukler (1976) for gas/Newtonian stratified flow; in particular, an extension to interfacial Andreussi and Persen (1987) correlation has been carried out for this work. In this regime, three-dimensional computational fluid dynamics simulations with Fluent volume of fluid (VOF) method were performed to compare the drag reduction ratio with experimental data and results from the steady state model. Taking advantage of 3D CFD capabilities, an attempt was made to estimate pressure gradients along pipes in order to evaluate non-Newtonian liquid wall friction factors and compare these values with standard correlations.

6.3 Governing equations of the stratified model

As explained in the chapter outline, the Taitel and Dukler (1976) model is considered for steady state gas-liquid flows (see figure 6.1), and therefore, momentum equations for two phase flow for either Newtonian or non-Newtonian systems reduce to a differential system (Bishop and Deshande, 1986)

$$-A_L\left[\rho_L\hat{\beta}\frac{\partial u_L^2}{\partial x}+\left(\frac{\partial p}{\partial x}\right)_{tp_L}\right]=\tau_{LW}S_L-\tau_{\mathrm{i}}S_{\mathrm{i}}+g\cdot\rho_L A_L\left[\frac{\partial h_L}{\partial x}-\sin\beta\right] \quad (6.1)$$

$$-A_G\left[\rho_G\hat{\beta}\frac{\partial u_G^2}{\partial x}+\left(\frac{\partial p}{\partial x}\right)_{tp_G}\right]=\tau_{GW}S_G+\tau_{\mathrm{i}}S_{\mathrm{i}}+g\cdot\rho_G A_G\left[\frac{\partial h_G}{\partial x}-\sin\beta\right] \quad (6.2)$$

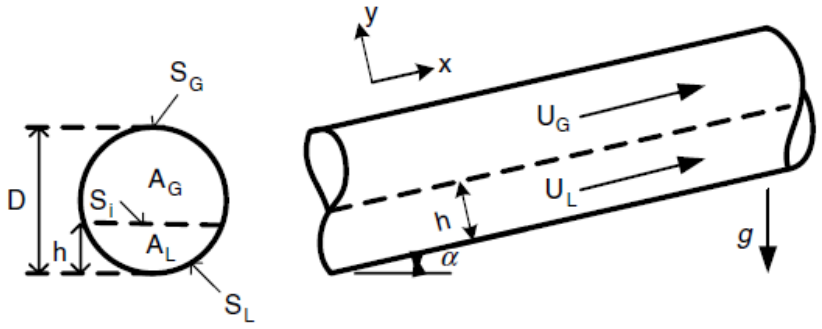

Figure 6.1: Illustration of geometry of the idealised stratified flow in pipeline

with u_k, A_k being respectively the velocity and flow cross-section area of the phase k (L for liquid, G for gas), ρ_k its density, S_k its wetted perimeter, h_k is the phase height, τ_{kW} and α the shear stress applied on the wall pipe by the phase and the angle of the inclination of the pipe. $\tau_{\mathrm{i}} S_{\mathrm{i}}$ represents the work exerted by the interfacial force between phases on the interface S_{i}, which is give in equaiton 2.14. $\left(\frac{\partial p}{\partial x}\right)_{tp_k}$ stands for the pressure gradient of the phase k in the two phase system. The phase wall τ_{kW} and interfacial τ_{i} shear stress were estimated from single phase flows and have the following general form:

$$\tau_{kj} = \frac{1}{2} f_k \rho_k (u_k - u_j)|u_k - u_j| \tag{6.3}$$

Here $\tau_i = \tau_{GL}$, and velocity on the wall $u_W = 0$.

The coefficient, $\hat{\beta}$ accounts for the kinetic energy correction term. For non-Newtonian shear-thinning, shear-thickening power law liquids that obey the Ostwald-de Waele rheology, the shear stress tensor τ_{ij} is related to the shear stress rate tensor θ_{ij} by equation 5.4.

The correction factor is given by

$$\hat{\beta} = \frac{2(2n+1)(5n+3)}{3(3n-1)^2} \tag{6.4}$$

where n represents the flow behaviour index.

Friction factors in the equation 6.3 in the case of turbulent gas and laminar liquid are given by

$$f_G = C_G{\cdot}\left(\frac{D_G{\cdot}\,u_L{\cdot}\,\rho_L}{\mu_G}\right)^{-m}$$
$$\text{and}\quad f_L = \frac{16}{Re_{MR}},\ \text{with}\ \ Re_{MR} = \frac{D_L^n{\cdot}\,u_L^{2-n}{\cdot}\,\rho_L}{8^{n-1}{\cdot}\,m{\cdot}\left(\frac{1+3{\cdot}\,n}{4{\cdot}\,n}\right)^n} \tag{6.5}$$

with coefficients $C_G = 0.079$ and and the consistency index $m = 0.25$, while μ_G is the viscosity of gas and Re_{MR} is the generalized Reynolds number of Metzner and Reed. For horizontal interfaces, a uniform steady state exists; hence, both potential and kinetic energies can be dropped from equation 6.1 and 6.2. One common way to extract extra information is by assuming (Lockhart and Martinelli, 1949) that in drag reduction experiments, $u_G >> u_L$ and $\left(\frac{\partial p}{\partial x}\right)_{tp_L} = \left(\frac{\partial p}{\partial x}\right)_{tp_G}$, where the second assumption is generally valid in the absence of interfacial level gradients and it is also an essential postulation in the Lockhart-Martinelli (L-M) factor calculation. Then, by eliminating the two phase pressure gradients $\left(\frac{\partial p}{\partial x}\right)_{tp}$, this leads to searching for equilibrium liquid height via an iteration procedure in relation 6.6 where velocities are taken as input fields.

$$\frac{\tau_{GW}S_G}{A_G} - \frac{\tau_{LW}S_L}{A_L} + \tau_{\mathrm{i}}S_{\mathrm{i}}{\cdot}\left(\frac{1}{A_G}+\frac{1}{A_L}\right) - g{\cdot}\,(\rho_L-\rho_G)\sin\alpha = 0 \tag{6.6}$$

Once the equilibrium holdup is obtained, the relation above for horizontal pipes can be reformulated by incorporating the shear stresses, friction factors and the rheology of the liquid expressions. Let χ^2 denote the Lockhart-Martinelli factor for liquids with rheology of an Ostwald-de Waele nature, and the general expression is rewritten in the reformulated form of that in Xu et al. (2007):

$$\chi^2 \cdot \Theta_L - \Theta_G \cdot \Gamma = 0$$

$$\text{where} \quad \Gamma = 1 - \frac{f_\text{i}}{f_G}\left(1 - \frac{u_L}{u_G}\right) \cdot |1 - \frac{u_L}{u_G}| \cdot \frac{\widetilde{S}_\text{i}}{\widetilde{S}_G}\left(1 + \frac{\widetilde{A}_G}{\widetilde{A}_L}\right) \tag{6.7}$$

$$\text{and} \qquad \Theta_L = \frac{\widetilde{S}_L \cdot \widetilde{u}_L^n}{\widetilde{A}_L \cdot \widetilde{D}_L^n},\ \Theta_G = \frac{\widetilde{S}_G \cdot \widetilde{u}_G^{2-m}}{\widetilde{A}_G \cdot \widetilde{D}_G^m}$$

Above, D stands for the pipe diameter, and all the parameters with tilde are non-dimensionalised as follows, $\widetilde{u_k} = \dfrac{u_k}{u_{Sk}}$, $\widetilde{D_k} = \dfrac{D_k}{D}$, $\widetilde{S_k} = \dfrac{S_k}{D}$ and $\widetilde{A_k} = \dfrac{A_k}{D^2}$, where u_{Sk} is the superficial velocity of the phase k. f_i is the interfacial friction factor.

Lockhart and Martinelli (1949) have suggested that liquid hold-up in the system is related to the drag reduction and to the Lockhart-Martinelli factor, χ^2, via a distinctive function. The generalised theoretical form of this function can be found in Taitel and Dukler (1976) and in Bishop and Deshande (1986). Following these authors and letting ϕ_G be the dimensionless pressure gradient ratio for the gas phase, the following is obtained:

$$\pi \cdot \phi_G^2 = \pi \cdot \frac{\Delta P_{tp}}{\Delta P_{spG}} = \widetilde{A}_L \cdot \Theta_L \cdot \chi^2 + \widetilde{A}_G \cdot \Theta_G$$

$$\text{where} \qquad \chi^2 = \frac{\Delta P_{sp_L}}{\Delta P_{sp_G}} \tag{6.8}$$

$$\text{and} \qquad \Delta P_{sp_k} = -\frac{4 \cdot \tau_{kW}}{D} = -\frac{2 \cdot f_k \cdot \rho_k \cdot u_k^2}{D}$$

The first relation in the equation 6.8 is obtained by summing momentum equations 6.1 and 6.2 for horizontal pipes. The second relation is the Lockhart-Martinelli factor definition, and the third is a simple balance of forces in single phase flow in circular pipe.

In these expressions, ΔP_{sp_L} and ΔP_{sp_G} represent the hypothetical pressure gradients that would exist in the pipe if the liquid or the gas flows alone in the pipe, and ΔP_{tp} stands for the pressure gradient when the gas and the liquid are flowing in the pipe.

Incorporating the first expression in the equation 6.7 into $\pi \cdot \phi_G^2$, the following is obtained:

$$\pi \cdot \phi_G^2 = \Theta_G \cdot \left(\widetilde{A}_L \cdot \Gamma + \widetilde{A}_G \right) \tag{6.9}$$

Using chain rules in the first relation in the equation 6.8 leads to the dimensionless pressure gradient for the liquid phase ϕ_L

$$\begin{gathered} \pi \cdot \phi_L^2 = \pi \cdot \frac{\Delta P_{tp}}{\Delta P_{sp_G}} \cdot \chi^{-2} \\ \text{or} \quad \pi \cdot \phi_L^2 = \widetilde{A}_L \cdot \Theta_L + \widetilde{A}_G \cdot \Theta_G \cdot \chi^{-2} \end{gathered} \tag{6.10}$$

Similarly, using the equation 6.7 into $\pi \cdot \phi_L^2$, gives:

$$\pi \cdot \phi_L^2 = \Theta_L \cdot \left(\widetilde{A}_L + \frac{\widetilde{A}_G}{\Gamma} \right) \tag{6.11}$$

From equations 6.7, a first expression of the Lockhart-Martinelli factor, χ^2 is obtained

$$\chi^2 = \frac{\Theta_G}{\Theta_L} \cdot \Gamma \tag{6.12}$$

An identical expression of the Lockhart-Martinelli factor is obtained from equations 6.9 and 6.11, that is

$$\chi^2 = \frac{\phi_G^2}{\phi_L^2} = \frac{\Theta_G}{\Theta_L} \cdot \frac{\widetilde{A}_L \cdot \Gamma + \widetilde{A}_G}{\widetilde{A}_L + \dfrac{\widetilde{A}_G}{\Gamma}} \tag{6.13}$$

The compatibility between the relations 6.12 and 6.13 is established for finite and non-singular values of Γ. The equation 6.11 indicates that the expression $\pi \cdot \phi_L^2$ becomes singular for $\lim \Gamma \to 0^+$.

The interfacial friction factor is one of the parameters that is essential in the specification of the function that links χ^2 to the flow fields. Several correlations

were reported in the literature; amongst them, Andreussi and Persen (1987) proposed an empirical correlation for the interfacial friction factor that is considered to be related to the gas friction factor via the dimensionless Froude number Fr,

$$\frac{f_{\mathrm{i}}}{f_G} = \begin{cases} 1.0 & \text{if } Fr \leq 0.36 \\ 1.0 + 29.7 \cdot (Fr - 0.36)^{0.67} \cdot \left(\dfrac{h_L}{D}\right)^{0.2} & \text{if } Fr > 0.36 \end{cases}$$

The dimensionless Froude number Fr for horizontal pipes is given by

$$Fr = u_G \cdot \left(\frac{\rho_G}{\rho_L - \rho_G} \cdot \frac{S_{\mathrm{i}}}{g \cdot A_G}\right)^{0.5} \tag{6.14}$$

The measurement of the drag reduction is given by the pressure drop ratio

$$\begin{aligned} \phi_R &= \phi_R\left(n, \widetilde{h}_L, \frac{u_L}{u_G}\right) \\ &= 1 - \phi_L^2 \\ &= 1 - \frac{\widetilde{S}_L \cdot \widetilde{u}_L^n}{\pi \cdot \widetilde{D}_L^n} \cdot \left(1 + \frac{\widetilde{A}_L \cdot \widetilde{S}_G}{1 - \dfrac{\pi \cdot D^4}{4} \cdot \dfrac{f_{\mathrm{i}}}{f_G} \cdot \left(1 - \dfrac{u_L}{u_G}\right) \cdot |1 - \dfrac{u_L}{u_G}| \cdot \widetilde{S}_{\mathrm{i}}}\right) \end{aligned} \tag{6.15}$$

Drag reductions occur when $\phi_R > 0$. The relation in 6.7 is similar to the one obtained in Xu et al. (2007), and here we adopt the ratio of physical velocities of liquid to gas is used as parameter.

6.4 Analytical result

Numerical experiments were conducted with CMC solutions, see table 6.1. These fluids are also considered in the paper of Xu et al. (2007).

Figure 6.2 illustrates the behaviour of the drag reduction factor as a function of the liquid holdup for $\frac{f_{\mathrm{i}}}{f_G} = 1$ Froude number independent. Figure 6.3 shows the

Table 6.1: Non-Newtonian CMC and Kaoline Liquid Phase Characteristics Taitel and Dukler (1976)

Non-Newtonian Phase	Density kg/m^3	m Flow Consistency Pa$\cdot s^n$	Flow Index n
CMC-1	0999.9	0.034	0.952
CMC-2	1000.0	0.407	0.765
CMC-3	1000.2	1.365	0.595
CMC-4	1000.4	2.434	0.350
Kaoline in Water	1360.0	4.25	0.175

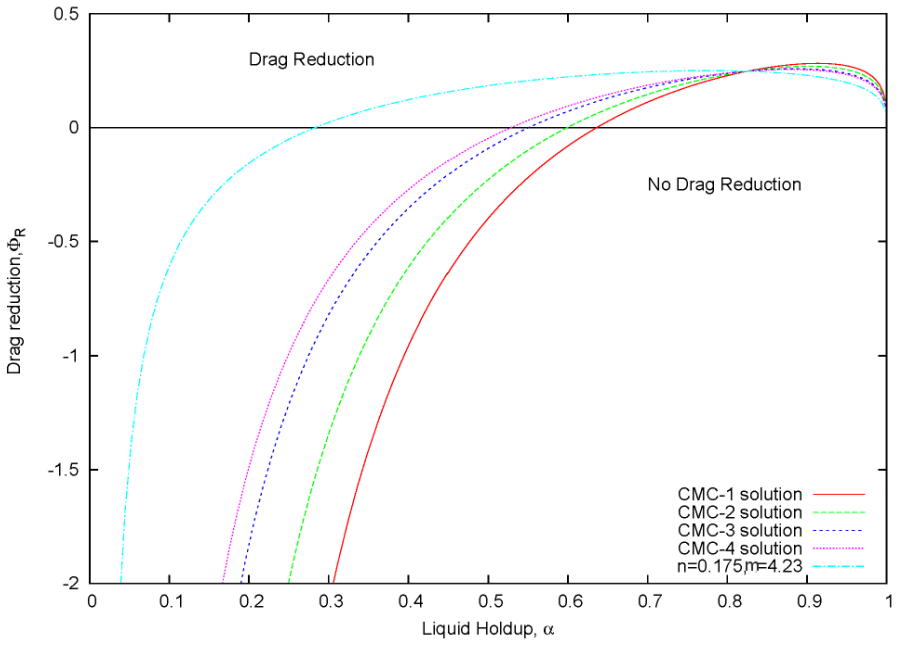

Figure 6.2: Drag reduction as function of the liquid holdup, Froude independent

drag reduction when the interfacial friction factor is related to Froude number.

It shows that the correlation role becomes noticeable for liquid film of $\alpha_L \leq 0.15$.

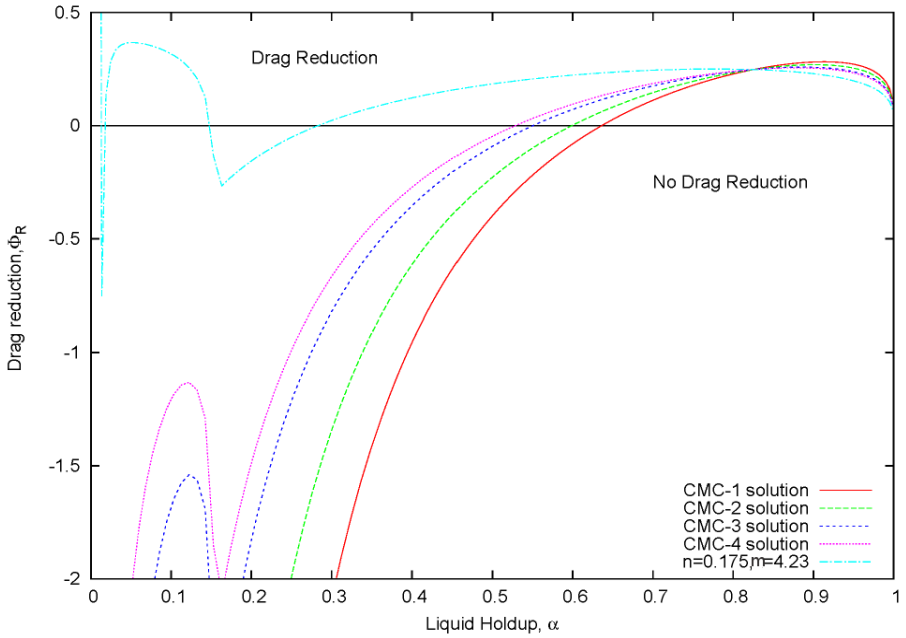

Figure 6.3: Drag reduction as function of the liquid holdup, Froude dependent

The maximum drag reduction attainable as a function of the index n and the integrated drag reduction are portrayed in Figures 6.4 and 6.5 with $\frac{u_L}{u_G} = 0.01$. The total or integrated drag reduction over a certain range of liquid hold-ups, performed with a trapezoidal integration method, is shown in Figure 6.5, and is defined by

$$I_{\phi_R}\left(n, \frac{u_L}{u_G}\right) = \int_{\phi_R>0} \phi_R\left(n, \widetilde{h}_L, \frac{u_L}{u_G}\right) \cdot d\widetilde{h}_L \tag{6.16}$$

Figures 6.6 and 6.7 illustrate the dependence of liquid hold-up on the flow rates ratio and on Lockhart Martinelli factor when the interfacial friction factor is compared with gas friction factor. Both cases show that at high L-M factor, the liquid hold-up varies slowly and is insensitive to the flow rates ratio u_{SL}/u_{SG}, but at lower L-M factor, it varies abruptly and is highly dependent on gas flow rates.

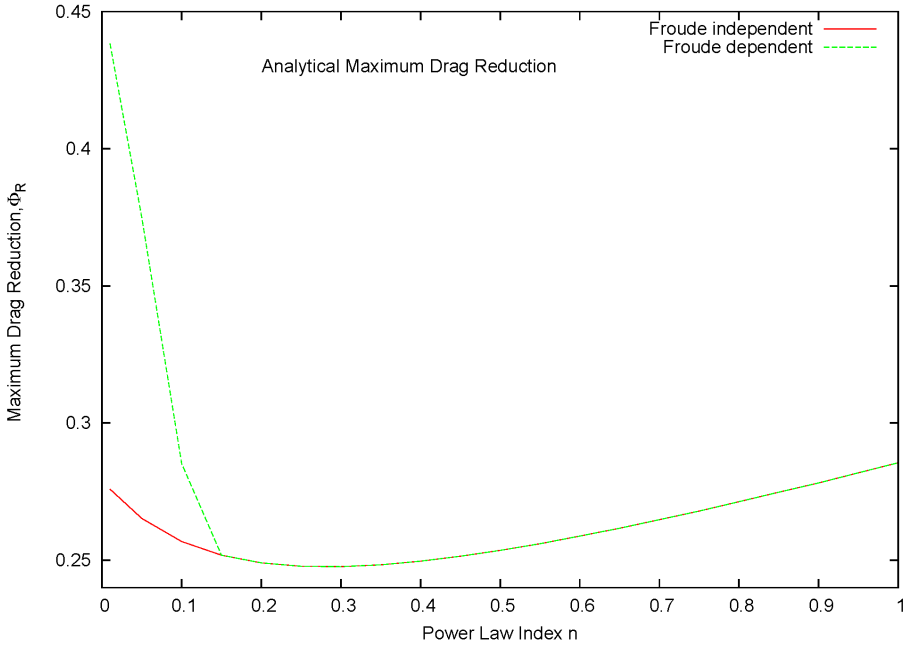

Figure 6.4: Maximum drag reduction with index

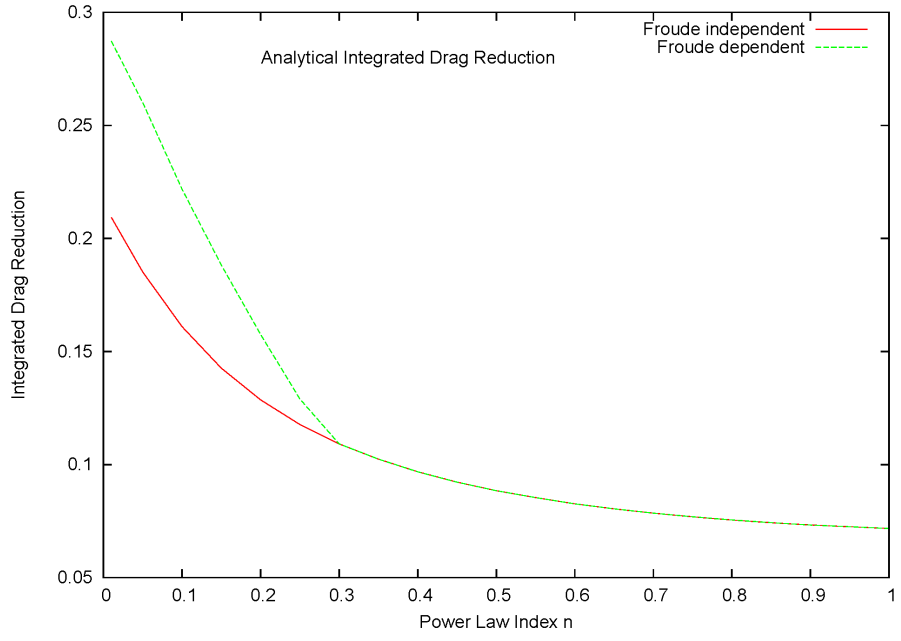

Figure 6.5: Integrated drag reduction with index

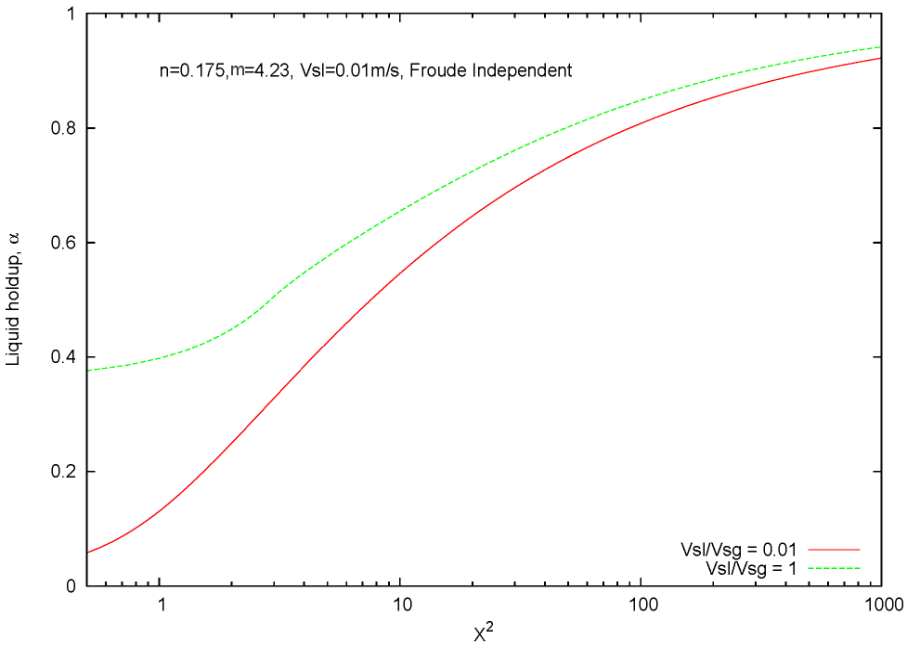

Figure 6.6: Lockhart-Martinelli factor, Froude independent

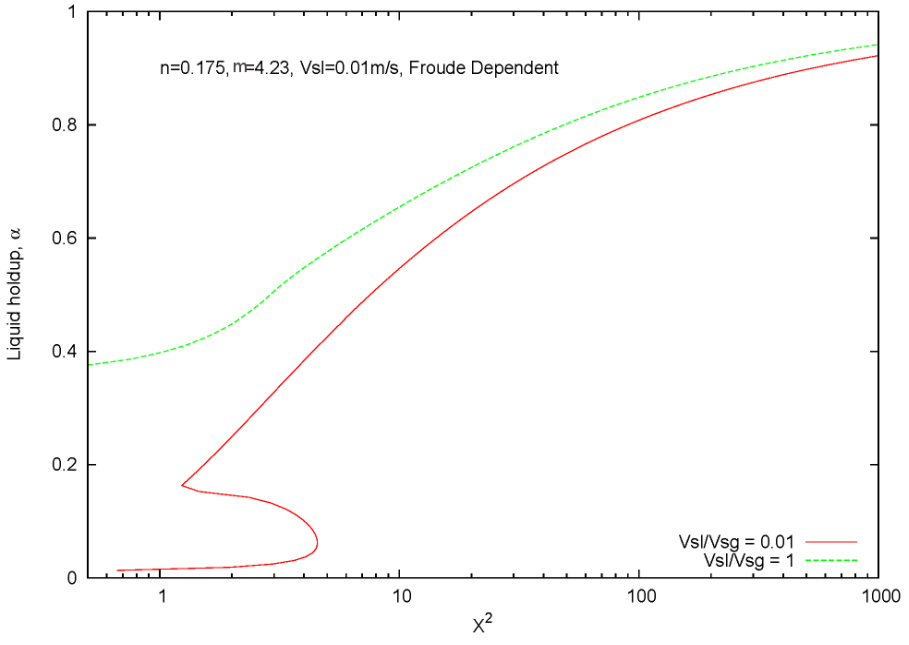

Figure 6.7: Lockhart-Martinelli factor, Froude dependent

In the case where Andreussi-Persen correlation is considered, for high gas flow rates, there is a critical interval of L-M with degenerate solutions for the liquid film holdup.

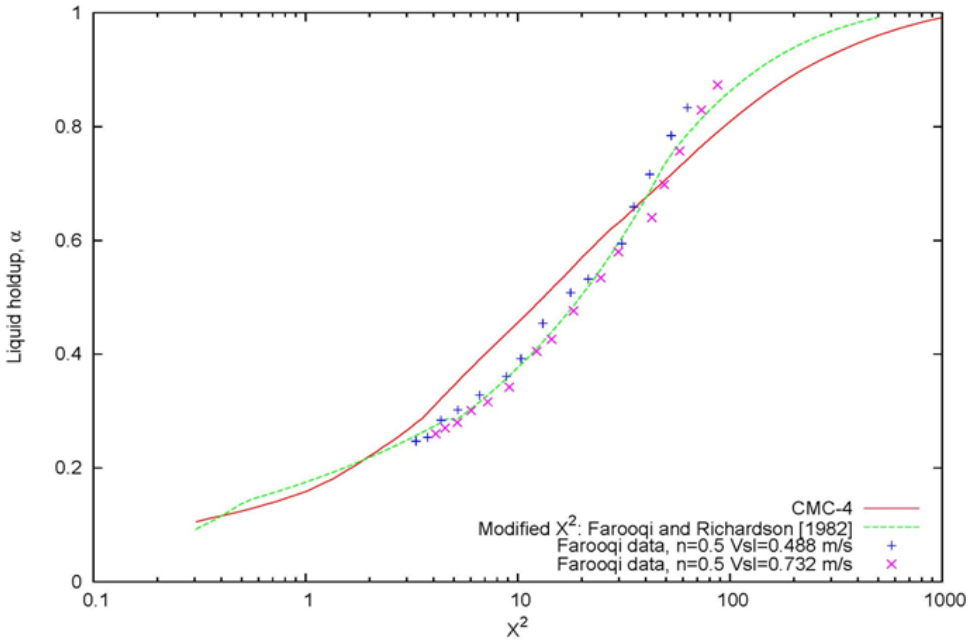

Figure 6.8: Comparison the present result with the modified χ^2 when $n = 0.5$

Figure 6.8 shows, the predicted liquid holdup was validated by experimental data and correlation that was review in equation 5.37. Here, our present work in some regions are over estimate, while they are underestimate in other regions, but the total error was no more than 9%.

6.5 CFD result

The validation of the analytical model of the drag reduction given by equation 6.15 is tested against experimental data from Farooqi, where Kaolin in water with air is used. The results are compared to the simulations obtained from 3D CFD VOF (volume of fluid) model.

6.5.1 Geometry and mesh

These simulations were conducted in a horizontal L-shaped pipe, whose mesh and specifications are shown in the table below. The length of the pipe upstream of

Table 6.2: Geometry and mesh specifications used for CFD

No. of Cells	No. of Faces	No. of Nodes	Length in m	Radius in m
1 091 667	3 310 740	1 129 542	9.00	0.05

the elbow is $1m$, while the part of the pipe down stream the elbow is $8m$. The mesh detail in the region of elbow is also reported.

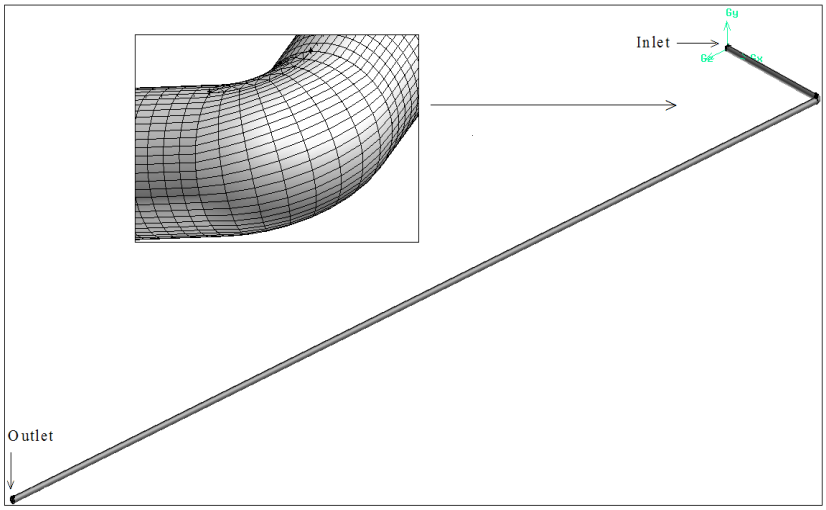

Figure 6.9: Geometry of L-pipe with detailed mesh (inset)

6.5.2 Mesh convergence study

CFD numerical simulations are computationally very expensive. One of the most significant factors influencing the computation time is the size of the grid. In order to identify the optimal mesh density to ensure the solution is independent

of the mesh resolution, a mesh sensitivity analysis has been carried out, in the construction and analysis of the CFD model. Three meshes were investigated and the adequate mesh results are studied. Below the table shows the convergence to the experimental data.

Table 6.3: Mesh convergence study for three 3D meshes.

Case	No. of Nodes	Drag reduction ratio	Experimental data
Mesh 1	56 4760	0.2	0.25
Mesh 2	1 129 542	0.27	0.25
Mesh 3	2 259 112	0.26	0.25

6.5.3 CFD set-up

The numerical simulations were carried out with the commercial CFD package Fluent. The second order upwind discretisation was used for both momentum and Turbulent $k-\epsilon$ equation. PISO algorithm, which was introduced in the Section 2.3.3, was chosen here as a pressure-velocity calculation procedure because of its good performance in finding a fast converged solution. The discretisation scheme that was used when solving volume fraction equations for the VOF explicit scheme is Geo-Reconstruct. These simulations were transient and the adaptive time step was used in these simulations and minimum time step size, and maximum time step size were set to 10^{-6} and 10^{-4} s respectively. The convergence criteria used were that all residuals should be smaller than 10^{-5} s. The inlet conditions were setup as a mass flow inlet boundary for each phase, and the outlet boundary condition was setup as a pressure outlet boundary. No slip was used to model the liquid velocity at the wall. The Global Courant Number was started from default which is 2.

6.6 The $k-\epsilon$ model

Newton and Behnia (2001) suggested that the functions of Lam and Bremhorst (1981) were amongst the best at predicting the general characteristics of the laminar sub-layer in turbulent pipe flow.

Lam and Bremhorst (1981) extended the $k-\epsilon$ model to the domain of the non-Newtonian fluids. Also, Malin (1997) has undertaken one of the first attempts to implement non-Newtonian properties in low-Reynolds number models, showing that a standard version of a Lam-Bremhorst low-Reynolds number was inadequate to describe velocity profiles and friction factors.

Standard $k-\epsilon$ Model was mentioned in section 2.3.2. In equation 2.38 and 2.39, for non-Newtonian fluids, μ is described in the following:

$$\mu = m\cdot \sqrt{\theta_{ij}\cdot \theta_{ij}}^{n-1} \tag{6.17}$$

Explicitly, the latter viscosity may be expressed by

$$\mu = m\cdot \left(\frac{1}{2}\cdot (\nabla\cdot \vec{u} + \nabla\cdot \vec{u}^T) : (\nabla\cdot \vec{u} + \nabla\cdot \vec{u}^T)\right)^{(n-1)/2} \tag{6.18}$$

The terms, f_1, f_2 and f_μ in the equations 2.39 are damping functions for the near wall, and they are expressed in Malin (1997) model, which differs from Lam-Bremhorst model only by the inclusion of an empirical parameter, $0.4 \leq m \leq 1.2$.

$$f_1 = 1 + \left(\frac{0.05}{f_\mu}\right)^3$$

$$\text{and} \qquad f_2 = 1 - exp(-\frac{R_t^2}{m^{\frac{1}{4}}}) \tag{6.19}$$

$$\text{while} \quad f_\mu = (1 - exp(-0.0165\cdot R_+))^2 \cdot \left(1 + \frac{20.5}{R_t}\right)$$

The specific Reynolds numbers are given by

$$R_t = \frac{\rho \cdot \ k^2}{\mu_t \cdot \epsilon}, \ R_+ = \frac{\rho \cdot \sqrt{k} \cdot y^+}{\mu_t} \tag{6.20}$$

where y^+ is the dimensionless normal distance to the wall for a wall bounded flow.

Low-Reynolds $k - \epsilon$ turbulence models require a grid with $y^+ \approx 1.0$ for a viscous sub layer regions. Finer grids are necessary in comparison with standard $k - \epsilon$ models (Missirlis et al. (2005)), this render low-Reynolds turbulence models expensive regarding CPU time consuming.

6.6.1 Fluid properties

The table below depicts the test conditions used in CFD, where u_{SL} and u_{SG} are the liquid and gas superficial velocities. The gas was considered compressible and the surface tension was taken as $\sigma = 0.070 N/m$. The density and the coefficients for the non-Newtonian liquid are $\rho_L = 1360 kg/m^3$, n=0.175, $m = 4.25 Pa \cdot s^n$.

Table 6.4: Flow conditions used for validation in stratified regimes

u_{SL}(m/s)	u_{SG}(m/s)	α_l	Re_{MR}	Re_G
0.244	0.297	0.640	70	875
	0.550	0.521		1620
	1.100	0.383		3205
	2.794	0.277		8517

Table 6.4 shows that the shear-thinning liquid is in laminar condition since the liquid Reynolds number is $Re_{MR} < 2000$, while the gas phase is mainly turbulent.

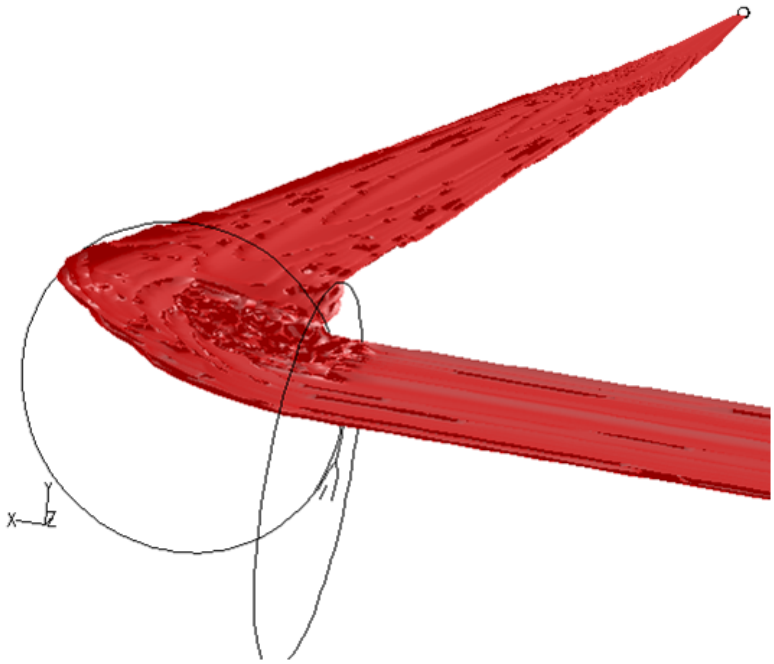

Figure 6.10: Stratified interface of the gas/shear-thinning liquid in L-shape pipeline

6.6.2 Validation and discuss of results

Figure 6.10 shows the interface of the gas/shear-thinning liquid in stratified flow regime. It can be seen that the interface of stratified flow is quite smooth.

Figure 6.11 shows the means of the liquid holdup time series at a cross sectional area. It can be figured out that, after a slug because of the initial condition, the fluid in the domain eventually arranges itself into stratified wavy flow condition.

Figure 6.12 shows that the steady stratified model is able to predict the pressure drop with good agreement with experimental data from Farooqi and Richardson (1982b). Furthermore, the agreement is extended to a wide range of gas flow rates. The distribution of the pressure drop with gas flow rate is also well described and follows the experimental profile. These profiles exhibit a maximum drag reduction of 0.335 for $u_{SG} \approx 0.8m/s$ and decrease more or less linearly as the gas flow rate increases.

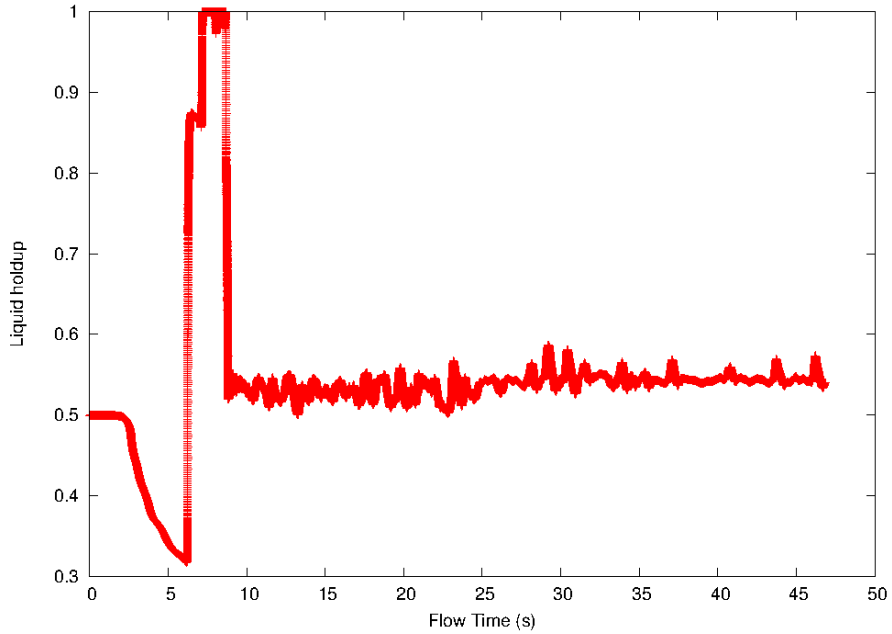

Figure 6.11: Liquid holdup traces at 7 m from the elbow for stratified wavy at $u_{SL} = 0.244m/s, u_{SG} = 1.1m/s$

The profile of drag reduction calculated from CFD also shows the same tendency, but over-estimates the maximum drag reduction. The discrepancy from the data is more apparent at high flow rates ratio. Although the VOF CFD model is a two phase and single field model, it gives globally satisfactory agreement with data.

6.6.3 Non-Newtonian liquid wall friction factor analysis

In this section, the attempt is to estimate the non-Newtonian liquid wall friction factor by combining CFD simulations with the two fluid stratified model.

The procedure is as follows: once the developed flow reaches the stratified regime, the pressure gradient is estimated from CFD simulations, and that quantity is substituted into gas momentum equation 6.2; hence, by iterating the momentum equation for the equilibrium height, the solution is then used in the equation 6.6, which is solved for f_L.

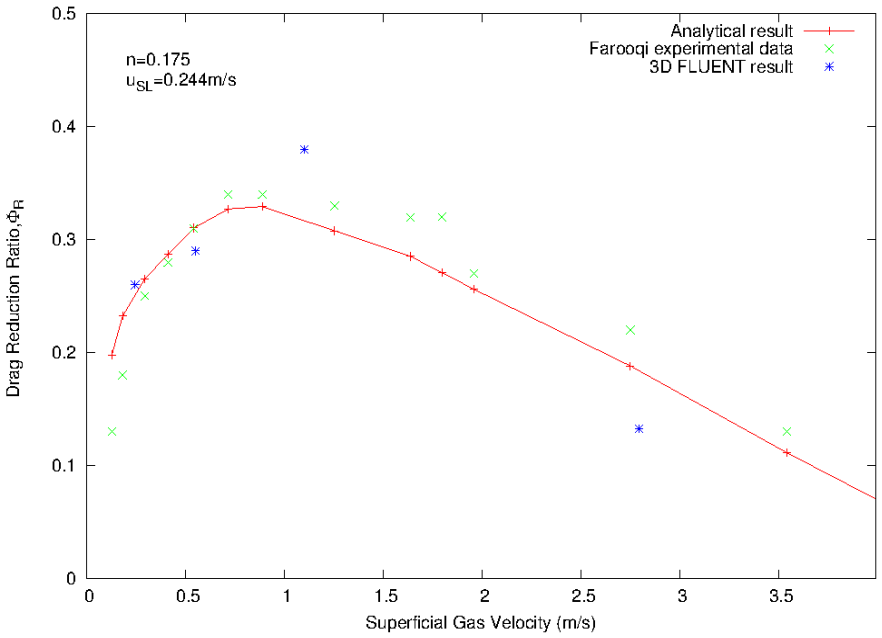

Figure 6.12: Drag reduction obtained with analytical form (equation 6.15) compared with experimental data (x) from Farooqi and Richardson (1982b) and with 3D CFD simulations ($*$)

$$\tau_{LW} = \frac{A_L}{A_G}\cdot \tau_{GW}\cdot \frac{S_{GW}}{S_{LW}} + \frac{A}{A_G}\cdot \tau_{\mathrm{i}}\cdot \frac{S_{\mathrm{i}}}{S_{LW}} \tag{6.21}$$

$$\text{and} \qquad f_L = 2\cdot \frac{\tau_{LW}}{\rho_L \cdot u_L^2}$$

The non-Newtonian liquid wall friction factor in either smooth or rough pipes is expressed by an empirical correlation in equation 6.5, similar to correlations for Newtonian fluids. The approach described above estimates the non-Newtonian liquid wall pipes friction factors, and they are compared to empirical correlations obtained from relation 6.5 in figure 6.13.

As in the previous Figure, CFD calculations give reasonable agreement with empirical correlations at low flow rates ratio $\frac{u_{SG}}{u_{SL}}$. At a given liquid flow rate, increasing disparity appears as gas flow rate increases.

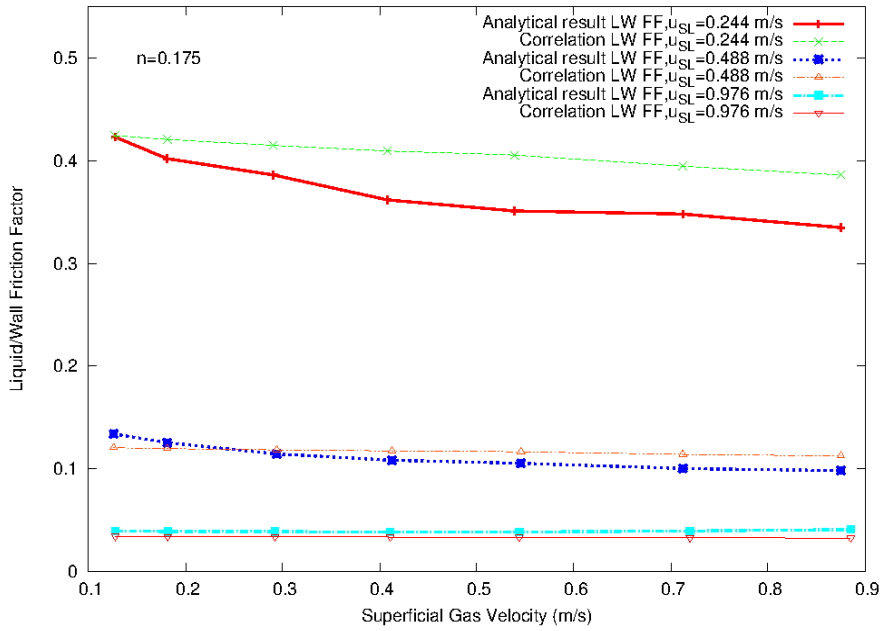

Figure 6.13: Non-Newtonian liquid wall friction factors: Comparison between empirical correlations and the procedure using CFD simulations

6.7 Conclusion

The accountability of the interfacial friction factor for the drag reduction was highlighted, especially at low liquid holdups. Due to the appearance of multiple solutions of liquid holdup, this suggests that gas liquid interface is unstable at high gas flow rate.

A mechanistic approach for two-phase steady invariant (fully stratified flows) gas and non-Newtonian liquids was tested and validated with experimental data. In comparing pressure gradients, it showed a great agreement with data for wide range of gas flow rates. Drag reduction ratio calculated from CFD also shows the same tendency, but over-estimates the maximum drag reduction. The discrepancy from the data is more apparent at high flow rates ratio. An attempt was made to evaluate non-Newtonian wall friction factors with the help of CFD, and a reasonable agreement was obtained with empirical correlations - apart from low liquid flow rate cases. The Andreussi and Persen (1987) correlation

could be considered in the CFD simulation to calculate the stratified flow using the User-Defined Functions.

In our case, we used the standard wall function $30 \leq y^+ \leq 300$, this lead to acceptable results for low gas velocity, but only produced reasonable results for high gas velocity, as shown in figure 6.12. On the other hand, it is suggested to use $y^+ \approx 1.0$ when enhanced wall function is turned on. In this case, with a pipe $9m$ long, I will end up with ≈ 8 million to 9 million cells, knowing that already with ≈ 1.2 million I have to use a time step of $10^{-6}s$ and I need at least 2 minutes of flow-time simulations.

6. TWO PHASE GAS/SHEAR-THINNING LIQUID STRATIFIED FLOW

References - 6

Andreussi, P. and Persen, L. (1987), 'Stratified gas-liquid flow in downwardly inclined pipes', *International Journal of Multiphase Flow* **13**(4), 565 – 575. (cited at page 114, 119, 132)

Bishop, A. and Deshande, S. (1986), 'Non-newtonian liquid-air stratified flow through horizontal tubes - ii', *International Journal of Multiphase Flow* **12**(6), 977 – 996. (cited at page 114, 117)

Farooqi, S. and Richardson, J. (1982b), 'Horizontal flow of air and liquid (newtonian and non-newtonian) in a smooth pipe. part ii: Average pressure drop', *Trans. IChemE* **60**(6), 323 – 333. (cited at page xv, 129, 131)

Lam, C. and Bremhorst, K. (1981), 'A modified form of the k-ϵ model for predicting wall turbulence', *Journal of Fluids Engineering, Transactions of the ASME* **103**(3), 456–460. (cited at page 127)

Lockhart, R. W. and Martinelli, R. C. (1949), 'Proposed correlation of data for isothermal two-phase, two-component flow in pipes', *Chemical Engineering Progress* **45**(1), 39 – 48. (cited at page 116, 117)

Malin, M. R. (1997), 'Turbulent pipe flow of power-law fluids', *International Communications in Heat and Mass Transfer* **24**(7), 977 – 988. (cited at page 127)

Missirlis, D., Yakinthos, K., Palikaras, A., Katheder, K. and Goulas, A. (2005), 'Experimental and numerical investigation of the flow field through a heat exchanger for aero-engine applications', *International Journal of Heat and*

Fluid Flow **26**(3), 440 – 458.
URL: *http://www.sciencedirect.com/science/article/pii/S0142727X04001675* (cited at page 128)

Newton, C. and Behnia, M. (2001), 'A numerical model of stratified wavy gasvliquid pipe flow', *Chemical Engineering Science* **56**(24), 6851–6861.
URL: *http://linkinghub.elsevier.com/retrieve/pii/S0009250901003220* (cited at page 127)

Taitel, Y. and Dukler, A. (1976), 'A theoretical approach to the lockhart-martinelli correlation for stratified flow', *International Journal of Multiphase Flow* **2**(5-6), 591 – 595. (cited at page 114, 117, 120)

Xu, J., Wu, Y., Shi, Z., Lao, L. and Li, D. (2007), 'Studies on two-phase co-current air/non-newtonian shear-thinning fluid flows in inclined smooth pipes', *International Journal of Multiphase Flow* **33**(9), 948 – 969. (cited at page 116, 119)

Chapter 7

Two phase gas/shear-thinning liquid slug flow

7.1 Introduction

Co-current flow of gas and liquid in horizontal pipes is a topic of considerable current interest, owing to the increasing importance of two-phase flow in process equipment and in long distance pipe lines. Of all the two-phase flow applications, the latter (involving mainly crude oil and nature gas systems) requires special attention regarding accurate calculation of pressure drop. When economic considerations are taken into account , the overwhelming majority of long distance lines operate in the slug flow regime.

Drag reduction by gas injection has been known for six decades, and 25 years ago, Chhabra et al. (1983), Farooqi et al. (1980) and, more recently, Xu et al. (2007) confirmed some of the existing experimental results.

7.2 Chapter outline

In this chapter, slug flow regime is investigated firstly, the mechanistic model of slug unit is reformulated, and its capability to agree with experimental data in

evaluating the pressure gradients is shown.

Fluent 3D CFD package Volume of fluid method was used, and simulations with an appropriate turbulence model, low Reynolds number $k-\epsilon$ initiated by Lam and Bremhorst (1981) were performed and supported the prediction of the previous slug unit model and its validity for wavy non-Newtonian flows. It has to be emphasised that the CFD model used in this work is a single fluid model (based on the mixture of gas and shear-thinning liquid) and, as opposed to the two fluid model, the turbulence and its dissipation are associated to the fluid mixture and not associated to each phase separately.

7.3 Slug unit model

Concerning slug flows, the mechanistic technique for intermittent flow is due to Dukler and Hubbard (1975), and it considers the slug flow regime as a sequence of periodical slug units travelling at a constant speed. The slug unit is formed by a liquid slug, followed by an elongated gas bubble travelling above a liquid film. In the past, several researchers added modifications and assumptions in the liquid film and gas interaction in order to improve the accuracy of the slug unit model or to extend its validation to wavy flows. An overview of these approaches is described in Mazza et al. (2010). Farooqi et al. (1980) considered suspensions rheology as the Bingham liquid model and predicted drag reduction within slug flow regime, and later Farooqi and Richardson (1982b) carried out tests with water mixed with additives of kaolin and water-glycerol solutions. Investigations on the liquid hold up led Farooqi and Richardson (1982a) to modify Lockhart-Martinelli factor in order to be applicable to power-law liquids. The adequacy of the modified factor has been further demonstrated for polymer solutions and CarboxyMethyl Cellulose solutions by Chhabra and Richardson (1984). Recently, Xu et al. (2009) showed that the two fluid model for stratified two phase flow and the mechanistic approach gives a good agreement with data concerning the drag reduction and the pressure drop for CMC solutions.

7.3.1 Mechanistic description

The slug unit concept originates from the assumption of the existence of an equilibrium state for slug flow regime. Let momentum equations of the system be considered in the following form:

$$\frac{\partial(\rho_k \cdot \alpha_k \cdot u_k)}{\partial t} + \frac{\partial(\rho_k \cdot \alpha_k \cdot u_k^2)}{\partial x} = 0 \tag{7.1}$$

For incompressible phases $k = G, L$, the above equation, as well as the continuity equations, reduce to generalised inviscid Burgers's equation.

$$\frac{D(\alpha_k \cdot u_k)}{Dt} = \frac{\partial(\alpha_k \cdot \ u_k)}{\partial t} + u_k \cdot \frac{\partial(\alpha_k \cdot u_k)}{\partial x} = 0 \tag{7.2}$$

Equation 7.2 shows that $[\alpha_k \cdot \ u_k](x,t)$ is invariant under the translation and admits implicit solutions:

$$\begin{aligned} \alpha_k(x,t) &= \eta_k(x - u_k \cdot t) \\ u_k(x,t) &= \psi_k(x - u_k \cdot t) \end{aligned} \tag{7.3}$$

The slug unit is defined by initial phase fraction $\alpha_k(x,0) = \eta_k(x)$ distribution, with associated phase velocity $u_k(x,0) = \psi_k(x)$.
Slug unit is a concept characterised by a slug body of liquid with length l_s, followed by liquid film and an elongated large bubble of gas. Its diameter is comparable to the pipe diameter D, and the length of the gas bubble and the liquid film are both represented by l_f.
The mechanisms behind the slug unit propagation are well understood and widely detailed in the literature. Briefly, a slug body is acting as sink of the upstream liquid film, and an equivalent amount of absorbed liquid is released downstream of the slug body to restore the film. Slug unit models suggest the existence of a marginally stable slug in the flow, and in these models, mass flow rate entering the slug body is equal to the mass flow rate leaving the body. These mechanisms suggest that the slug body propagates with a higher speed u_s than that of the film

u_f. The mass balance in the slug unit can be deduced using the mass conservation of each phase while the unit is evolving. A schematic representation of the slug unit is depicted in Figure 7.1. The mass balance of gas and liquid along the slug

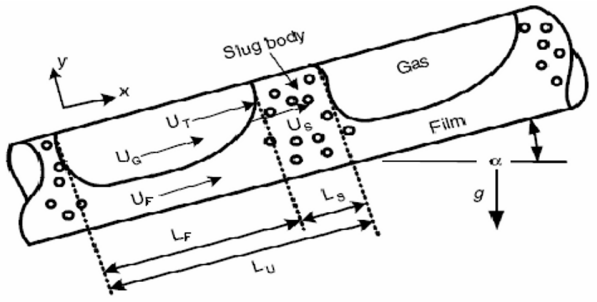

Figure 7.1: Schematic view of slug unit

unit is

$$l_u \cdot u_{SL} = l_f \cdot \alpha_f \cdot u_f + l_S \cdot \alpha_S \cdot u_S$$
$$l_u \cdot u_{SG} = l_f \cdot (1 - \alpha_f) \cdot u_G + l_S \cdot (1 - \alpha_S) \cdot u_S \tag{7.4}$$

where $u_S = u_{SG} + u_{SL}$ and u_f are the slug or mixture and liquid film velocities, while α_S is the liquid holdup in the slug body, and α_f is the liquid holdup over the film zone.

For slug unit stability (conservation of slug unit length), it is necessary that the volumetric mass of liquid entering the slug per unit time is conserved across the control volume of the slug unit. Therefore, if u_t stands for the slug front (translational) velocity, then

$$(u_S - u_t) \cdot \alpha_S = (u_f - u_t) \cdot \alpha_f \tag{7.5}$$

It is understood that the translational velocity is well approximated (Bendiksen, 1984) by $u_t = 1.2 \cdot u_S + 0.54 \cdot \sqrt{g \cdot D}$.

Equations 6.6, 7.1 and 7.2, together with the momentum equations provide the formulation of the slug unit model that allows for an estimate of the average pressure gradient along the unit

$$\begin{aligned}
\left(\frac{\mathrm{d}p}{\mathrm{d}x}\right)_{SU} &= \frac{2}{D}\cdot f_S \rho_S u_S^2 \cdot \frac{l_S}{l_u} + \frac{4}{\pi D^2}\left(\tau_{GW}\cdot S_G + \tau_{LW}\cdot S_L\right)\cdot \frac{l_f}{l_u} \\
A\cdot\left(\frac{\mathrm{d}p}{\mathrm{d}x}\right)_{SU} &= \tau_{SW}\cdot S_S \cdot \frac{l_S}{l_u} + \left(\tau_{GW}\cdot S_G + \tau_{LW}\cdot S_L\right)\cdot \frac{l_f}{l_u} \qquad (7.6) \\
A\cdot\left(\frac{\mathrm{d}p}{\mathrm{d}x}\right)_{SU} &= \tau_{SW}\cdot S_S + \tau_{GS}\cdot S_G + \tau_{LS}\cdot S_L
\end{aligned}$$

where SU stands for slug unit, while S_G and S_L are the gas and liquid wetted perimeters. In the first relation above, f_S and ρ_S are the mean values of slug friction factor and slug density, and are given by the barycentric form of each phase, and u_S stands for the superficial mixture or slug velocity. In the second relation, $A = \dfrac{\pi D^2}{4}$ represents the cross section surface of the pipe, and by analogy, one can define the slug wall shear stress, the slug wetted perimeter and the shear stresses difference, respectively, by

$$\begin{aligned}
\tau_{SW} &= \frac{1}{2}\cdot f_S \cdot \rho_S \cdot u_S^2 \\
S_S &= \pi \cdot D \qquad (7.7) \\
\tau_{KS} &= \left(\tau_{KW} - \tau_{SW}\right)\cdot \frac{l_f}{l_u} \geq 0
\end{aligned}$$

Note that $l_S = l_u - l_f$ and $S_S = S_L + S_G$ were used to reformulate the slug unit momentum equation 7.2.

7.3.2 Computational solution

The computation of the solution for the calculation of pressure gradient for slug flow regime using the slug unit model requires the following: D, u_{SL}, u_{SG}, ρ_L,

ρ_G, m, n, μ_G and the superficial tension σ_L.

Considering that the film zone is in equilibrium, the pressure gradients in gas and in liquid are equal; thus, the equation 7.8 holds

$$\frac{\tau_{fW} S_f - \tau_{\mathrm{i}} S_{\mathrm{i}}}{A_f} = \frac{\tau_{GW} S_G + \tau_{\mathrm{i}} S_{\mathrm{i}}}{A_G} \tag{7.8}$$

In order to close the system of equations for slug unit model, the correlation of Andreussi et al. (1993) is used to calculate the slug liquid holdup.

$$h_S = 1 - \frac{u_S/\sqrt{g\cdot D} - F_o}{u_S/\sqrt{g\cdot D} + 2400\cdot B_o^{-3/4}}$$

$$F_o = 2.6\,(1 - 2\cdot(0.025/D)^2) \tag{7.9}$$

$$B_o = \frac{(\rho_L - \rho_G)\cdot g\cdot D^2}{\sigma_L}$$

Above, B_o stands for Bond number.

The set of equations 7.4 to 7.9, with the shears stresses and the geometrical variables in the cylindrical pipes, constitute a complete and autonomous system that is analytically solved for the wetted angle θ, u_G, u_f, f_f, f_G and $\frac{l_f}{l_u}$. Once these quantities are obtained, the pressure drop along the slug unit is calculated.

It can be seen from figure 7.2 that the slug unit formulation shows an excellent agreement with the experimental data for low flow rates ratio $\frac{u_{SG}}{u_{SL}}$ in figure 7.2. It also corroborates the absence of drag reduction at high liquid flow rates. A clear disagreement appears between data and slug unit results at high gas flow rates.

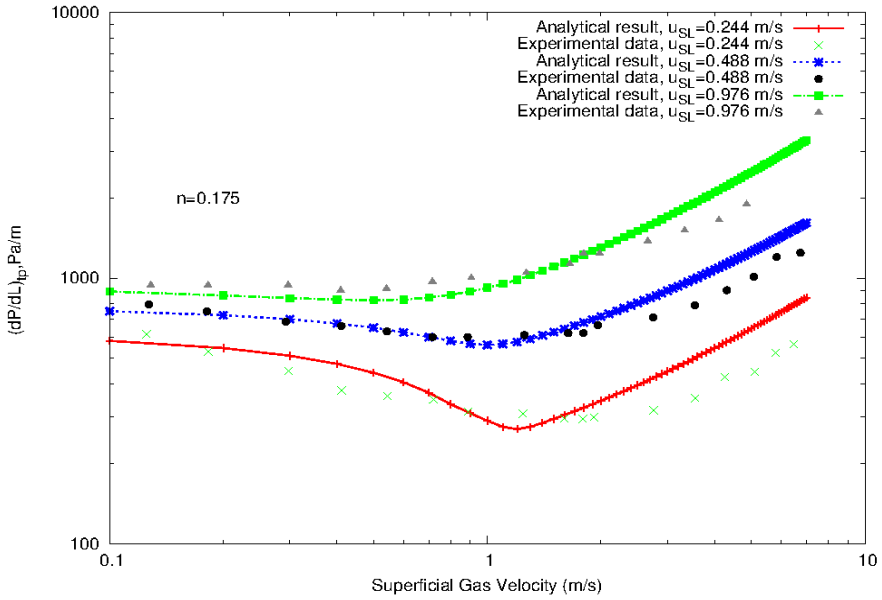

Figure 7.2: Drag reductions computed by the procedure above compared to the measured drag reductions from Farooqi and Richardson (1982b).

7.4 Numerical results using CFD

In this section, a limited number of specific cases of flow conditions from from Farooqi and Richardson (1982b) were selected for performing 3D CFD. The CFD setup has been introduced in the Chapter 6 and will keep same in here.

These cases are illustrated in the table 7.1. The gas was considered compressible and the surface tension was taken as $\sigma = 0.070 N/m$. The density and the coefficients for the non-Newtonian liquid are $\rho_L = 1360 kg/m^3$, n=0.175, $m = 4.25 Pa \cdot s^n$.

As in the stratified tests, the shear-thinning liquid phase remains in laminar condition, while the gas is in turbulent condition for most cases.

Figure 7.3 illustrates the comparison of pressure gradients obtained from CFD simulations and from data. A satisfactory agreement between CFD and data is outlined above for pressure gradients. The discrepancy that is noticeable above can be understood if one keeps in mind that the VOF model is a single fluid equation. The transverse components of the pressure gradient and their

Table 7.1: Flow rates used in CFD for slug regimes

u_{SL}(m/s)	u_{SG}(m/s)	α_l	Re_{MR}	Re_G
0.488	0.181	0.834	249	531
	0.411	0.674		1229
	0.887	0.484		2672
	1.637	0.380		4977
0.976	0.284	0.831	884	877
	0.525	0.725		1624
	1.200	0.522		3783
	1.717	0.444		5524

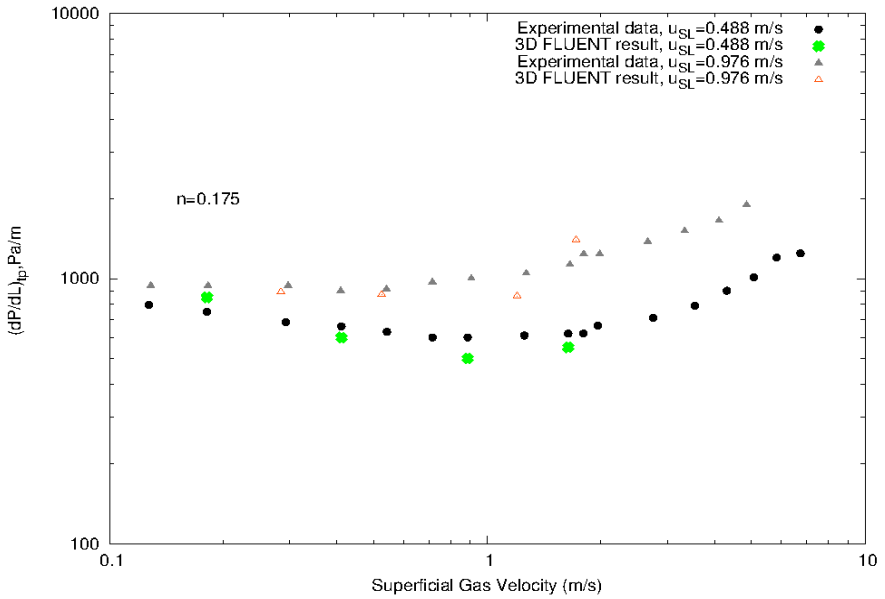

Figure 7.3: Pressure gradients obtained from CFD single fluid model compared to pressure gradients measured from data

corresponding transverse components of friction forces were considered, and also

the compressibility of the gas was taken into consideration. Gradient pressures reported in Figure 7.3 were recorded at sections $z = 4m$, $z = 6m$ and $z = 7m$ downstream the elbow.

The pictures below concern the case with superficial velocities $u_{SL} = 0.488m/s$ and $u_{SG} = 0.887m/s$. Snapshots of a slug at two stages (upstream and downstream the elbow) while travelling across the elbow, and its volume fraction, velocity magnitude, dynamic pressure and static pressure are reported.

In each picture, the flow circulates from the bottom right (inlet), crosses the elbow, and turns right to the top right (outlet).

Static pressure is always higher at the tail of the slug, in contrast with the velocity that is higher at the slug front than in its tail. Because of the difference of liquid and gas velocity, a small wave in interface can be found in each figure. High volume fraction of liquid is present at the elbow, as expected, and the slug body shows entrapped gas bubbles.

It is noticeable that the slug body, while travelling, exchanges momentum with the elbow, and this is shown through the speed drop at the slug front and the pressure drop at the tail of the slug.

Time traces of liquid holdup and static pressure at $4m$,$6m$,$7m$ from the elbow in two phase gas/shear-thinning slug flow are introduced in the appendix D.

7.5 Conclusions

The mechanistic model of the slug unit shows a remarkable agreement with experimental data in evaluating the pressure gradients. As it has been observed by Chhabra and Richardson (1999), when the gas superficial velocity increases, the pressure gradient first decreases, then reaches a minimum corresponding to the maximum drag reduction, before starting to increase and then surpassing the value corresponding to the single phase liquid flow condition.

As the non-Newtonian liquid (shear-thinning) superficial velocity increases, the drag reduction gained by gas injection becomes insignificant; therefore, this technique is not advisable under high liquid flow rates.

Concerning the slug flow regimes, slug unit approach is viewed as a system of inviscid Burgers's equations that originates from the existence of an equilibrium state for slugging regime. The slug unit model showed a good agreement with data at low gas flow rates. At high gas flow rates, a clear inconsistency exists between the results from slug unit model and the data. This is probably due to the fact that at high gas flow rates, transverse components of pressure gradient and their counterpart, transverse components of frictions forces should be considered.

The CFD model, although it is a single fluid, showed an acceptable agreement with both data and the mechanistic model for slug flow regimes. These results may be improved in many ways, possibly using refined meshes or a modified source term contained in superficial tension for a better estimate of friction forces components. This would be of benefit for enhancing the capabilities of mechanistic models.

Discrepancy between data, mechanistic model is expected. Mechanistic model is based on two-fluid approach. The limitations of the mechanistic approach are known. Mechanistic model considers the turbulence only via friction factors and it does not take into account the diffusion of the liquid flow under the entrainment of the gas flow. From figure 7.2 it can be seen that the discrepancy between data and the model is significant at high gas flow rates, when the gas starts to be highly turbulent.

From figure 7.3 discrepancy between experimental data and CFD appears here to be increasing with increasing gas flow rates. The turbulent effects are averaged over the liquid and gas. The volume of fluid model in CFD could not account for a separated turbulence model for each phase, contrary to the data, the shear-thinning liquid phase is laminar, while the gas phase is mainly turbulent.

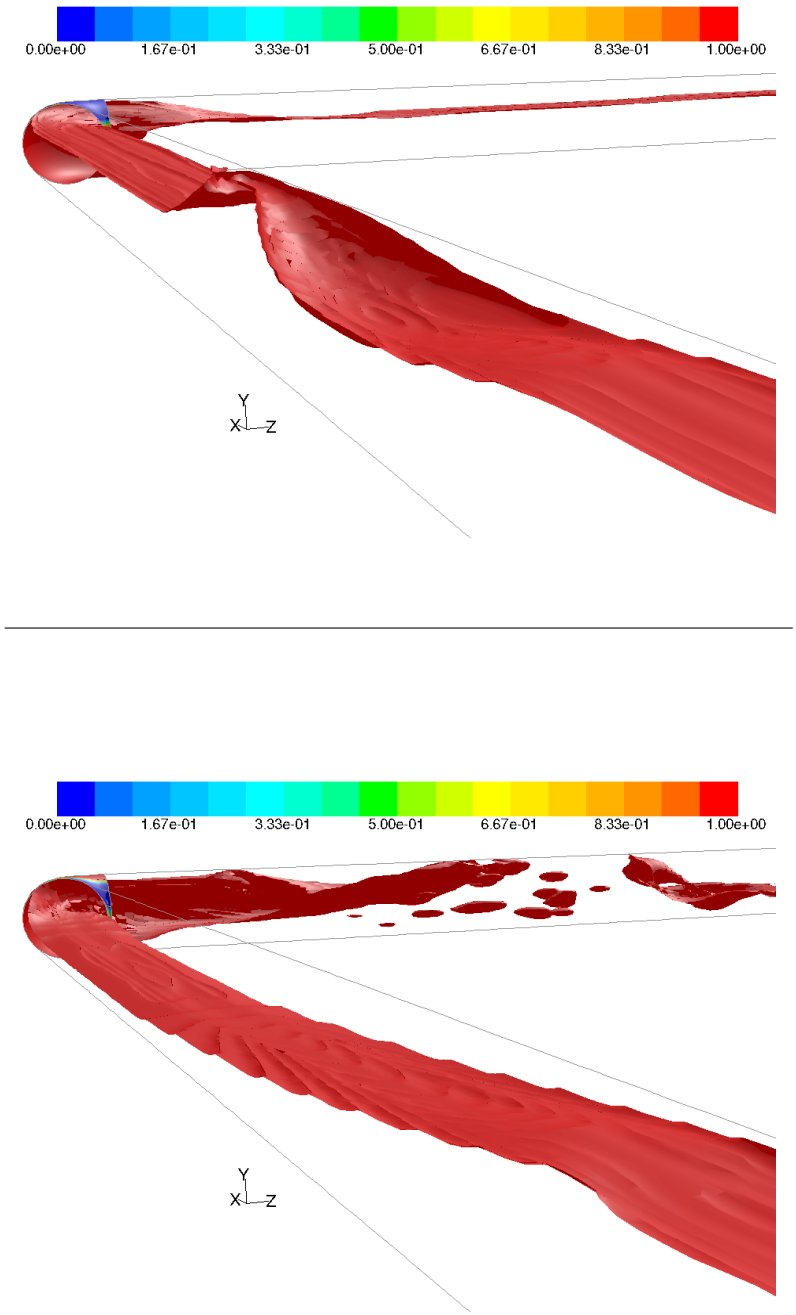

Figure 7.4: Slug (top to bottom) upstream and downstream the elbow: Liquid volume fraction

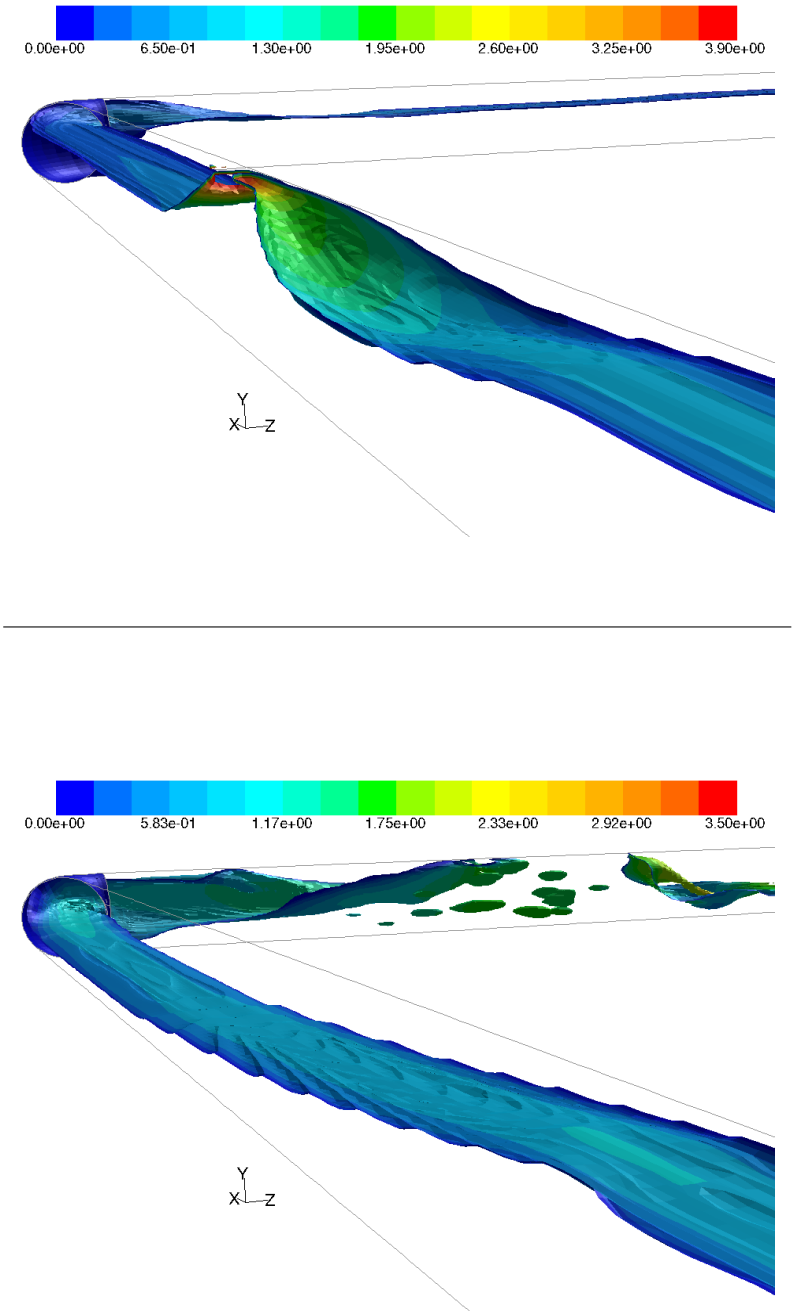

Figure 7.5: Slug (top to bottom) upstream and downstream the elbow: Liquid interface velocity

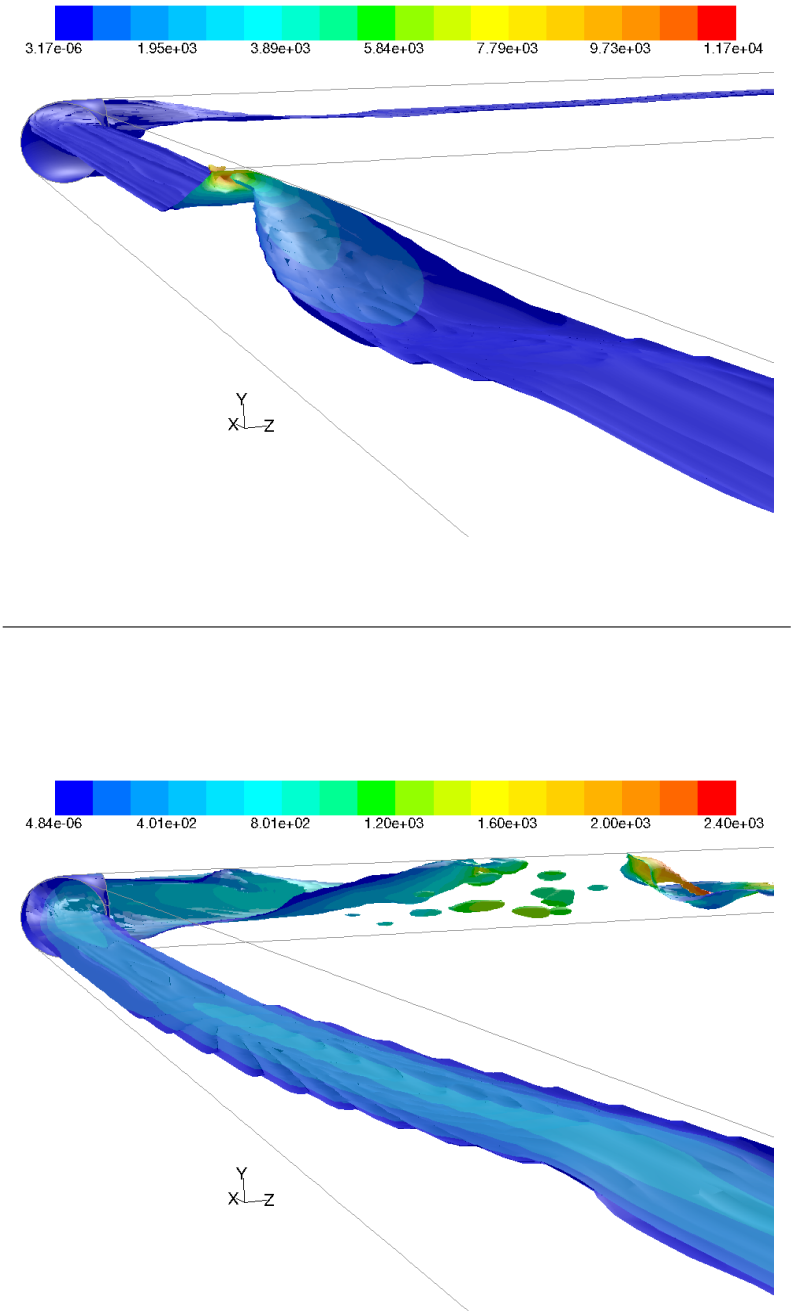

Figure 7.6: Slug (top to bottom) upstream and downstream the elbow: Dynamic pressure

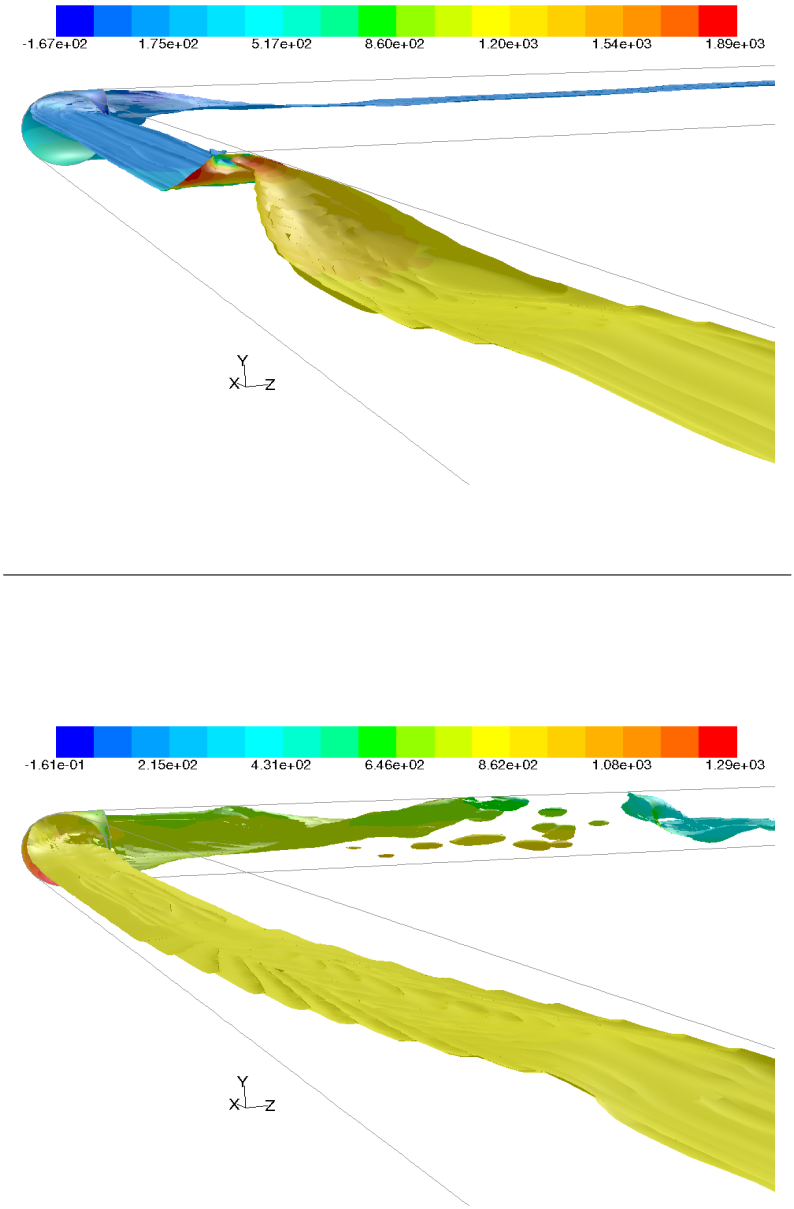

Figure 7.7: Slug (top to bottom) upstream and downstream the elbow: Static pressure

References - 7

Andreussi, P., Minervini, A. and Paglianti, A. (1993), 'Mechanistic model of slug flow in near-horizontal pipes', *AIChE Journal* **39**(8), 1281–1291. (cited at page 142)

Bendiksen, K. H. (1984), 'An experimental investigation of the motion of long bubbles in inclined tubes', *International Journal of Multiphase Flow* **10**(4), 467 – 483. (cited at page 140)

Chhabra, R. P., Farooqi, S. I., Richardson, J. F. and Wardle (1983), 'Co-current flow of air and shear-thinning suspensions in pipes of large diameter', *Chemical Engineering Research and Design* **61**, 56 – 61. (cited at page 137)

Chhabra, R. P. and Richardson, J. F. (1984), 'Prediction of flow pattern for the co-current flow of gas and non-newtonian liquid in horizontal pipes', *The Canadian Journal of Chemical Engineering* **62**(4), 449 – 454. (cited at page 138)

Chhabra, R. P. and Richardson, J. F. (1999), *Non-Newtonian flow in the process industries*, Butterworth-Heinemann. (cited at page 145)

Dukler, A. E. and Hubbard, M. G. (1975), 'A model for gas-liquid slug flow in horizontal and near horizontal tubes', *Industrial & Engineering Chemistry Fundamentals* **14**(4), 337 – 347. (cited at page 138)

Farooqi, S. I., Heywood, N. I. and Richardson, J. F. (1980), 'Drag reduction by air injection for suspension flow in a horizontal pipeline', *Transactions of the Institution of Chemical Engineers* **58**(1), 16–27. (cited at page 137, 138)

Farooqi, S. and Richardson, J. (1982a), 'Horizontal flow of air and liquid (newtonian and non-newtonian) in a smooth pipe. part i: A correlation for average liquid holdup', *Trans. IChemE* **60**, 292 – 305. (cited at page 138)

Farooqi, S. and Richardson, J. (1982b), 'Horizontal flow of air and liquid (newtonian and non-newtonian) in a smooth pipe. part ii: Average pressure drop', *Trans. IChemE* **60**(6), 323 – 333. (cited at page xv, 138, 143)

Lam, C. and Bremhorst, K. (1981), 'A modified form of the k-ϵ model for predicting wall turbulence', *Journal of Fluids Engineering, Transactions of the ASME* **103**(3), 456–460. (cited at page 138)

Mazza, R., Rosa, E. and Yoshizawa, C. (2010), 'Analyses of liquid film models applied to horizontal and near horizontal gas-liquid slug flows', *Chemical Engineering Science* **65**(12), 3876 – 3892. (cited at page 138)

Xu, J., Wu, Y., Shi, Z., Lao, L. and Li, D. (2007), 'Studies on two-phase co-current air/non-newtonian shear-thinning fluid flows in inclined smooth pipes', *International Journal of Multiphase Flow* **33**(9), 948 – 969. (cited at page 137)

Xu, J., xiang Wu, Y., Li, H., Guo, J. and Chang, Y. (2009), 'Study of drag reduction by gas injection for power-law fluid flow in horizontal stratified and slug flow regimes', *Chemical Engineering Journal* **147**(2-3), 235 – 244. (cited at page 138)

Chapter 8

Conclusion and Futher work

8.1 Conclusion

One-dimensional two-fluids models were presented firstly, in order to solve two-phase flow problems. Closure laws for pressure terms and shear stress, used in this two-fluids model, were introduced also. Because of the complexity of the two-fluids model, explicit finite volume approach, $AUSMDV^*$, adopted for solving the two-phase flow models, was introduced in detail. Except for the one-dimensional two-phase model, the three dimensional Volume of Fluid VOF model was presented. Additionally, $k-\epsilon$ turbulence model was described to consider the turbulence of the mixture velocity.

Slug flow was introduced and different slug frequency and slug length correlations were reviewed. Then a slug test case was simulated with the two fluids single pressure model (SPM-4) in the EMAPS framework, and average slug length and slug frequency, calculated from simulations, were compared with the correlations. A good agreement of slug frequency was obtained compared with Manolis (1995) correlation, but the slug length shows to be slightly lower than the experiments, although the predictions are within the range.

The AMR strategy was introduced with a gradient error criterion; but this error criterion can not flag all the regions which need be refined in slug flow. A new

method was proposed here to deal especially with the slug case. A good agreement was achieved, with high speed-up compared with uniform mesh.

Non-Newtonian fluids and their mathematics models were thoroughly reviewed. Then, analytical velocity distribution in steady laminar flow was given, and totally matched the result from 2D Fluent. The pressure gradient was also calculated in turbulent flow. The velocity profile for a shear-thinning fluid is much flatter than the profile for a shear-thickening fluid.

After a theoretical study of steady non-Newtonian flow in circular tubes, gas-shear-thinning two-phase flows through an horizontal tube was conducted. Special attention was given to the influence of liquid phase properties on flow pattern, liquid holdup, pressure drop and drag reduction. Although gas-non-Newtonian two-phase flow has less attention compared with gas-water two-phase flow, it was observed that the properties of non-Newtonian fluid had a minimal effect on the flow pattern in horizontal and near horizontal flows. Drag reduction phenomenon is noticed by Farooqi and Richardson (1982b), Heywood and Charles (1979) and Dziubinski (1995).

The Heywood and Charles (1979) model for horizontal flow was modified for stratified flow in an horizontal pipe for the average void fraction and pressure drop of the mixture flow of a gas-non-Newtonian liquid. Predictive models of void fraction and dimensionless pressure drop were presented for the stratified flow of gas and non-Newtonian liquid, obeying the power-law model. Results indicate a good agreement for the liquid holdup data and the dimensionless pressure drop. 3D Fluent numerical results also are in agreement with the experimental data from Farooqi.

The pressure gradient model for non-Newtonian slug flow extended from gas-Newtonian slug flow was studied in this thesis. A good agreement was obtained between the predicted and experimental results, and 3D Fluent has the capability of predicting the pressure gradient in gas-shear-thinning fluid slug flow.

As it has been observed by Chhabra and Richardson (1999), when the gas superficial velocity increases, the pressure gradient first decreases, then reaches

a minimum corresponding to the maximum drag reduction, before starting to increase and then surpassing the value corresponding to the single phase liquid flow condition.

As the non-Newtonian liquid (shear-thinning) superficial velocity increases, the drag reduction gained by gas injection becomes insignificant; therefore, this technique is not advisable under high liquid flow rates.

This study also opened a door for developing the EMAPS to extend capabilities of the approach in order to account for the effect when liquid is shear-thinning flow.

Two papers have been published about gas-non-Newtonian two phase flow, in Jia et al. (2011*a*) and Jia et al. (2011*b*).

8.2 Suggestions for future work

There are some suggestions for future work in order to improve the capabilities of the EMAPS code, some of the possibilities are inherent to the extension of the code itself to other flow regimes, or by coupling the code with a commercial code. This latter possibility would be adequate for simulating flow lines with branches and junctions.

- Implementing non-Newtonian model as well as heavy oil and slurry models in transient EMAPS code. This can be achieved either by implementing adequate friction correlations or by directly incorporating viscous diffusive terms in the momenta equations. Validation of this development is required.
- AMR refinement criterion has to be extended in order to encompass gas -oil and gas-non-Newtonian flow regimes other than slug flows; for example wavy and bubbly flows.
- Improving the numerical scheme and introducing multi-time step: This is necessary when simulations involve slow heavy oil or slurry with fast flowing gas.

- More different models should be exploited to apply the complex situation in gas-non-Newtonian flow; for example, Herschel-Bulkley fluid, which is a kind of shear-thinning fluid with yield stress.
- Extended investigations on slug terrain and in very large flow lines are needed to test the speed up capability and accuracy of the results of the code.
- Coupling 1D EMAPS code with a 3D CFD commercial code: This is to simulate network of pipes: 1D code can be used for long single lines while 3D code in regions with junctions or with complex shapes.

References - 8

Chhabra, R. P. and Richardson, J. F. (1999), *Non-Newtonian flow in the process industries*, Butterworth-Heinemann. (cited at page 154)

Dziubinski, M. (1995), 'A general correlation for two-phase pressure drop in intermittent flow of gas and non-newtonian liquid mixtures in a pipe', *Chemical Engineering Research and Design* **73**(5), 528 – 534. (cited at page 154)

Farooqi, S. and Richardson, J. (1982b), 'Horizontal flow of air and liquid (newtonian and non-newtonian) in a smooth pipe. part ii: Average pressure drop', *Trans. IChemE* **60**(6), 323 – 333. (cited at page 154)

Heywood, N. I. and Charles, M. E. (1979), 'The stratified flow of gas and non-newtonian liquid in horizontal pipes', *International Journal of Multiphase Flow* **5**(5), 341 – 352. (cited at page 154)

Jia, N., Gourma, M. and Thompson, C. (2011*a*), 'Non-newtonian multi-phase flows: On drag reduction, pressure drop and liquid wall friction factor', *Chemical Engineering Science* **66**(20), 4742 – 4756. (cited at page 155)

Jia, N., Gourma, M. and Thompson, C. (2011*b*), Simulation of gas non-newtonian two phase slug flow pressure drop, *in* '19th International Conference on Applied Simulation and Modelling', Crete, Greece. (cited at page 155)

Manolis, I. G. (1995), High Pressure Gas-Liquid Slug Flow, PhD thesis, Department of Chemical Engineering and Chemical Technology, Imperial College of Science, Technology and Medicine, London, UK. (cited at page 153)

Appendix A

EMAPS implementation of AMR

A.1 Introduction

In this appendix, the AMR algorithms that were implemented in the EMAPS framework will be introduced. The purpose is to provide the reader with general ideas on how this AMR strategy works. Followed this, some numerical validation cases will given, except for the slug case which was studied in chapter 4.

A.2 AMR algorithms

The functions required by the AMR strategy, which can be found in Omgba-Essama (2004), are introduced here:

- Control
- Integration
- Boundary collection
- Regridding
- Error estimation

- Flagging
- Correction
- Projection

Figure A.1 is the integration process used in the EMAPS AMR subroutine.

A.3 Numerical validation

A.3.1 Shock wave test case

The first non-linear example is the shock wave case which is based on the invisicid Burgers equation $\frac{\partial U}{\partial x} + \frac{1}{\partial x}(\frac{1}{2}U^2) = 0$. When the initial velocities are $U_L = 2.0m/s$, and $U_R = 0.5m/s$, and the initial shock position is $x_{shock} = 5m$. Figure A.2 present the distribution of refinement levels and velocity at time = $15s$. These computations use adaptive gridding, with one initial patch of 100 coarse cells and 4 levels of refinement. The figures clearly show the robustness and effectiveness of the AMR algorithm, as the mesh distribution along the pipe automatically evolves with the flow, with fine meshes concentrated near discontinuities where they are needed, while coarse cells are used far away from the discontinuity. For this case, the level 4 always is set for the domain where the discontinuity occurs.

Figure A.3 shows the result with AMR, whose adaptive level is 4, is not only more accurate than the result with 100 unif cellsorm cells, but also more so than the result with 400 uniform cells. The result with 800 uniform cells is overlapped by the result with AMR, which means they have the same accuracy. When adaptive level is 4, numbers of pipeline cells are only 350. Although there are only 350 cells with AMR, more grids are generated in the place where shock occurs than the 400 uniform grids.

Table A.1 shows the execution time recorded for the integration of the shock wave case after 20 seconds flow time. As shown, the AMR method significantly accelerates the computation compared to uniform grid. The Speed-up will be

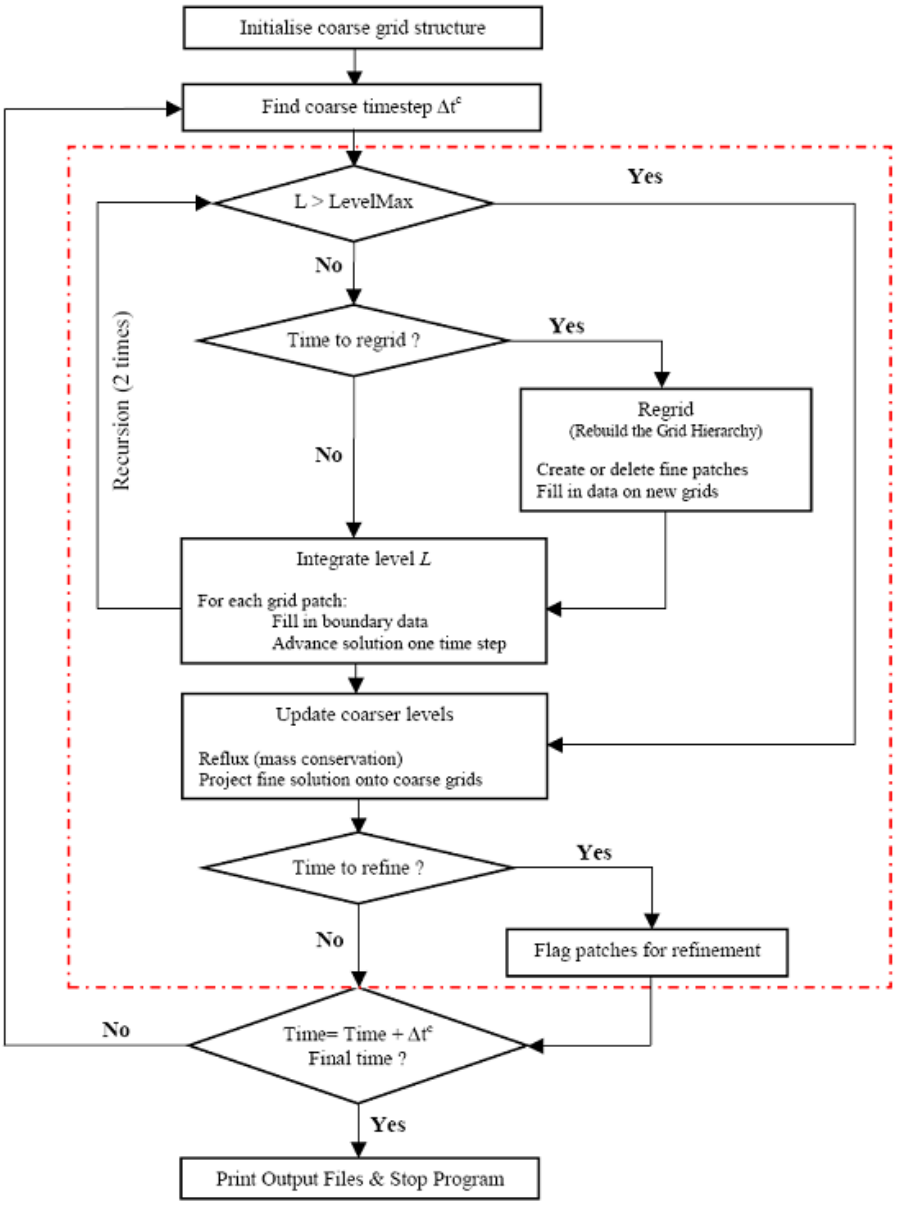

Figure A.1: Flow chart that describes the adaptive mesh refinement algorithm,(Omgba-Essama, 2004)

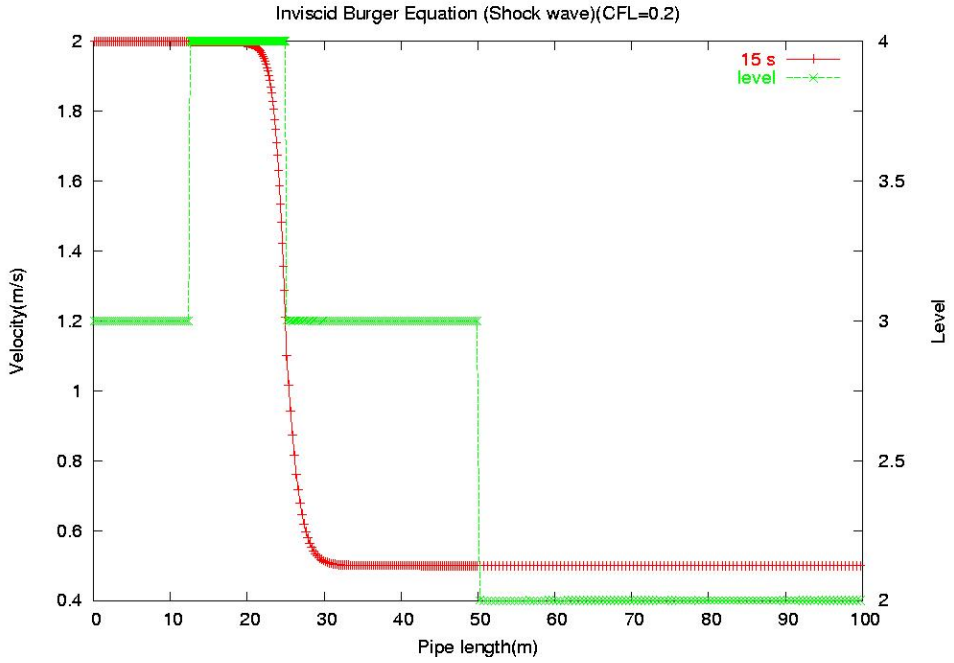

Figure A.2: Distribution of refinement levels and velocity at time = $15s$

outstanding when the high level of refinement is adopted, which is 5.7 when level 5 is chosen.

A.3.2 Faucet test case

This popular problem, devised by Ransom (1987), consists of a liquid stream entering a vertical solution space at the top and falling under the action of gravity to form a stream of uniformly decreasing cross-section. It is illustrated schematically in figure A.4, and the specifications of the problem are given as:

- Length of the vertical pipe: $12m$
- Diameter for the vertical pipe: $1m$
- Operating fluids: air and water ($\rho_G = 1.16kg/m^3$, $\rho_L = 998kg/m^3$)
- Flow temperature: $T = 20\,^{\circ}\mathrm{C}$

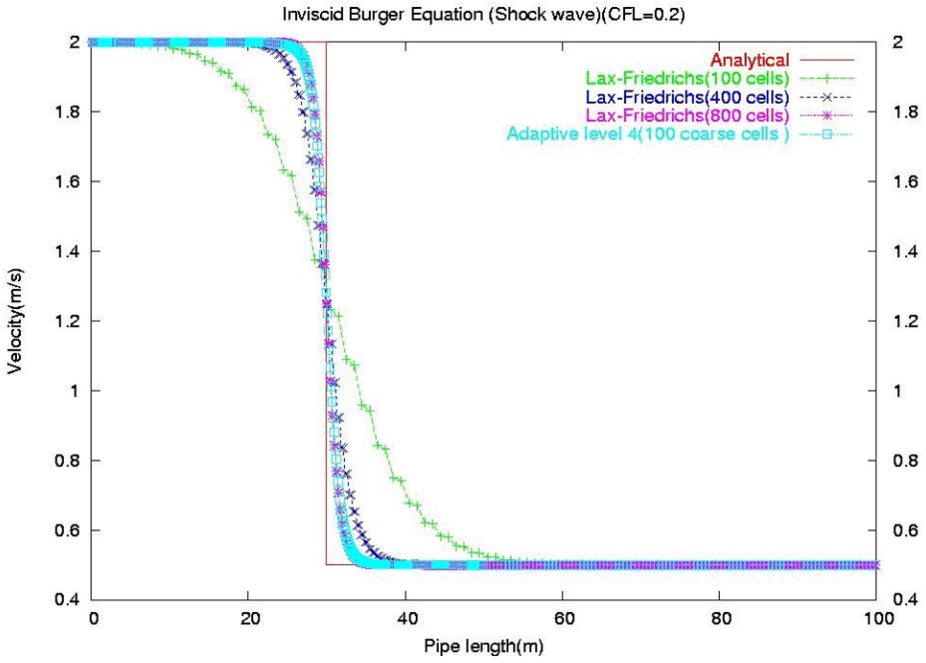

Figure A.3: Comparison of the results using the uniform and adaptive grids at time $= 20s$

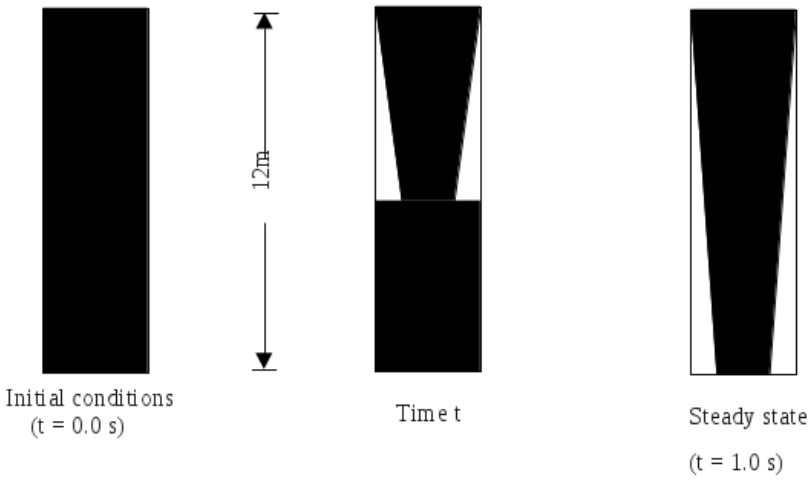

Figure A.4: Schematic of the water faucet test case

Figure A.5 presents the numerical results of the gas holdup with the analytical solutions, for different grids. The curve using the adaptive mesh refinement, which has been adaptively refined 4 times, starting at 50 coarse cells, is overlapped

Table A.1: Running time of Burger shock wave test case using different grids and AMR

Level of Refinement (Based on 100 cells)	Timings (s)		Speed-up
	Uniform	AMR	
1	0.06 (100 cells)	-	-
2	0.13 (200 cells)	0.11	1.18
3	0.39 (400 cells)	0.17	2.29
4	1.21 (800 cells)	0.38	3.18
5	3.19 (1600 cells)	0.56	5.70

with the results using 200 uniform cells - and they are more accurate than the results using 100 uniform cells. This makes the AMR scheme very attractive, as a similar convergent solution can be achieved for a fraction of the computational time compared to the uniform grid.

Table A.2 shows the recorded execution time of the water faucet test case after 0.5 seconds flow time. It can be seen that the AMR method significantly accelerates the computation compared to uniform grid. It is clearly shown that the levels of refinement have significant effect on the speed up, and as the level of refinement increases, the speed up increases sharply while achieving the same accuracy.

A.4 Wave gowth

The numerical wave growth of the incompressible model (Pressure free model-Watson) and the compressible (SPM4) models of EMAPS for an air-water mixture velocity of $2.4m/s$ are investigated. For the case, which is between the

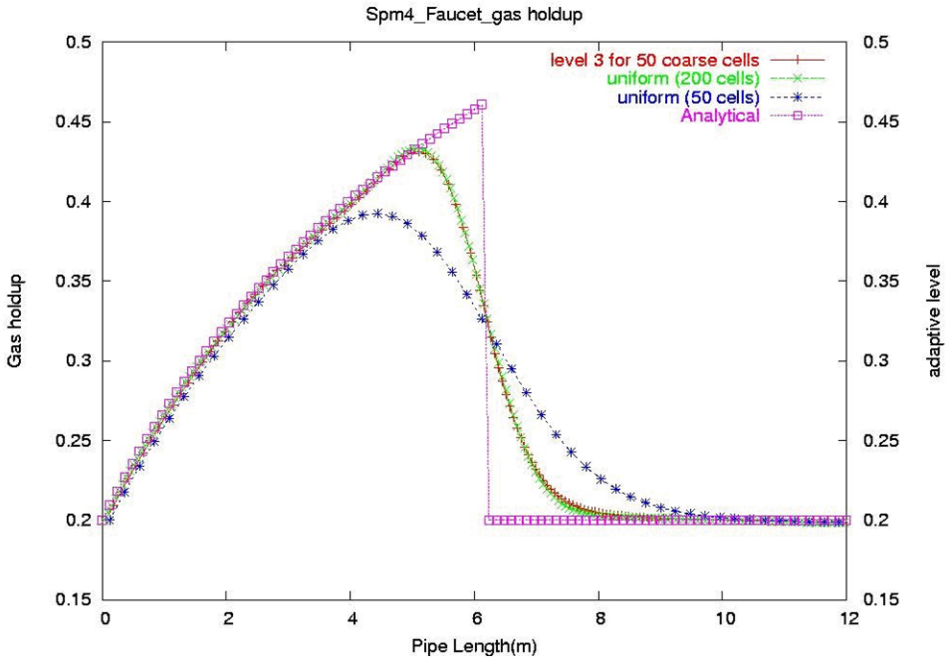

Figure A.5: Analytical comparison of the results using the uniform and adaptive grids for gas holdup at time = $0.5s$

Table A.2: Running time of SPM4 faucet test case using different grids and AMR

Level of Refinement (Based on 50 cells)	Timings (s)		Speed-up
	Uniform	AMR	
1	13.5 (50)	-	-
2	51.67 (100)	34.72	1.48
3	202.16 (200)	80.61	2.51
4	809.47 (400)	202.87	3.99

inviscid Kelvin Helmholtz (KH) and the viscous KH transition lines, the details are as follows:

- Air/water at atmospheric conditions
- Diameter for the vertical pipe: $1m$
- Operating fluids: air and water: ($\rho_G = 1.21kg/m^3$, $\rho_L = 998kg/m^3$)
- Fluids viscosity: ($\mu_G = 1.7710^{-5}kg/m\cdot s$, $\mu_L = 1.1410^{-3}kg/m\cdot s$)
- Boundary condition: $U_{SG} = 2.0m/s$, $U_{SL} = 0.4m/s$
- Small perturbation of the initial holdup with $A_O = 1\%$, $x_s = 15m$, and $x_f = 23m$, see figure A.6

$$\begin{cases} \alpha_{L\_initial} = \alpha_L^{eq}\left[1 + A_0 \sin\left(\frac{\pi}{4}\left(x - x_s\right)\right)\right] & if \quad x \in [x_s, x_f] \\ \alpha_{L\_initial} = \alpha_L^{eq} & otherwise \end{cases}$$

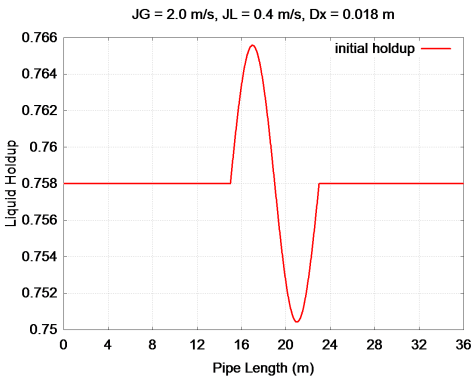

Figure A.6: Initial liquid holdup for wave growth

The EMAPS code is run for 10 seconds and the time evolution of the liquid holdup profile is plotted in figure A.7.

It can be seen from figure A.8 that the highest level was put where the wave is, and that the highest level is moving with the wave. Time evolution of the liquid holdup (left label) and Taitel-Dukler Kelvin-Helmholtz result (right label) are plotted here in figure A.9. It is clearly shown that they have a similar shape. In

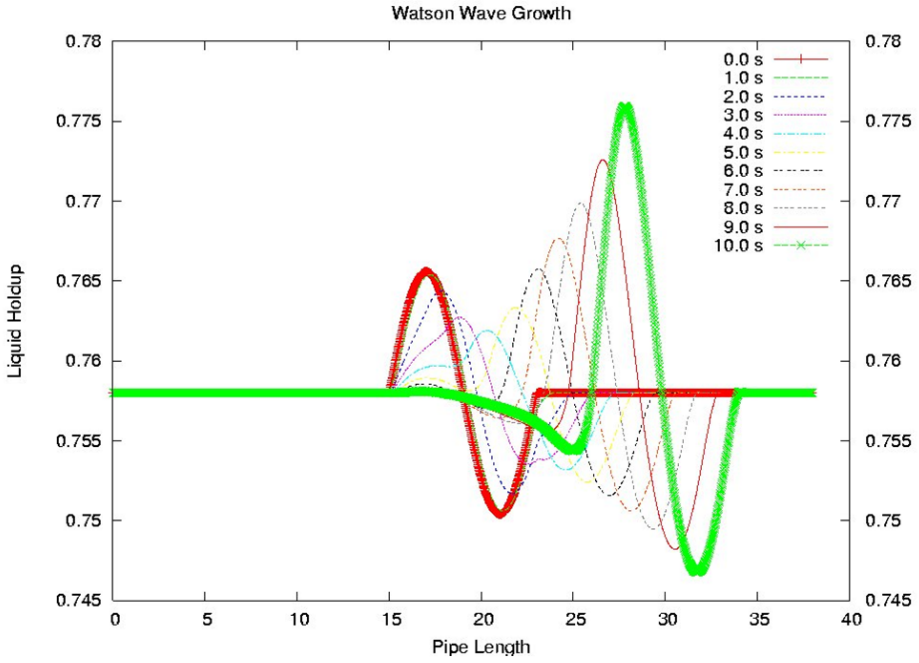

Figure A.7: Time evolution of the liquid holdup profile in the pipe

figures A.9 a and b, the Taitel-Dukler Kelvin-Helmholtz results in the whole pipe are smaller than zero, which means it is still in the stratified flow zone. However, in figures A.9 c and d, the Taitel-Dukler Kelvin-Helmholtz results in the wave top are already greater than zero, which means the wave starts to transit from stratified flow to slug flow.

Table A.3 and A.4 is the running time of the wave growth, using Watson and SPM4 model, respectively. It is clearly shown that the AMR method significantly accelerates the computation compared to uniform grid. However, speed-up for the AMR simulation using SPM4 is higher than the one using Watson, because the compressible SPM4 model is more complex than the incompressible Watson model. The effect will be more obvious when the complex model is chosen.

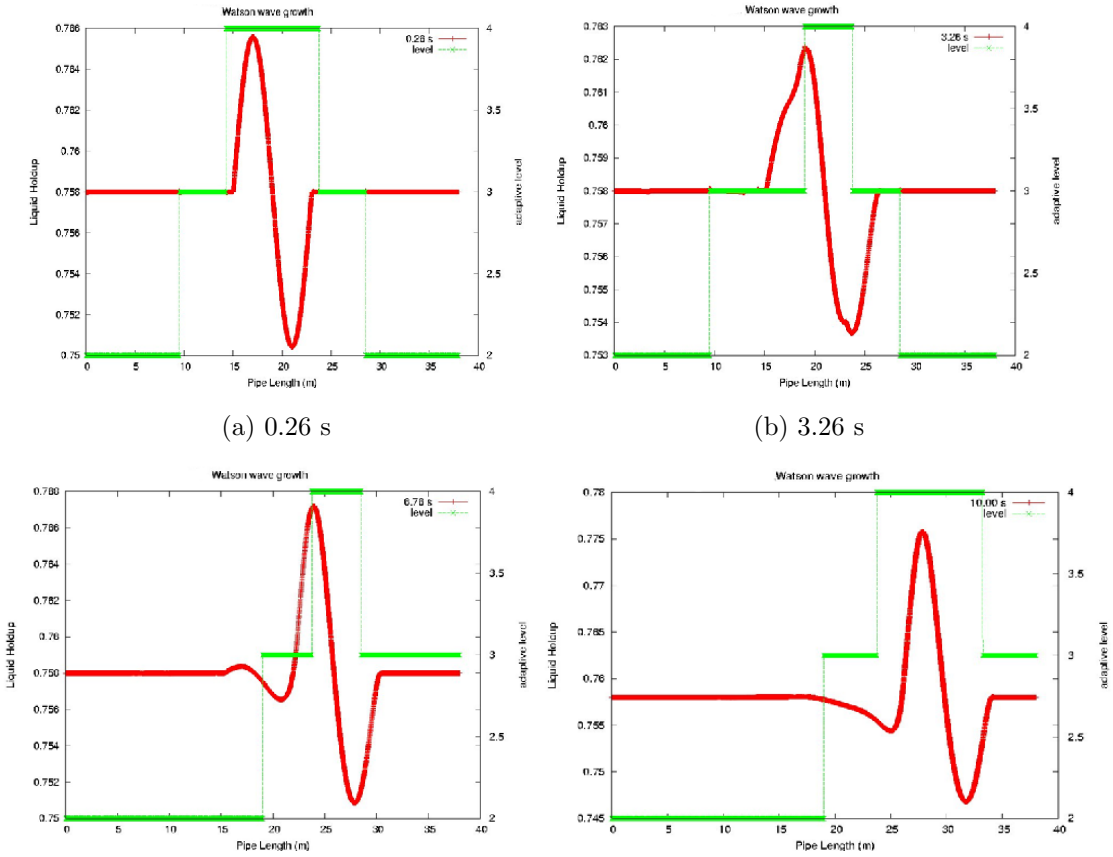

(a) 0.26 s

(b) 3.26 s

(c) 3.76 s

(d) 10 s

Figure A.8: Time evolution of the liquid holdup with adaptive grid

A.5 Reference A

Omgba-Essama, C. (2004), Numerical Modelling of Transient Gas-Liquid Flows (Application to Stratified and Slug Flow Regimes, PhD thesis, Cranfield University, UK. (cited at page xvi, 159, 161)

Ransom, V. H. (1987), Faucet flow, oscillating manometer, and expulsion of steam by sub cooled water, *in* G. Hewitt, J. Delhaye, and N. Zuber,

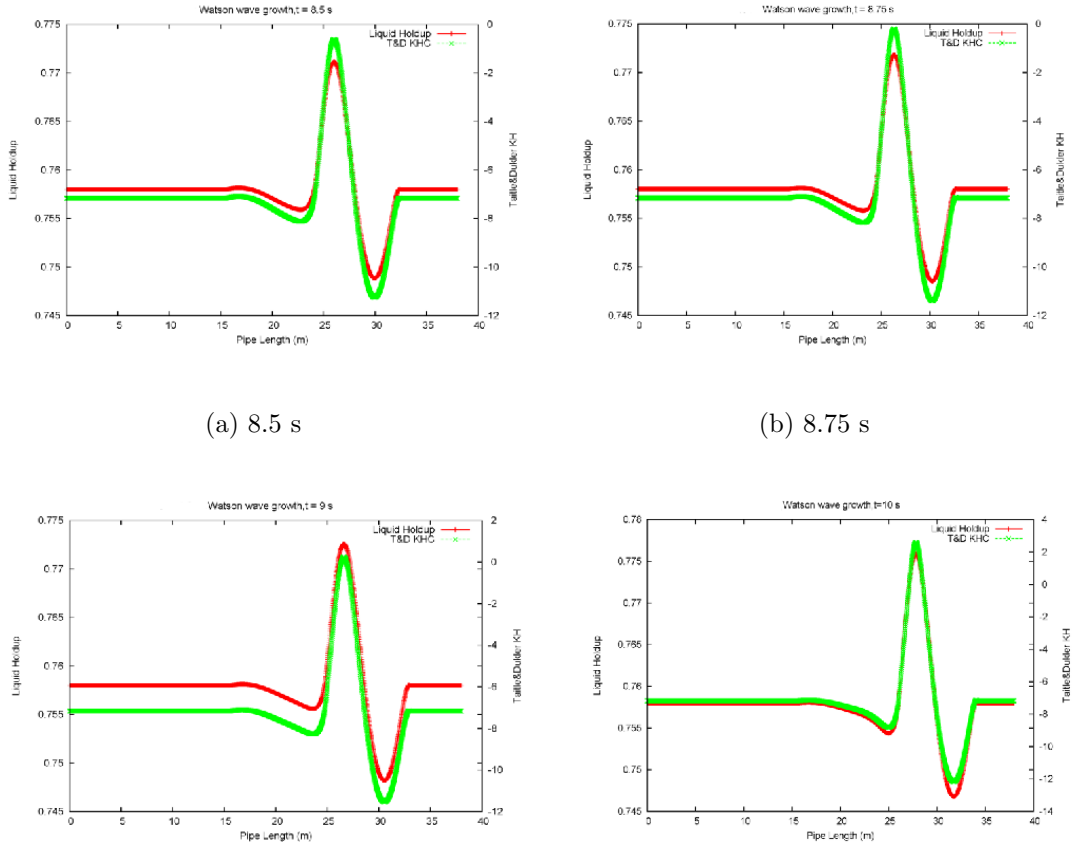

(a) 8.5 s

(b) 8.75 s

(c) 9 s

(d) 10 s

Figure A.9: The transition from stratified to slug flow of wave peak

eds, 'Multiphase Science and Technology', Vol. 3, Hemisphere Publishing Corporation. (cited at page 162)

Table A.3: Running time of Watson wave growth test case using different grids and AMR

Level of Refinement (Based on 50 cells)	Timings (s)		Speed-up
	Uniform	AMR	
1	18.861 s (2000 cells)	-	-
2	70.250 s (4000 cells)	42.544 s	1.65
3	283.224 s (8000 cells)	123.254 s	2.298
4	18Min16s (16000 cells)	281.087 s	3.899

Table A.4: Running time of SPM4 wave growth test case using different grids and AMR

Level of Refinement (Based on 50 cells)	Timings (s)		Speed-up
	Uniform	AMR	
1	45.960 s (500 cells)	-	-
2	201.67 s (1000 cells)	110.20 s	1.83
3	833.063 s (2000 cells)	328.05 s	2.54
4	48m43s (4000 cells)	12m11 s	4.02

Appendix B

Non-Newtonian power-law fluids velocity profile

B.1 Laminar steady flow

The velocity profiles for different values of n calculated from equation FLUENT with $0.1m/s$ inlet velocity in laminar flow will display in this section.

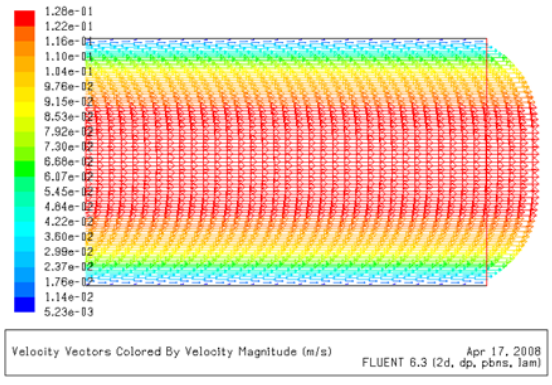

Figure B.1: Outlet velocity profile when power-law index $n = 0.4$ with $0.1m/s$ inlet velocity in laminar flow

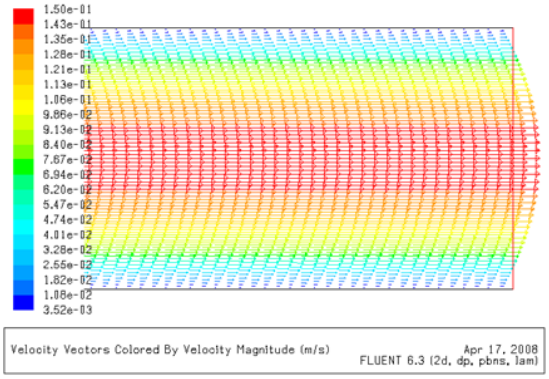

Figure B.2: Outlet velocity profile for Newtonian with $0.1m/s$ inlet velocity in laminar flow

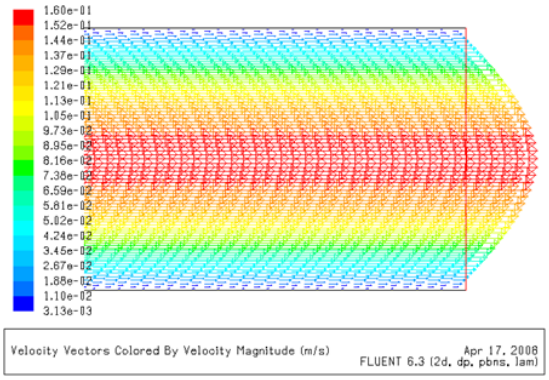

Figure B.3: Outlet velocity profile when power-law index $n = 1.5$ with $0.1m/s$ inlet velocity in laminar flow

B.2 Turbulent flow

The velocity profiles for different values of n calculated from equation FLUENT with $1m/s$ inlet velocity in turbulent flow will display in this section.

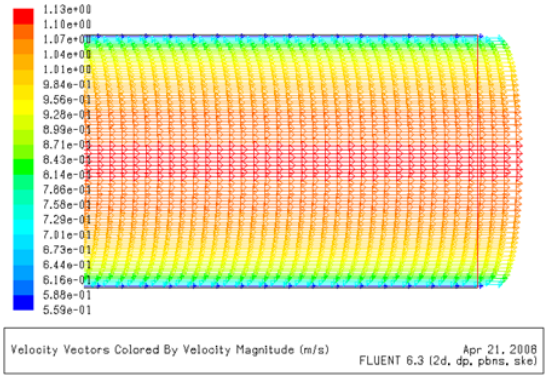

Figure B.4: Outlet velocity profile when power-law index $n = 0.4$ with $1m/s$ inlet velocity in turbulent flow

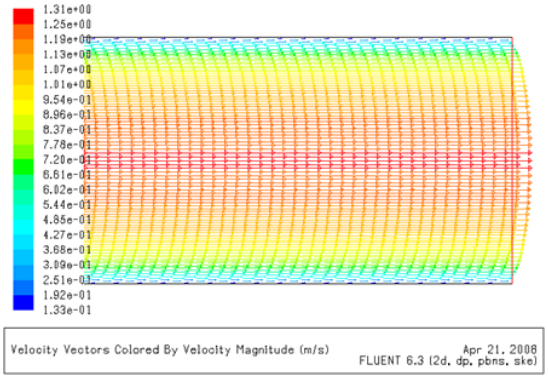

Figure B.5: Outlet velocity profile for Newtonian with $1m/s$ inlet velocity in turbulent flow

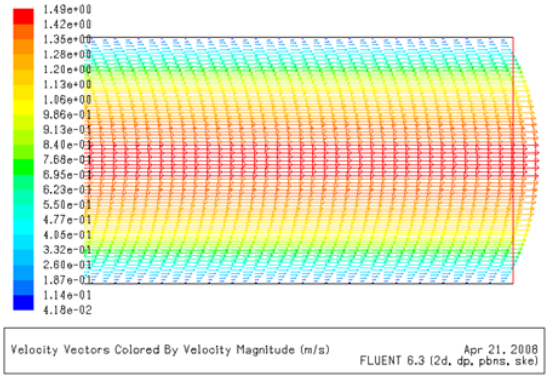

Figure B.6: Outlet velocity profile when power-law index $n = 1.5$ with $1m/s$ inlet velocity in turbulent flow

Appendix C

Generalised Reynolds number for the flow of non-Newtonian time-independent fluids

C.1 Metzner and Reed Reynolds number

This chapter will introduce how to define an appropriate Reynolds number, which will result in a unique friction factor-Reynolds number curve for all non-Newtonian time-independent fluids in laminar flow in a tube, introduced by Chhabra and Richardson (1999). Metzner and Reed (1955) start from the equation 2.28, and then the ratio of shear stress to wall shear stress can be written:

$$\frac{\tau_{rz}}{\tau_w} = \frac{r}{R} \tag{C.1}$$

As mentioned in equation 2.30, the volumetric flow rate is:

$$Q = \int_0^R 2\pi r V_z \mathrm{d}r \tag{C.2}$$

Integration by parts leads to:

$$Q = \pi r^2 V_z\big|_0^R + \int_0^R \pi r^2 (-\frac{\mathrm{d}V_z}{\mathrm{d}r})\mathrm{d}r \tag{C.3}$$

The boundary condition of the wall is no-slip, $V_z = 0$ at $r = R$, so the first term in the right hand side is zero in equation C.3, and it can be re-written:

$$Q = \int_0^R \pi r^2 (-\frac{\mathrm{d}V_z}{\mathrm{d}r})\mathrm{d}r \tag{C.4}$$

Changing the variable of integration from r to τ_{rz} according to C.1

$$r = R(\frac{\tau_{rz}}{\tau_z}); \quad dr = R\frac{\mathrm{d}\tau_{rz}}{\tau_z} \tag{C.5}$$

When $r = 0, \tau_{rz} = 0$ at the middle of the pipe and $r = R, \tau_{rz} = \tau_w$ at the walls of the pipe, substitution in equation C.4 gives:

$$Q = \frac{\pi R^3}{\tau_w^3} \int_0^{\tau_w} \tau_{rz}^2 f(\tau_{rz})\mathrm{d}\tau_{rz} \tag{C.6}$$

First multiplying both sides of equation C.6 by τ_w^3 and then differentiating with respect to τ_w gives

$$\frac{\mathrm{d}}{\mathrm{d}\tau_w}\left\{\tau_w^3\left(\frac{Q}{\pi R^3}\right)\right\} = \frac{\mathrm{d}}{\mathrm{d}\tau_w}\int_0^{\tau_w} \tau_{rz}^2 f(\tau_{rz})\mathrm{d}\tau_{rz} \tag{C.7}$$

Applying the Leibnitz rule to the integral on the right-hand side gives:

$$3\tau_w^2\left(\frac{Q}{\pi R^3}\right) + \tau_w^3\frac{\mathrm{d}}{\mathrm{d}\tau_w}\left(\frac{Q}{\pi R^3}\right) = \tau_w^2 f(\tau_w) \tag{C.8}$$

Then, the equation C.8 over the number 4 on both sides and further rewrite the left-hand side:

$$f(\tau_w) = (-\frac{\mathrm{d}V_z}{\mathrm{d}r})_{wall} = \frac{4Q}{\pi R^3}\left\{\frac{3}{4} + \frac{1}{4}\cdot\frac{\frac{\mathrm{d}(4Q/\pi R^3)}{4Q/\pi R^3}}{\frac{\mathrm{d}\tau_w}{\tau_w}}\right\} \tag{C.9}$$

In terms of average velocity V and pipe diameter D,

$$(-\frac{\mathrm{d}V_z}{\mathrm{d}r})_{wall} = \frac{8V}{D}\left\{\frac{3}{4} + \frac{1}{4}\cdot\frac{\mathrm{d}\log(8V/D)}{\mathrm{d}\log\tau_w}\right\} \tag{C.10}$$

Here, $(8V/D)$ is the wall shear rate for a Newtonian fluid and is referred to as the nominal shear rate for a non-Newtonian fluid. Alternatively, writing it in terms of the slope of $\log\tau_w - \log(8V/D)$ plot's,

$$\dot{\gamma_w} = (-\frac{\mathrm{d}V_z}{\mathrm{d}r})_{wall} = (\frac{8V}{D})(\frac{3n+1}{4n}) \tag{C.11}$$

where $n = (\mathrm{d}\log\tau_w/\mathrm{d}\log(8V/D))$ which is not constant at all range of shear rates. The index n is the slop of the log-log plots of the wall shear stress τ_w versus $(8V/D)$ in the laminar region, and the index n is the flow behaviour of time-independent non-Newtonian fluids.

Shear stress expression can be obtained from equation C.11 and is shown in the following:

$$\tau_w = \frac{D}{4}\left(\frac{-\Delta P}{L}\right) = m\left(\frac{3n+1}{4n}\right)^n\left(\frac{8V}{D}\right)^n \tag{C.12}$$

Substituting for τ_w in terms of the friction factor, $f = \tau_w/(1/2)\rho V^2$, equation C.12 becomes:

$$f = \frac{2}{\rho V^2}m\left(\frac{3n+1}{4n}\right)^n\left(\frac{8V}{D}\right)^n \tag{C.13}$$

Now, a Reynolds number could be defined in the following so that in the laminar flow regime, it is related to $f = \frac{16}{\mathrm{Re}_{MR}}$ as it is for Newtonian fluids.

$$\mathrm{Re}_{MR} = \frac{\rho V^{2-n}D^n}{8^{n-1}m\left(\frac{3n+1}{4n}\right)^n} \tag{C.14}$$

C.2 Reference C

Chhabra, R. P. and Richardson, J. F. (1999), *Non-Newtonian flow in the process industries*, Butterworth-Heinemann. (cited at page 175)

Metzner, A. B. and Reed, J. C. (1955), 'Flow of non-newtonian fluids - correlation of the laminar, transition, and turbulent-flow regions', *AIChE Journal* **1**(4), 434 – 440. (cited at page 175)

Appendix D

Time trace in two phase gas/shear-thinning slug flow

D.1 Time trace of the liquid holdup

Once a slug has been initiated, it is observed that in order to follow the development process of the slug, a set of time traces of liquid holdup are obtained at $4m$,$6m$,$7m$ from the elbow, as indicated in figure D.1. It can be observed that in order to pick up liquid, there must be enough liquid in the stratified flow in front of the slug, which means a minimum liquid level of the liquid film is required. This means that if a slug already exists, it will exist as long as the condition of equally picking up and shedding liquid is met - and if the film in front of the slug is not enough to maintain the slug, it will decay.

Another interesting observation is that under this condition, it can be seen that the slug is always initiated from the inlet of the pipe, and then it follows a development process as it travels along the pipe.

D.2 Time trace of the static pressure

The profile of mean static pressure traces for different positions is shown in figure D.2; it can be observed that pressure increases continuously from the figure D.2 a to c, and static pressure suddenly increases when a slug passes by.

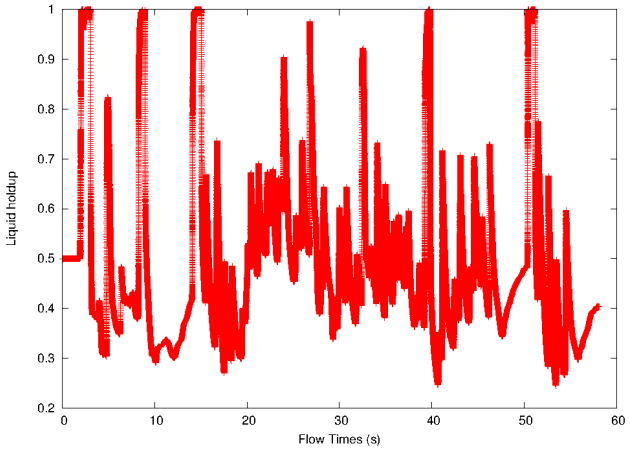

(a) at $4m$ from the elbow

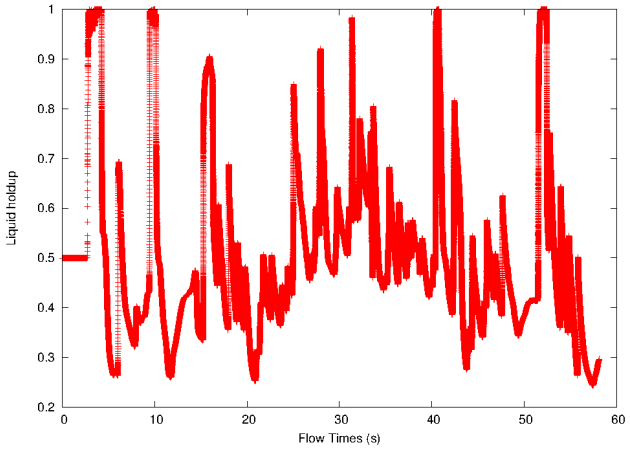

(b) at $6m$ from the elbow

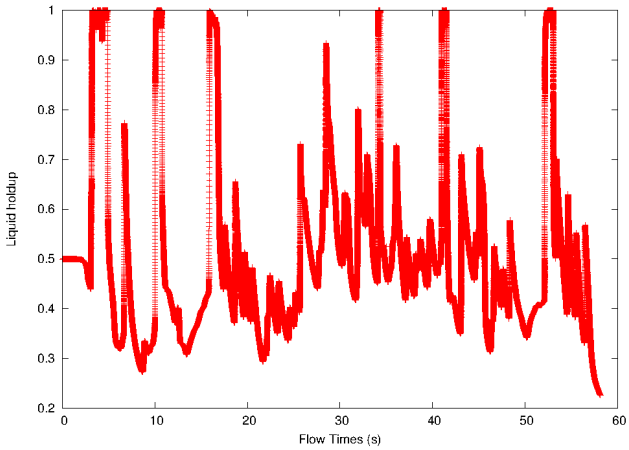

(c) at $7m$ from the elbow

Figure D.1: Liquid holdup traces for slug flow at $u_{SL} = 0.488m/s, u_{SG} = 0.887m/s$

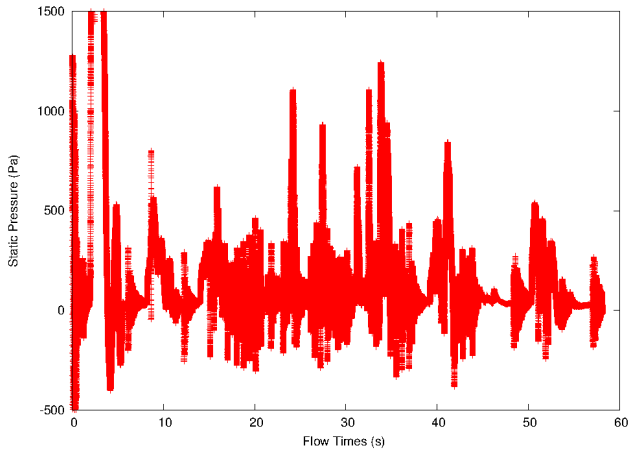

(a) at $4m$ from the elbow

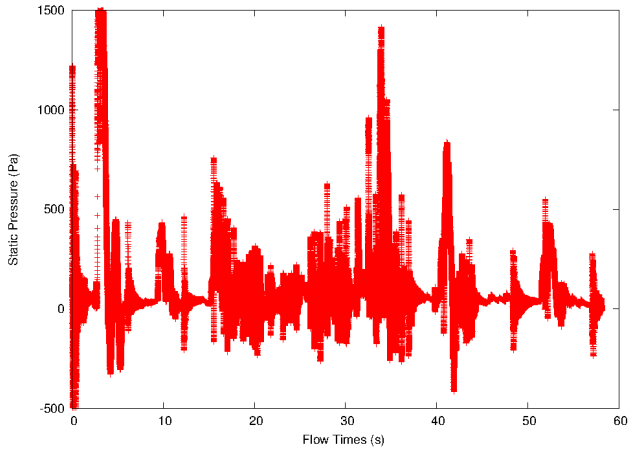

(b) at $6m$ from the elbow

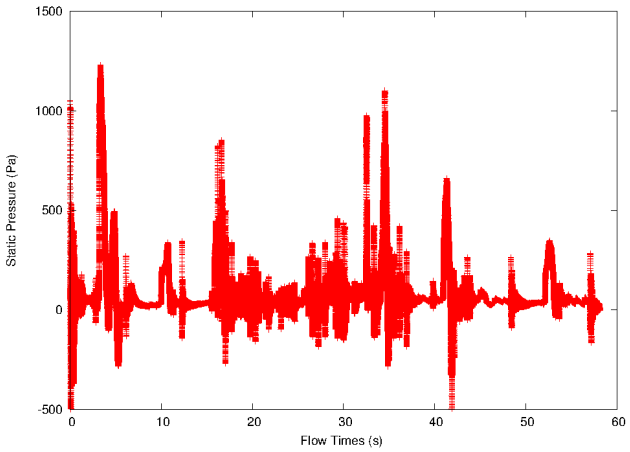

(c) at $7m$ from the elbow

Figure D.2: Area-weighted average static pressure traces for slug flow at $u_{SL} = 0.488m/s, u_{SG} = 0.887m/s$

Appendix E

Liquid-liquid core annular flow steady state model in a vertical pipe

E.1 Introduction

In this appendix, the normal two-phase steady state model was chosen to study the liquid-liquid annular flow core radius in a vertical pipe, as shown in the figure E.1.

E.2 Liquid-liquid annular flow steady state model

Two fluids steady state model was introduced here:

$$-A_W(\frac{dP}{dx})_{TP} - \tau_W S_W + \tau_I S_I - \rho_W A_W g \sin\alpha = 0 \tag{E.1}$$

$$-A_O(\frac{dP}{dx})_{TP} - \tau_I S_I - \rho_O A_O g \sin\alpha = 0 \tag{E.2}$$

E. LIQUID-LIQUID CORE ANNULAR FLOW STEADY STATE MODEL IN A VERTICAL PIPE

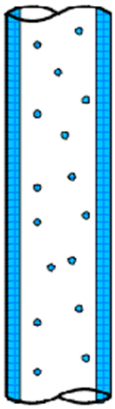

Figure E.1: Vertical annular flow regime

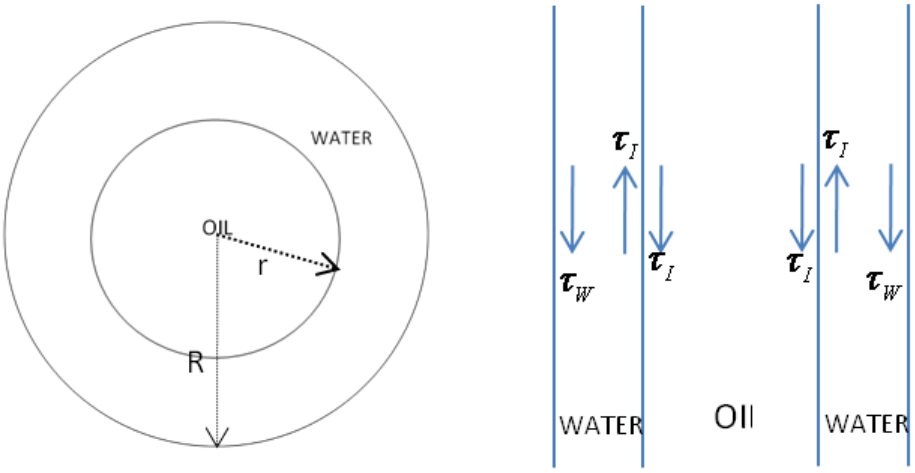

Figure E.2: Description of the vertical annular flow: cross-section and side views of a core annular flow in a vertical pipe

Combining equation E.1 and E.2 by eliminating the two-phase Pressure gradient $(\frac{dP}{dx})_{TP}$, then

$$-\frac{\tau_W S_W}{A_W}+\tau_I S_I\left(\frac{1}{A_O}+\frac{1}{A_W}\right)-(\rho_W-\rho_O)\,g\sin\alpha=0 \tag{E.3}$$

where A_W, A_O, S_I and S_W are geometric parameters that only depend on the oil phase radius r, which is shown in the figure E.2 and are defined in the following.

- Area for each phase:

$$A_W=\frac{\pi}{4}D^2-\pi r^2, \qquad A_O=\pi r^2 \tag{E.4}$$

- Wetted perimeter:

$$S_W=\pi D, \qquad S_I=2\pi r \tag{E.5}$$

The quantity τ_W is shear stress. It is calculated by empirical correlations for the friction factors. Among this, τ_I is the shear stress between the liquid phase and the gas phase. It is associated with the interfacial friction factor f_I

- Shear stress :

$$\tau_W=f_W\frac{\rho_W U_W^2}{2}, \qquad \tau_I=f_I\frac{\rho_O\,(U_O-U_W)\,|U_O-U_W|}{2} \tag{E.6}$$

where water wall friction factor f_W and interfacial friction factor f_I gives:

- Friction factor:

$$f_W=C_W\mathrm{Re}_W^{-a}, \qquad f_O=C_O\mathrm{Re}_W^{-b}, \qquad f_I=f_O \tag{E.7}$$

The coefficients C_W, a respectively have values of 0.046 and 0.25 if the flow is turbulent ($Re_K > 2100$), or 16 and 1 if the flow is laminar ($Re_K < 2100$); the values are same with C_O, b.
where the Reynolds number $\mathrm{Re_k}$ is defined as:

- Reynolds number:

$$\mathrm{Re}_W = \frac{D_W U_W \rho_W}{\mu_W}, \qquad \mathrm{Re}_O = \frac{D_O U_O \rho_O}{\mu_O} \tag{E.8}$$

The hydraulic diameter D_k is defined as:

- Hydraulic diameter:

$$D_W = \frac{4A_W}{\pi D}, \qquad D_O = \frac{4A_O}{2\pi h} \tag{E.9}$$

E.3 Validations

The specifications of flow are summarised as:

- Pipe length: 5.1 m
- Diameter: $25mm$
- Operating fluids: oil and water
- Fluids density: $\rho_O = 960kg/m^3$, $\rho_L = 1000kg/m^3$
- Fluids viscosity: $\mu_O = 0.20kg/ms$, $\mu_L = 0.0013kg/ms$
- Flow temperature: $T = 298\mathrm{K}$
- Initiation inlet superficial velocity: $U_{so} = 0.3m/s, U_{sw} = 0.3m/s$

The analytical oil core radius was compared with the 3D Fluent result using the Eulerian-Eulerian model simulated by Gourma and Thompson (2011), as shown in figure E.3.

where L is the pipe length from inlet and U_{SG}, U_{SO} are the water superficial velocity and oil superficial velocity in that pipe cross section, respectively. It can be seen from table E.1 that the oil core radius calculated by the steady state model has great agreement with the result simulated with the 3D fluent by Gourma and

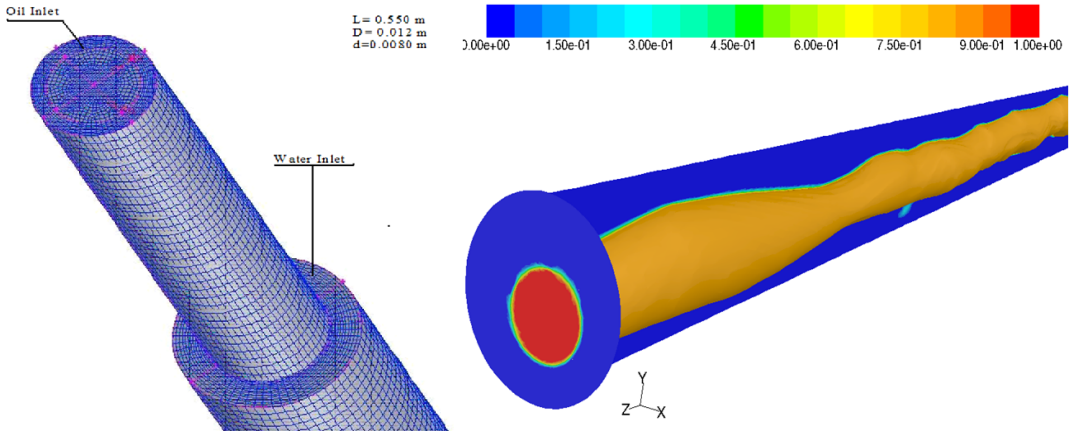

(a) (b)

Figure E.3: Left: Mesh for the core annular flow in a vertical pipe. Right: Volume fraction distribution: Gravity is pointing to +z axis. (Gourma and Thompson, 2011)

	Steady state oil core radius (m)	3D FLUENT oil core radius (m)
$L = 0.35$ $U_{so} = 0.1259m/s$ $U_{sw} = 0.6198m/s$	0.0024039	0.0025
$L = 0.45$ $U_{so} = 0.152m/s$ $U_{sw} = 0.618m/s$	0.0025989	0.0027

Table E.1: Comparison the oil core radius with the 3D fluent result

Thompson (2011). This result proves that the two fluids steady state model has the capability to calculate the core radius for the core annular flow in a vertical

pipe.

E.4 Reference E

Gourma, M. and Thompson, C. P. (2011), Calculation of core annular flows in vertical pipes, Technical report, AMAC, Cranfield University. (cited at page xvii, 186, 187)

Nomenclature

Roman Symbols

ΔP	pressure drop	Pa
A	flow cross-section area of the phase	m^2
B_{fk}	body or gravity force of the k-phase	Pa/m
D	pipe diameter	m
D_k	hydraulic diameter of the phase k	m
f	friction factor	
g	acceleration due to gravity	m/s^2
h	the phase height	m
k	turbulent kinetic energy	$m^2 s^{-2}$
l	liquid length	m
m	fluid consistency index	Pas^n
M_{ki}	interfacial stress force of the k-phase	Pa/m
M_{kw}	wall stress force of the k-phase	Pa/m
n	the flow behaviour index,dimensionless	
P_c	pressure correction term of the liquid phase	Pa

Re_{MR}	Reynolds number of non-Newtonian liquid phase	
S	wetted perimeter	m
T_i	interfacial shear force	Pa/m
T_{kw}	wall shear force of the k-phase	Pa/m
u	flow velocity of the phase	m/s
u_k	velocity of the k-phase	m/s
u_{SG}	superficial velocity of the phase gas	m/s
u_{SL}	superficial velocity of the phase liquid	m/s

Greek Symbols

α	liquid holdup	
α_k	volume fraction of the phase k	
β	the angle of the inclination of the pipe	rad
ϵ	turbulent dissipation energy	$m^2 s^{-2}$
Γ_k	mass transfer term of the k-phase	$kg/(m^3 s)$
λ_L	slug length	m
μ	viscosity	$kg/(ms)$
ω_S	slug frequency	
ρ	density	kg/m^3
$\dot{\gamma}$	shear rate	$1/s$
μ	Newtonian or apparent viscosity	$Pa \cdot s$
τ	shear stress in fluid	Pa

Subscripts

f liquid film in slug unit

G gas phase

GW gas wall

i interfacial

k phase k, L for liquid, G for gas

ki interfacial and the k-phase

kW phase k and wall

L liquid phase

LW liquid wall

s slug body in slug unit

sp single phase

tp two phase

u slug unit

Acronyms

AMR adaptive mesh refinement

AUSM Advection Upstream Splitting Method

AUSMD Advection Upstream Splitting Method using flux Difference splitting scheme

AUSMDV Advection Upstream Splitting Method hybrid flux Difference splitting (FDS) and flux Vector splitting (FVS) schemes

AUSMV Advection Upstream Splitting Method using flux Vector splitting scheme

CMC CarboxyMethylo Cellulose

FDS flux Difference splitting scheme

FVS flux Vector splitting scheme

KH Kelvin-Helmholtz

TD KH Taitel-Dukler Kelvin-Helmholtz

VOF volume of fluid